# Sustained effects of influenza A virus infection on allergic airway inflammation in two mouse models with a focus on macrophages and dendritic cells

**Thesis**

for the degree of

**doctor rerum naturalium (Dr. rer. nat.)**

approved by the Faculty of Natural Sciences of Otto von Guericke University Magdeburg

by M.Sc. Belinda Camp

born on 21.12.1995 in Goslar

Examiner: PD Dr. Sabine Stegemann-Koniszewski
Prof. Dr. Matthias Gunzer

submitted on: 24. Mai 2024

defended on: 25. Oktober 2024

# Preamble

Parts of the results of this thesis were published in:

**Camp B.**, Jorde I., Sittel F., Pausder A., Jeron A., Bruder D., Schreiber J. and Stegemann-Koniszewski S.

"Comprehensive analysis of lung macrophages and dendritic cells in two murine models of allergic airway inflammation reveals model- and subset-specific accumulation and phenotypic alterations"

Frontiers in Immunology. 15:1374670; 2024; doi: 10.3389/fimmu.2024.1374670

Text sections from the above-mentioned publication were used in **sections 2, 3, 4.1 and 5**.

# Vorwort

Teilergebnisse der vorliegenden Arbeit wurden veröffentlicht in:

**Camp B.**, Jorde I., Sittel F., Pausder A., Jeron A., Bruder D., Schreiber J. and Stegemann-Koniszewski S.
"Comprehensive analysis of lung macrophages and dendritic cells in two murine models of allergic airway inflammation reveals model- and subset-specific accumulation and phenotypic alterations"
Frontiers in Immunology. 15:1374670; 2024; doi: 10.3389/fimmu.2024.1374670

Textabschnitte der oben genannten Publikation wurden in den **Abschnitten 2, 3, 4.1 und 5** verwendet.

# Contents

# List of publications – results of this thesis

**Camp B.**, Jorde I., Sittel F., Pausder A., Jeron A., Bruder D., Schreiber J. and Stegemann-Koniszewski S.

"Comprehensive analysis of lung macrophages and dendritic cells in two murine models of allergic airway inflammation reveals model- and subset-specific accumulation and phenotypic alterations"

Frontiers in Immunology. 15:1374670; 2024; doi: 10.3389/fimmu.2024.1374670

# List of publications - others

**Camp, B**., Stegemann-Koniszewski, S., Schreiber, J.

"Infection-Associated Mechanisms of Neuro-Inflammation and Neuro-Immune-Crosstalk in Chronic Respiratory Diseases"

International Journal of Molecular Sciences, 2021, 22, 5699; doi: 10.3390/ijms22115699

Kopenhagen, A., Ramming, I., **Camp, B**., Hammerschmidt, S., Fulde, M., Müsken, M., Steinert, M., Bergmann, S.

„*Streptococcus pneumoniae* Affects Endothelial Cell Migration in Microfluidic Circulation"

Frontiers in Microbiology, 2022; doi: 10.3389/fmicb.2022.852036

# Conference contributions

**Camp, B.**, Wu, Q., Jorde, I., Lücke, E., Kershaw, O., Schreiber, J., Stegemann-Koniszewski, S. „Long-term modulation of the lung monocyte/macrophage compartment following resolved IAV infection and its consequences for allergic airway inflammation in a mouse model." Poster presentation. 62. Kongress der Deutschen Gesellschaft für Pneumologie und Beatmungsmedizin e.V. (DGP), Leipzig, 2022

**Camp, B.**, Wu, Q., Jorde, I., Kershaw, O., Schreiber, J., Stegemann-Koniszewski, S. „IAV infection has long-term effects on the lung monocyte/macrophage compartment and modulates subsequent allergic airway inflammation in a mouse model." Poster presentation. Joint Meeting of German Society for Immunology (DGfI) and Austrian Society for Allergology and Immunology (ÖGAI), Hannover, 2022

**Camp, B.**, Jorde, I., Jeron, A., Schreiber, J., Stegemann-Koniszewski, S. „A characterization of the lung macrophage and dendritic cell compartment in allergic airway inflammation following influenza A virus infection comparing peripheral versus respiratory sensitization." Poster presentation. Joint Meeting of German Society for Immunology (DGfI) and Société Francaise d´Immunologie (SFI), Straßburg, 2023

**Camp, B.**, Jorde, I., Jeron, A., Schreiber, J., Stegemann-Koniszewski, S. „A comparison of peripheral versus respiratory sensitization in allergic airway inflammation following influenza A virus infection with regard to macrophages and dendritic cells in the lung." Poster presentation. The Autumn School of the German Society for Immunology (DGfI), Merseburg, 2023

# Abstract

Allergic asthma is the most common form of bronchial asthma, a frequent chronic inflammatory respiratory disease. It is highly heterogeneous and the predisposing factors, drivers of inflammation and pathomechanisms remain elusive in many points, including the relevance of respiratory infections. Influenza A virus (IAV) is a respiratory virus that can have sustained effects on local immunity. Only few data are available on how these effects modulate allergic airway inflammation (AAI). In the lung, a complex network of macrophages and DC contributes to the induction, regulation and resolution of immune responses. Multiple subsets have been described and there is increasing evidence for their distinct roles in AAI. Further, respiratory viral infections are postulated as the one of the main causes for allergic asthma. This thesis followed the hypothesis, that IAV infection sustainably affects lung macrophages and DC and thereby modulates subsequently induced AAI.

Macrophage and DC subsets were comprehensively characterized by spectral flow cytometry in two common mouse models of AAI. Subset- as well as model-specific characteristics with respect to cell numbers and functional marker expression were observed comparing ovalbumin (OVA)-mediated and house dust mite (HDM)-mediated AAI. Significantly increased numbers of alveolar macrophages (AM), $CD103^+$ and $CD11b^+$ DC as well as increased CD80 expression by $CD11b^+$ DC were observed in the HDM model, concurrent with significantly increased levels of lung T cells, B cells as well as respiratory interleukin (IL)-4 and IL-17A, but decreased serum total IgE levels.

IAV infection resulted in significantly increased levels of respiratory serum albumin and IL-12p40 levels as well as numbers of AM and interstitial macrophages (IM) 39 days post infection, however without strong effects on the analyzed macrophage and DC subsets. AAI induced after recovery from IAV infection was significantly modulated with regard to decreased total serum IgE levels and Th2 cytokine production. Overall, there was a trend for amelioration of AAI by previous IAV infection, which was AAI model-specific.

Taken together, the results of this thesis highlight the importance of model-specific aspects in mouse models of allergic asthma, underline the potential of IAV infections to form long-lasting effects on the lung immune micromilieu and show that resolved infection has the potential to suppress key features of AAI. These data display a valuable basis for future research into IAV-mediated functional alterations in lung macrophages and DC as well as how these shape allergic inflammation in the context of resolved viral infection.

# Zusammenfassung

Allergisches Asthma ist eine häufige, chronisch-entzündliche Atemwegserkrankung. Ihre Ausprägung ist sehr heterogen und die prädisponierenden Faktoren, Treiber der Entzündung und Pathomechanismen sind in vielen Punkten, einschließlich der Bedeutung von Atemwegsinfektionen, unklar. Das Influenza-A-Virus (IAV) ist ein häufiges Atemwegsvirus, das langfristige Auswirkungen auf die lokale Immunität haben kann. Hierzu und darüber, wie eine nachfolgend auftretende allergische Atemwegsentzündung (AAI) moduliert wird, gibt es nur wenige klinische und experimentelle Daten. In der Lunge trägt ein komplexes Netzwerk von Makrophagen und dendritischen Zellen (DC) zur Induktion und Regulierung von Immunantworten bei. Es werden jeweils mehrere Untergruppen beschrieben und es gibt zunehmende Belege für ihre Rolle in der AAI. In dieser Arbeit wurde die Hypothese verfolgt, dass eine IAV-Infektion Makrophagen und DC in der Lunge nachhaltig beeinflusst und dadurch eine nachfolgend induzierte AAI moduliert.

In zwei Mausmodellen des allergischen Asthmas wurden Makrophagen und DC mittels spektraler Durchflusszytometrie umfassend charakterisiert. Dabei wurden subpopulations- und modellspezifische Merkmale beobachtet. Im Vergleich zu einem Ovalbumin-vermittelten Modell wurde in einem Hausstaubmilben-vermittelten Modell eine signifikant verstärkte Akkumulation von Alveolarmakrophagen (AM), $CD103^+$ und $CD11b^+$ DC sowie eine verstärkte Expression von CD80 auf $CD11b^+$ DC bei gleichzeitig signifikant erhöhten respiratorischen T- und B Zellzahlen sowie Interleukin (IL)-4- und IL-17A-Spiegeln, aber reduziertem Gesamt-IgE-beobachtet.

Die durchgemachte Infektion mit IAV führte nach 39 Tagen zu signifikant erhöhten Serumalbumin- und IL-12p40-Spiegeln in der BAL sowie zu einer signifikant erhöhten Anzahl von AM und interstitiellen Makrophagen in der Lunge, wobei deren einzelne Subpopulationen kaum verändert waren. In der nachfolgend induzierten AAI zeigte sich in Bezug auf den Gesamt-IgE-Spiegel im Serum und die Th2-Zytokinproduktion eine signifikante Modulation. Insgesamt zeigte sich ein teilweise modell-anhängiger Trend zur Abschwächung der AAI durch eine vorangegangene IAV-Infektion.

Die Ergebnisse dieser Arbeit unterstreichen die Bedeutung modell-spezifischer Beobachtungen in der Erforschung des allergischen Asthmas. Weiter verdeutlichen sie das Potenzial von IAV-Infektionen, langanhaltende Auswirkungen auf die Lunge zu vermitteln und zeigen, dass die durchgemachte Infektion Mechanismen der allergischen Entzündung unterdrücken kann. Diese Daten stellen eine Grundlage für künftige Forschungen zu funktionellen Veränderungen von pulmonalen Makrophagen und DC nach IAV Infektion und wie diese die allergische Entzündung unterdrücken können, dar.

# List of abbreviations

| | |
|---|---|
| % | Percent |
| /° | Per well |
| × g | Multiple of the gravitational acceleration |
| ° | Well |
| °C | Degree Celsius |
| µg | Micrograms |
| µl | Microliter |
| µm | Micrometer |
| AAI | Allergic airway inflammation |
| ACK | Ammonium chloride potassium |
| AF | Autofluorescence |
| AF700 | Alexa Fluor™ 700 |
| Ag | Antigen |
| AHR | Airway hyper-reactivity |
| alum | Aluminum hydroxide |
| AM | Alveolar macrophages |
| a.o. | Alum only |
| APC | Antigen-presenting cell |
| APC | Allophycocyanin |
| APC/Cy7 | Allophycocyanin-cyanine 7 |
| BAL | Bronchoalveolar lavage |
| BAM | Bronchus-associated macrophages |
| BV421/510/711 | Brilliant Violet 421/510/711 |
| c | Concentration |
| cDC | Conventional dendritic cell |

List of abbreviations

| | |
|---|---|
| $CO_2$ | Carbon dioxide |
| d | Day(s) |
| DAMPs | Damage-associated molecular patterns |
| DC | Dendritic cell |
| Der p | *Dermatophagoides pteronyssinus* |
| Der f | *Dermatophagoides farinae* |
| DNAse | Deoxyribonuclease |
| AEC | Airway epithelial cells |
| e.g. | *exempli gratia* (for example) |
| EDTA | Ethylenediaminetetraacetic acid |
| ELISA | Enzyme-linked immunosorbent assay |
| *et al*. | *et alii* (and others) |
| FACS | Fluorescence-activated cell sorting |
| FCS | Fetal calf serum |
| FCS | Forward scatter |
| FcεRI | Fc epsilon receptor I |
| FMO | Fluorescence minus one |
| GM-CSF | Granulocyte-macrophage colony-stimulating factor |
| h | Hour(s) |
| HA | Hemagglutinin |
| HDM | House dust mite |
| HRP | Horseradish peroxidase |
| *i.n.* | Intranasal/intranasally |
| *i.p.* | Intraperitoneal/intraperitoneally |
| *i.t.* | Intratracheal/intratracheally |
| IAV | Influenza A virus |

List of abbreviations

| | |
|---|---|
| ICAM-1 | Intracellular cell adhesion molecule 1 |
| IFN | Interferon |
| Ig | Immunoglobulin |
| IgE | Immunoglobulin E |
| IL | Interleukin |
| ILC2 | Group 2 innate lymphoid cells |
| IM | Interstitial macrophages |
| IMDM | Iscove's modified dulbecco's medium |
| IVC | Individually ventilated cage |
| KB520 | Kiravia Blue 520 |
| kDa | Kilodalton |
| kg | Kilograms |
| $KHCO_3$ | Potassium hydrogen carbonate |
| LPS | Lipopolysaccharide |
| M | Molar |
| MBP | Major basic protein |
| MFI | Mean fluorescence intensity |
| mg | Milligrams |
| MHC | Major histocompatibility complex |
| min | Minute(s) |
| ml | Milliliter |
| mM | Millimolar |
| n | Sample size |
| NA | Neuraminidase |
| NaCl | Sodium chloride |
| NAM | Nerve-associated macrophages |
| $NH_4CL$ | Ammonium chloride |

List of abbreviations

| | |
|---|---|
| NLRs | Nod-like receptors |
| ns | Non-significant |
| NS1 | Nonstructural protein 1 |
| $O_2$ | Oxygen |
| OD | Optical density |
| OVA | Ovalbumin |
| p | Probability |
| PAMPs | Pathogen-associated molecular patterns |
| PBS | Phosphate-buffered saline |
| PE | Phycoerythrin |
| PE/Cy7 | Phycoerythrin/Cyanin 7 |
| PerCP/Cy5.5 | Peridinin-chlorophyll proteins cyanine 5.5 |
| PFA | Paraformaldehyde |
| pg | Picogram |
| pH | Hydrogen ion exponent |
| PRRs | Pattern recognition receptors |
| recMacs | Monocyte-derived recruited macrophages |
| RIG-I | Retinoic acid induced gene 1 like receptor |
| rpm | Rounds per minute |
| RSV | Respiratory syncytial virus |
| RT | Room temperature |
| *S. aureus* | *Staphylococcus aureus* |
| Spark YG593 | Spark yellow-green 593 |
| SPF | Specific-pathogen free |
| SSC | Side scatter |
| TCR | T cell receptor |
| TGF-β | Transforming growth factor β |

List of abbreviations

| | |
|---|---|
| Th cell | T helper cell |
| Th1 cell | T helper cell 1 |
| Th17 cell | T helper cell 17 |
| Th2 cell | T helper cell 2 |
| TLR | Toll-like receptor |
| TMB | 3,3', 5,5'-Tetramethylbenzidine |
| TSLP | Thymic stromal lymphopoietin |
| UMAP | Uniform Manifold Approximation and Projection |
| UV | Ultraviolet |
| vs | Versus |
| β-Me | 2-Mercaptothanol |

# List of figures

# List of tables

# 1 Introduction

## 1.1 Bronchial asthma

Bronchial asthma is one of the most common chronic inflammatory respiratory diseases and is estimated to affect more than 300 million patients worldwide (Lambrecht *et al.* 2015). The estimated prevalence of asthma in 2019 was the highest in the African region (11.3 %) and the lowest in the southeast Asia region (8.8 %) (Song *et al.* 2022). The symptoms and intensity of asthma vary over time and include wheezing, chest tightness, coughing and shortness of breath (Holgate *et al.* 2015). Bronchial asthma is further characterized by airway hyper-reactivity, airway narrowing, airway wall remodeling and mucus overproduction (Papi *et al.* 2018). The remodeling processes include an increase of the airway smooth muscle mass, thickening of the subepithelial basement membrane, neuronal proliferation, angiogenesis and metaplasia of goblet cells (Mims 2015) (see figure 1, p. 2). Next to others, immunological factors, age and sex influence the development of asthma (Holgate *et al.* 2015).

Asthma is an extraordinarily heterogeneous disease (Carr *et al.* 2016). Traditionally, two types of asthma were discriminated: allergic (extrinsic) and non-allergic (intrinsic) asthma. About 60 % of adults and the majority of children suffer from allergic asthma (Vogelmeier *et al.* 2017). Allergic asthma is typically characterized by a T helper type 2 cell (Th2) dominated immune response towards aeroallergens like house dust mite (HDM), fungal spores or pollen (Lambrecht *et al.* 2015). The immune response manifests through the production of allergen-specific immunoglobulin E (IgE)-antibodies, the release of Th2-inflammatory mediators such as interleukin-4 (IL-4), IL-5 and IL-13 as well as the recruitment of eosinophils and basophils (Foster *et al.* 2017, Caminati *et al.* 2018). Non-allergic or intrinsic asthma is characterized by a lack of specific IgE responses and the adaptive immune system such as Th2 cells is not involved. Furthermore, intrinsic asthma develops later in life and is more common in women (Romanet-Manent *et al.* 2002, Peters 2014).

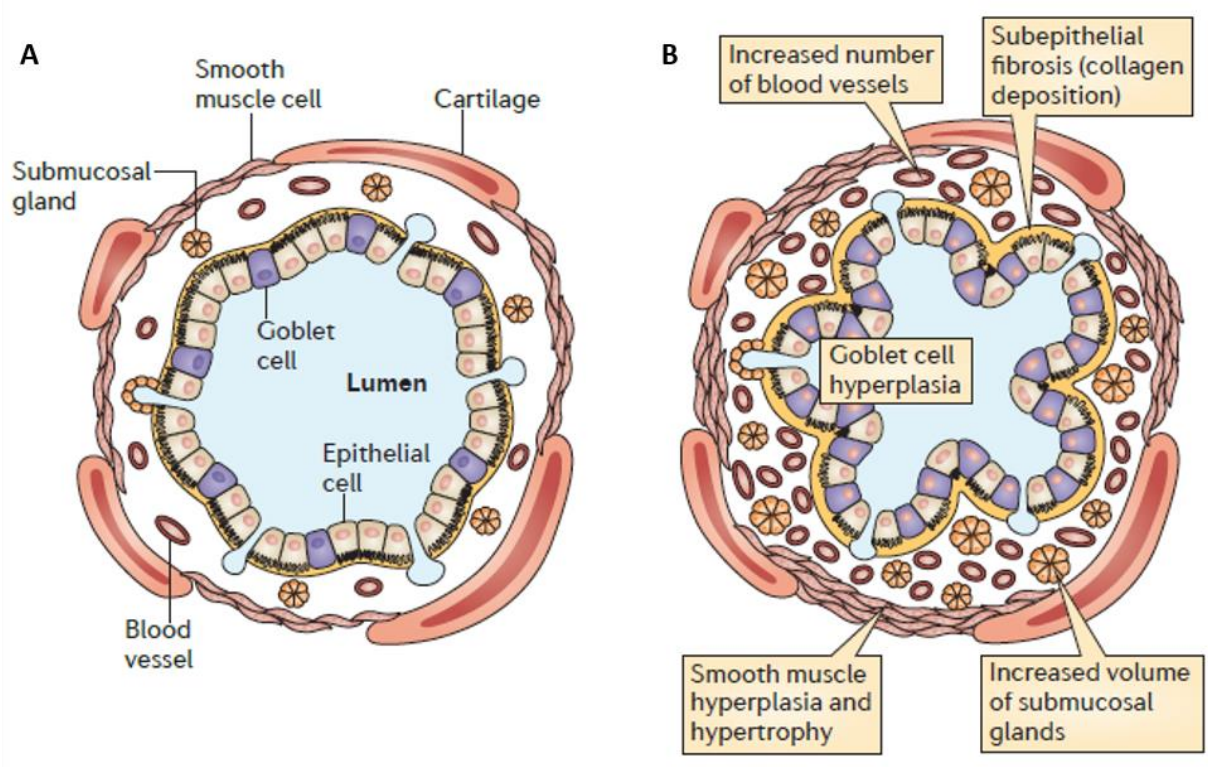


**figure 1: Airway pathology in asthma.** (adapted from Fahy 2014)
Airway structures in medium-sized (A) healthy airways and (B) in a patient with asthma. The airways in asthma show structural remodeling including goblet cell hyperplasia, subepithelial fibrosis and increases in smooth muscle volume as well as increased numbers of blood vessels.

The disease endotype clearly differs from a disease phenotype and describes a subtype of a condition, defined by distinct mechanistic pathways (Kuruvilla *et al.* 2019). Today, asthma is divided into more than two subtypes: type 2-high asthma and type 2-low asthma, which can further be divided into several endotypes depending on e.g. inflammatory mediators, activation stimuli and the onset of the disease. Type 2-high asthma is the most common endotype. The initial exposure to an allergen induces its uptake by antigen presenting cells (APC) resulting in an allergen-specific Th2 response mainly mediated by Th2 cells, IgE-producing B cells and group 2 innate lymphoid cells (ILC2s). This response includes the secretion of cytokines such as IL-4, IL-5 and IL-13. Elevated IgE titers and eosinophilia

characterize the disease (Lambrecht *et al.* 2015). It is more challenging to define type 2-low endotypes due to the lack of identified biomarkers. Common among all forms of asthma is that the symptoms are triggered by allergens, respiratory infections, cold air, stress, tobacco, medication or pollutants (Holgate *et al.* 2015).

### 1.1.1 Pathophysiology of allergic asthma

In adaptive immune responses, characteristic Th1, Th2 and Th17 responses are balanced (Eberl 2016). Th1 cells secrete the key cytokines interferon (IFN)-γ and tumor necrosis factor (TNF)-α in response to infections with intracellular viruses and bacteria. Th2 cells secrete IL-4, IL-5 and IL-13 to target parasitic organisms. Th17 cells secrete the cytokines IL-17, IL-6, IL-22 and TNF-α and play a role in tissue inflammation and activation of neutrophils to combat extracellular bacteria (Kaiko *et al.* 2008). In allergic asthma, this balance is shifted towards a Th2-dominated response during the immune response. The strong secretion of IL-4, IL-5 and IL-13 results in a suppression of Th1 and Th17 responses and ultimately leads to allergic airway inflammation (AAI). In this, various of structural cells, cells of the innate and the adaptive immune system and a variety of humoral factors are involved (Luo *et al.* 2022).

#### 1.1.1.1 Airway epithelium

Airway epithelial cells (AEC) form a natural barrier towards the environment and represent the first line of defense against microorganisms, gases and allergens. According to their protective function, AEC expresses pattern recognition receptors to detect and respond to pathogen-associated molecular patterns (PAMPs) or damage-associated molecular patterns (DAMPs). The activation of these receptors leads to the release of cytokines and chemokines which attract and activate immune cells to orchestrate subsequent immune responses (Lambrecht *et al.* 2012). Allergens such as HDM can lead to a loss of cell-cell contact due to

their enzymatic activities that compromise barrier integrity (Papi *et al.* 2018) and it is reported that patients with asthma show a diminished integrity of the respiratory epithelium (Wan *et al.* 1999). AEC activation initiates the local network of dendritic cells (DC) *via* IL-33, thymic stromal lymphopoietin (TSLP) and granulocyte-macrophage colony–stimulating factor (GM-CSF) to coordinate the subsequent immune response (Lambrecht *et al.* 2009). Further, in patients, higher levels of IL-25 are associated with a greater airway hyper-responsiveness, higher levels of serum IgE and higher airway and blood eosinophils (Cheng *et al.* 2014). Together, IL-25, IL-33 and TSLP act as epithelial alarmins (Whetstone *et al.* 2022). In some murine models of eosinophilic asthma, these cytokines contribute to the formation of a Th2-response by responding in a TLR4/Myd88-dependent manner (Hammad *et al.* 2009). Pathogen replication and the immune response to the infection strongly affect the respiratory epithelium during respiratory infections (Denney *et al.* 2018).

#### 1.1.1.2 Key effector cells and mediators of allergic asthma

DC are professional APC of the lung immune system that sample the inhaled air for antigens into the airway lumen. Upon antigen encounter and uptake, they migrate to the draining lymph nodes, where they present the antigens to antigen-specific B and T cells (Holt 2000). Subsequently, this interaction between APC (i.e. DC) and lymphocytes induces specific responses. These are influenced and characterized by the presence or absence of specific co-stimulatory molecules as well as cytokines. Peptide-presentation *via* major histocompatibility complex-II (MHC II) molecules on the DC surface, along with the influence of epithelial-derived cytokines, leads to the differentiation of antigen-specific T cells into Th2-type T cells and the activation of allergen-specific Th2-cells (Holgate *et al.* 2015). The most efficient ligand on APC to prime naïve T cells is the OX40 ligand (OX40L) on DC (Ohshima *et al.* 1997). Allergen-specific Th2 cells secrete the pro-allergic cytokines IL-4, IL-5, IL-9, IL-13 and GM-CSF, which in turn lead to B cell class-switching and the IgE, mast cell and eosinophilic responses which are

characteristic for allergic asthma (see figure 2, p. 6) (Kay 2006). The triggering of an allergen-specific immune response and its Th2 polarization are fundamental to allergic asthma. Nevertheless, it is unclear in many respects how this allergic sensitization occurs in affected patients and needs further investigations.

IL-4 and IL-13 are described as the main cytokines involved in the pathogenesis of allergic responses, including airway remodeling by stimulation of mucus producing cells and fibroblasts, the induction of B cell class switching to produce IgE and the upregulation of adhesion molecules enabling the migration of leukocytes to the airways (Steinke *et al.* 2001, Wills-Karp 2004, Hall *et al.* 2014). IL-5 is the major cytokine driving the activation of eosinophil precursors, the recruitment of eosinophils from the bone marrow and their survival in the periphery. Studies on mice have demonstrated an increased infiltration with eosinophils in the lungs following mite antigen treatment, a phenomenon not seen in IL-5 deficient knockout mice (Shimizu *et al.* 2013). The activation of eosinophils leads to the release of pro-inflammatory mediators such as major basic protein (MBP) and they possess the ability to release different interleukins, chemokines, TNF-α and TGF-β that altogether drive eosinophilic inflammation (Bandeira-Melo *et al.* 2002).

Mast cells play a critical role in immediate allergic reactions. Fc epsilon receptor I (FcεRI) expression on their surface allows them to bind free IgE. Re-exposure of a sensitized individual to an allergen causes crosslinking of mast cell surface FcεRI receptors by the allergen binding to FcεRI-bound IgE. This results in the activation and degranulation of mast cells, which thereby release a variety of different mediators such as leukotrienes, histamine as well as proteases and prostaglandins (Amin 2012). Increased concentrations of these mediators lead to the contraction of smooth muscle cells and mucous secretion and promote inflammation (Roquet *et al.* 1997, O'Byrne 2000). There are many pathways, by which the close localization of mast cells with airway smooth muscle cells might lead to disordered function of smooth muscles in the airways (Bradding *et al.* 2006).

The shape, intensity and combination of the described inflammatory pathways and mechanisms are very heterogeneous between patients with allergic asthma. This leads to individual variations in the symptoms, severity and course of the disease and a wide range of treatment regimens.

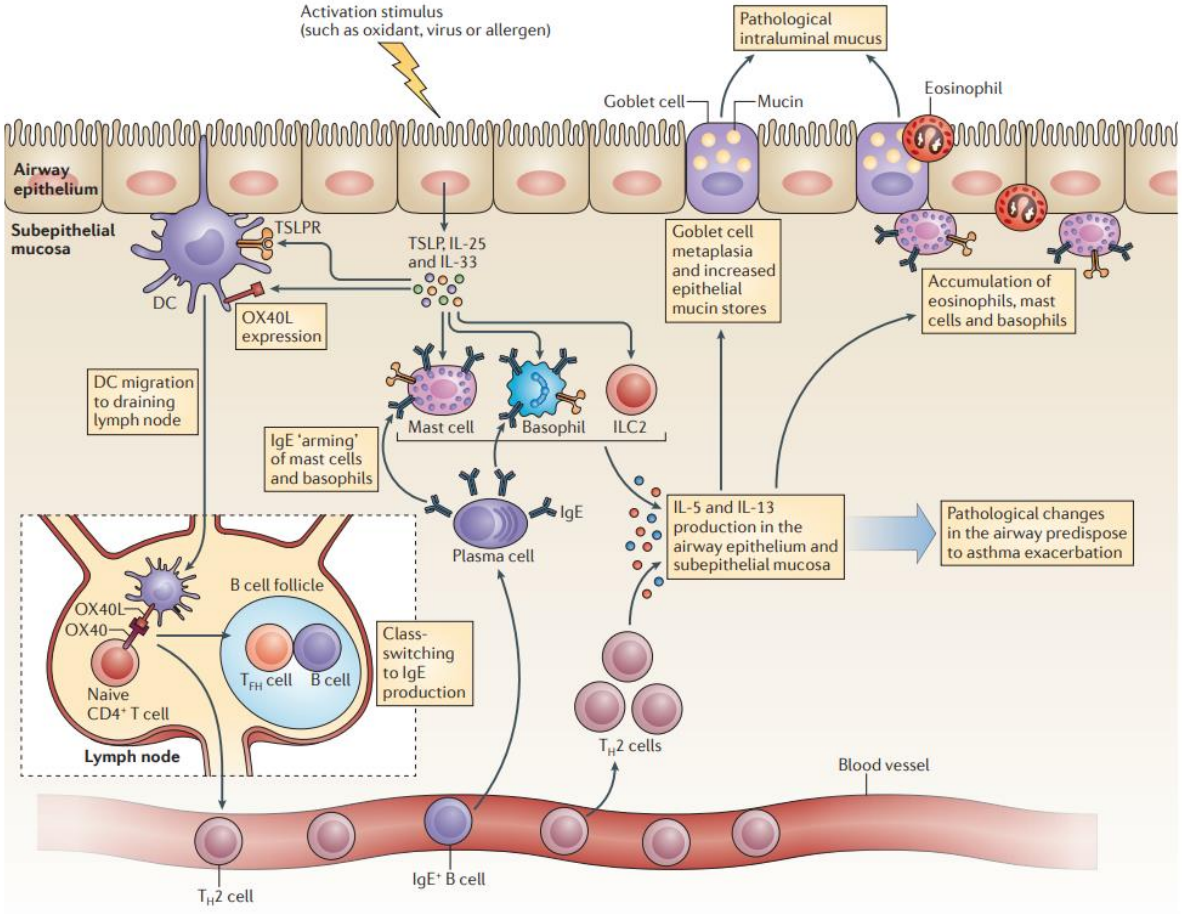


**figure 2: The type 2 immune response in asthma.** (taken from Fahy 2014)
After sensing of an activating stimulus like an allergen, the epithelium releases different cytokines like IL-25, IL-33 and TSLP, which induce the expression of OX40L on DC to promote their mobilization to local draining lymph nodes. In the draining lymph nodes, the activation of naïve $CD4^+$ T cells takes place, which then migrate to the B cell zones and differentiate to T follicular helper cells ($T_{FH}$ cells), translocate into the circulation and complete their maturation to T helper cells type 2 (Th2 cells). The produced IL-4 from $T_{FH}$ cells mediates an IgE class-switch in B cells, while IL-5 and IL-13 produced by Th2 cells mediate remodeling and inflammatory changes in the airway mucosa as well as the accumulation of eosinophils, mast cells and basophils.

#### 1.1.1.3 Current therapies for allergic asthma

Over the decades, with the availability of improved, specific therapeutics the treatment strategy in allergic asthma has changed from a “one-fits-for-all” model to a personalized approach. Nevertheless, effective therapy for allergic asthma is accompanied by a number of difficulties, including the complexity of the molecular mechanisms underlying the symptoms and the disease spectrum. The individual treatment is based on an assessment of the patient´s symptom control, risk factors and comorbidities (Shay *et al.* 2015). A common, rather unspecific treatment of Th2-high asthma are inhaled corticosteroids (Woodruff *et al.* 2009). However, a notable subgroup of patients with this endotype suffers from uncontrolled asthma despite corticosteroid treatment. In these, one of the most recent approaches of treating the associated chronic inflammation is the assessment of biomarkers with the potential to guide treatments that target specific inflammatory pathways. To date, a number of biologic therapies have been approved including inhibitors of IgE, IL-5 and TSLP. For inhibiting IgE, the monoclonal antibody omalizumab was approved, which depletes IgE and thereby weakens mast cell and basophil reactions. Additionally, the effects of IgE on dendritic cells are blocked (Boulet *et al.* 1997, Fahy *et al.* 1997). Furthermore, therapeutics that target IL-5 are approved. Mepolizumab is a monoclonal antibody that binds IL-5 to block its interaction with the α-chain of the IL-5 receptor (IL-5Rα) (Egan *et al.* 1999). Tezepelumab is an antibody directed against the epithelial cytokine TSLP. As TSLP is produced in response to various inhaled triggers (allergens, viruses and other airborne irritants) and leads to the activation of antigen-presenting cells, tezepelumab thus intervenes early in the inflammatory process (DGP). To inhibit IL-13, four antibody therapeutics were tested, which prevent the binding of IL-13 to its two receptors. Examples for IL-13 inhibitors are dupilomap and lebrikizumab (Noonan *et al.* 2013, Hanania *et al.* 2016, Bourdin *et al.* 2024).

For Th2-low asthma there remains a lack of effective controller medication without a solution at present. This lack arises from the fact, that Th2-low asthma is not responsive to corticosteroids (Woodruff *et al.* 2009). Moreover, patients with Th2-low asthma probably

constitute a mix of multiple disease endotypes (see 1.1) that each affect relatively small subgroups of patients.

Although many patients with Th2-high asthma benefit from these therapeutic approaches, a large subgroup of patients that do not respond to the currently available treatments remain and there are unmet therapeutic needs. Further, the available therapeutic agents do not yet lead to a cure of the disease and generally have to be administered continuously, with frequent re-evaluation of the treatment. For this reason, the prevention of sensitization is a fundamental step in the development of asthma. Here, numerous risk factors play a decisive role.

#### 1.1.1.4 Risk factors for allergic asthma

Nowadays, multiple environmental and genetic risk factors for developing allergic asthma are known and they are just as variable as the individual disease. The most prominent environmental risk factor is tobacco smoke that augments T2-type like responses (Feleszko *et al.* 2006). Studies show that prenatal or postnatal exposure to passive smoking increases the risk of developing asthma significantly in children (Li *et al.* 2005).

Increasing air pollution, caused by rising urbanization and population growth, and the presence of environmental allergens are also risk factors for developing allergic asthma. Children sensitized to aeroallergens during early childhood are more likely to experience asthma than non-sensitized children (Platts-Mills *et al.* 2001, Torrent *et al.* 2007).

Next to environmental factors, physical and psychological conditions like obesity or stress can increase the risk of developing asthma. Obesity during childhood is associated with the severity of asthma (Mebrahtu *et al.* 2015). The gut microbiome has a strong influence on the developing immune system, and in turn on allergic asthma, *via* the gut-lung axis. There is also evidence that the respiratory microbiome varies with asthma phenotype, endotype and disease severity (Campbell *et al.* 2023).

There is the hygiene hypothesis according to which the development of asthma is favored by the lack of exposure to microorganisms. A correlation between increasing incidence of allergic diseases and at the same time decreasing incidence of infectious diseases, driven by vaccines, increased use of antibiotics and improved hygiene and urbanization has been observed in western industrial countries (Bach 2002, van Tilburg Bernardes *et al.* 2017).
Furthermore, genetic risk factors can also play an important role in the development of asthma. Today, for several candidate genes in every chromosome an association with asthma has been identified (Bijanzadeh *et al.* 2011, Ntontsi *et al.* 2021). Studies revealed for example, that asthma risk alleles positively correlate with orosomucoid-like 3 (ORMDL3) which affects the serum ICAM-1 (intracellular cell adhesion molecule-1), known for regulating leukocyte recruitment from circulation to sites of inflammation and is significantly associated with asthma (Bijanzadeh *et al.* 2009, Bui *et al.* 2020).

The prevention of asthma is therefore an important strategy to reduce the incidence of the disease. Studies suggested that the intake of vitamin D or fish oil during pregnancy could decrease the risk of wheezing in pre-school children. Further, the ban of smoking in enclosed public places significantly reduced hospital admission rates for asthma (von Mutius *et al.* 2020). Microbial interventions with prebiotics and probiotics are also coming into focus.

In contrast to protective effects of microbial factors, viral upper respiratory tract infections with human rhinoviruses (RV), respiratory syncytial virus (RSV), influenza and parainfluenza virus as well as coronaviruses were commonly identified as the main cause of asthma (Busse *et al.* 2010). Viral replication in the respiratory tract can cause damage in epithelial cells and thereby destroy the first line of defense against other pathogens as well as allergens (Veerapandian *et al.* 2018). RV strain-specific antibody levels were associated with the severity of symptoms related to asthma in children 4 to 6 years of age (Megremis *et al.* 2018) and several studies have reported an association between RSV and school-age asthma (Jartti *et al.* 2020). Mechanistically, however, many questions remain unanswered as to how viral

infections affect existing asthma, the development of asthma or the inflammatory phenotype in allergic asthma.

### 1.1.2 Mouse models of allergic asthma

The development of animal models for studying allergic asthma has received a lot of research attention. Animal models are of crucial importance for the analysis of the pathomechanisms underlying allergic diseases as well as the identification of strategies for prophylaxis and novel therapeutic targets. At the same time, transferability to clinical allergic asthma is limited due to the complexity of AAI on the one hand and differences between experimental animals and humans on the other hand.

Pathomechanisms of AAI have been studied in several species including mice (Nials *et al.* 2008), rats (Motta *et al.* 2004), guinea pigs (Toward *et al.* 2004), rabbits (Gascoigne *et al.* 2003), ferrets (Aoki *et al.* 2000), dogs (Barrett *et al.* 2003), sheep (Bischof *et al.* 2003) and non-human primates (Ayanoglu *et al.* 2011). Most species besides humans, cats and horses however, do not spontaneously develop asthma (Bates *et al.* 2009).

Mice are the most frequently used animals due to several advantages, such as easy housing and breeding, relatively short generation times and the availability of many genetic variants and research reagents. Mouse models of acute allergic asthma have successfully reproduced features of human allergic asthma such as high levels of IgE, eosinophilic airway inflammation, goblet cell hyperplasia and airway hyper-responsiveness (AHR) (Aun *et al.* 2017). Multiple mouse models of AAI have been described in the literature and multiple important contributions to our understanding of the pathophysiology of allergic asthma, such as many disease mediators, have been identified in these models (Nials *et al.* 2008).

There are no clear implications as to which mouse model is best suited for which scientific question related to allergic asthma. While a number of studies reported that not all mouse strains show similar effects with respect to AAI, the most common mouse strains used in this

context are BALB/c and C57BL/6. While BALB/c mice are IgE-high/Th2 immune responders, C57BL/6 mice are described as IgE-low/Th1 immune responders (Bousquet *et al.* 2000, Herz *et al.* 2004, McMillan *et al.* 2004). At the same time, more genetic strains, such as gene-specific knock-out strains, are available on the C57/BL6 background.

Next to different mouse strains, the choice of the allergen must be considered. The most commonly used antigen to induce AAI in mice is chicken ovalbumin (OVA), although it does not display a frequent allergen in humans. OVA is inexpensive, can easily be produced in high quantity and various research reagents and genetically modified mouse strains, such as T cell receptor transgenic mice, are available. Typically, in treatment protocols for OVA-AAI, mice are sensitized together with the adjuvant aluminum hydroxide (alum) *via* intraperitoneal (*i.p.*), intradermal or subcutaneous injections. This OVA-specific sensitization is followed by an airway OVA-challenge, in which OVA is administered several times intranasally (*i.n.*), intratracheally (*i.t.*) or aerosolized (Kumar *et al.* 2008). The most common method for the application of the allergen challenge is *i.n.*, because the administered allergen dose can be precisely controlled (Sjöberg *et al.* 2017, Khumalo *et al.* 2020). While OVA as a model-antigen harbors numerous advantages, mice also can develop tolerance against OVA after repeated exposure (Fröde *et al.* 2005, Aun *et al.* 2017).

There are alternative acute models of allergic asthma using naturally occurring allergens such as house dust mite (HDM). Here, sensitization takes place *via* the pulmonary route without the need of any adjuvant (Jacquet 2011). Commonly used HDM extract consists of *Dermatophagoides pteronyssinus* (Der p) or *D. farinae* (Der f) with Der p being the most widespread one. Its mite allergen Der p 1 has been identified as being able to induce inflammatory cytokine release and to stimulate pulmonary inflammation as well as Th2 cell and IgE humoral responses (Doras *et al.* 2018). Its intrinsic enzymatic activity and immunogenicity makes HDM a suited allergen to study AAI in mice (Aun *et al.* 2017). Mice treated with HDM develop bronchial inflammation, airway remodeling and epithelial damage (Mostafa *et al.* 2022).

Other natural allergens used in animal models for AAI are derived from fungi (*Aspergillus*

*fumigatus*, *Alternaria alternata*), cotton dust, *Ascaris* antigens, cockroach extracts, latex and ragweed (*Hevea brasiliensis*) (Zosky *et al.* 2007).

Approaches using cockroach extracts like from the species *Blatella germanica* have shown, that the protein Bla g 2 is a potent allergen and it can be identified in 60%–80% of patients allergic to domestic cockroaches (Arruda *et al.* 1995).

It is well known, that fungi are among the main allergens in asthmatics. Fungi which are often used for the induction of AAI are *Aspergillus fumigatus* or *Alternaria alternata* (Aun *et al.* 2017). Mice sensitized with *Aspergillus* or *Alternaria* are characterized by developing high levels of eosinophilia, IgE and lung inflammation (Takazono *et al.* 2017).

Ragweeds are flowering plants belonging to the aster family *Asteraceae* and are the main cause of health problems in the sensitized population. Ragweed pollen is responsible for allergic reactions in humans and often occurs seasonally (Taramarcaz *et al.* 2005).

Nonetheless, the allergic inflammation and AHR typically resolve after the last challenge in these mouse models (McMillan *et al.* 2004), while human asthma mostly is a chronic condition.

Taken together, there are large variations in the described animal models of AAI, which differ in host species, allergen and sensitization/challenge protocols. Ultimately, the selection of an appropriate model needs to consider the hypothesis to be investigated. In general, applicability of animal models is limited as they are not able to mimic all features and phenotypes of human asthma. Nevertheless, they harbor a number of advantages as experimental models of AAI: Key immunological and histological processes of AAI can be reproduced and it is possible to investigate pathomechanisms with a wider perspective and in more controlled settings as it would be possible in humans.

## 1.2 Influenza A virus (IAV)

Influenza viruses are subdivided into IAV, influenza B virus and influenza C virus, of which IAV is the most common and pathogenic type (Busse *et al.* 2010). IAV is an RNA virus from the *Orthomyxoviridae* family. It consists of the nucleocapsid with nucleoprotein-associated RNA in eight segments, a lipid membrane and the surface antigens hemagglutinin (HA), neuraminidase (NA) and the matrix proteins 1 and 2 (Hutchinson *et al.* 2013, Yoon *et al.* 2014). Influenza is a contagious viral infection of the respiratory tract occurring seasonally mostly in the winter, depending on the climatic and geographical situations (Bridges *et al.* 2003). IAV infection manifests with fever, headache, weakness, red eyes, sore throat, dry cough and nasal discharge and can cause severe or life-threatening complications (Nakagawa *et al.* 2017, Clohisey *et al.* 2019).

Secondary bacterial infections, e.g. with *Streptococcus pneumonia* or *Staphylococcus aureus* (*S. aureus*), can lead to a higher morbidity and mortality in IAV patients. Influenza damages the airway and lung epithelium and tissue and thus promotes bacterial colonization, which can favor the development of a bacterial superinfection (Mikušová *et al.* 2022). Further, IAV infection modulates antibacterial defense by affecting various immune mechanisms in the lung (Rynda-Apple *et al.* 2015).

### 1.2.1 The immune response to IAV and pathomechanisms of IAV infection

Seasonal influenza is transmitted *via* droplets dispersed into the air by infected people. From infection to illness, the incubation period is about 2 days (WHO). IAV infections range from a mild upper respiratory tract infection to severe lower respiratory tract infection (Peteranderl *et al.* 2016). IAV primarily replicates in the respiratory epithelium (Kalil *et al.* 2019). After entering the host, the HA receptor-binding site of the virus attaches to the cell surface (Gamblin *et al.* 2010). The HA-mediated binding to the receptor triggers endocytosis of the virion (Dou *et al.* 2018). IAV is recognized by the innate immune system through pattern

recognition receptors (PRRs). PRR are predominantly expressed on cell membranes as well as in the cytoplasm of cells of the immune system (Żeromski *et al.* 2020). The PRRs that recognize IAV belong to the classes of toll-like receptors (TLRs), nod-like receptors (NLRs) and retinoic acid induced gene 1 (RIG-I) like receptors, with RIG-I being one of the main receptor to recognize the intracellular single-stranded RNA (ssRNA) of IAV (Chen *et al.* 2018). The activation of host cells by PRR ligation is followed by a pro-inflammatory response (Akira *et al.* 2006, Berri *et al.* 2014). The activation of specific transcription factors results in the initiation of interferons (IFN). Type I and type III IFNs play an important role in the antiviral response (Chen *et al.* 2018). The production of cytokines results in the activation and recruitment of leukocytes into the lungs, which in turn release further cytokines in a positive-feedback loop. In some cases, excessive levels of these signaling molecules are produced, leading to a "cytokine storm" (Tscherne *et al.* 2011, Walsh *et al.* 2011). Furthermore, there is a correlation between the production of cytokines and the recruitment of neutrophils, macrophages, B and T lymphocytes to the lung, that are responsible for viral clearance and at the same time can lead to tissue damage (Li *et al.* 2015) (figure 3, p. 15).

In order for IAV to replicate successfully in the host, the pathogen requires several mechanisms that prevent it from being recognized and cleared.

Frequent point mutations and the possibility for whole gene segment recombination in IAV lead to antigenic drift and antigenic shift, respectively. These have resulted in highly pathogenic strains, e.g. H1N1 which is to date the most lethal one (Palese *et al.* 2011). Next to changes in surface proteins that compromise recognition by immunological memory, IAV produces various proteins that target the IFN signaling pathway and drive successful infection. The most potent inhibitor of the IFN signaling pathway is the nonstructural protein 1 (NS1), which interacts with cellular proteins *via* different mechanisms and inhibits the activation of IFN-I (Rashid *et al.* 2023).

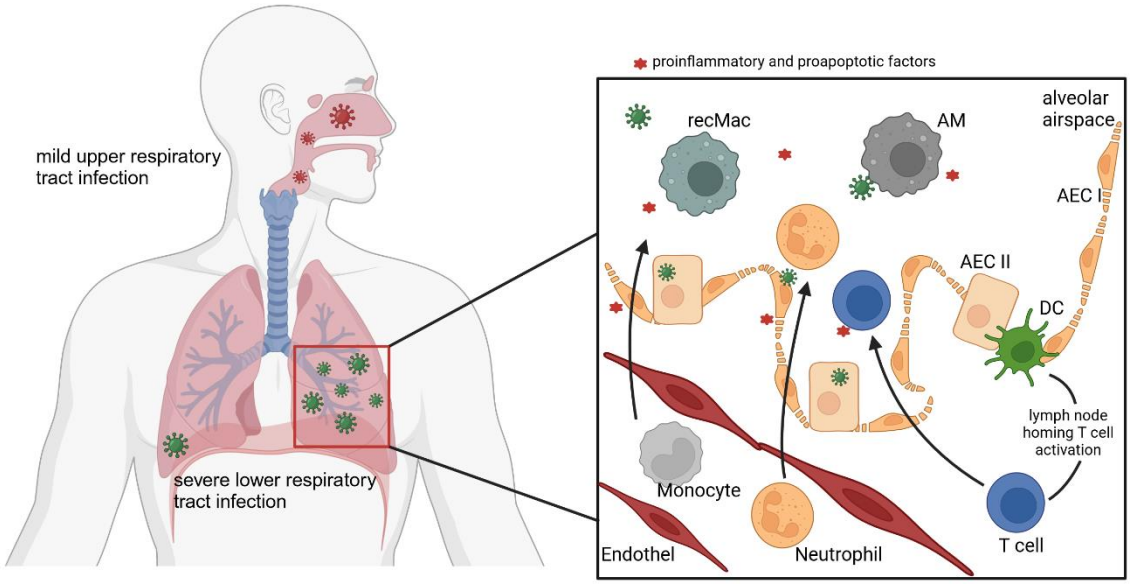


**figure 3: Key players in IAV-induced lung injury.** (adapted from Peteranderl *et al.* 2016)
In severe IAV infection, the virus spreads to the lower respiratory tract. Here, resident alveolar macrophages (AM) and dendritic cells (DC) sense IAV infection of alveolar epithelial type I (AECI) and type II (AECII) cells. Cytokine release in the alveolar lumen leads to the recruitment of monocyte-derived macrophages (recMac) as well as neutrophils from the blood vessels to the site of infection. DC migration further induces generation of antigen-specific T cells. Created with BioRender.com.

### 1.2.2 Mouse models of IAV infection

*Ex vivo* systems for the investigation of viral infections cannot replace the complexity required for the characterization of the immune response to infection or vaccination. For studying viral infections, different animal models can be found in the literature. The most commonly used animal models for influenza research are mouse and ferret models. Although they are not a natural host, mice can be experimentally infected with a variety of human influenza viruses, some of which have been adapted to mice *via* several passages. For this purpose, the wild-type mouse strains C57/BL6 and BALB/c were mainly used, which show innate and adaptive immune responses similar to those observed in humans (Bodewes *et al.* 2010). Clinical signs of acute IAV infection in mice are lethargy, anorexia, weight loss and occasionally paralysis

(Roubidoux *et al.* 2021). Mouse-adapted virus strains used in experimental mouse models include A/Puerto Rico/8/1934 (PR8), A/WSN/1933 (WSN) and B/Lee/1940. Upon infection, mice can display a sublethal or lethal infection, depending on the viral strain and dose (Thangavel *et al.* 2014).

### 1.2.3 Long-term effects of IAV infection on the host

During influenza infection, epithelial and immune cells in the upper and possibly the lower respiratory tract are targeted, resulting in inflammation (Yu *et al.* 2011, Ong *et al.* 2019). In healthy individuals, the infection is usually resolved within seven days (Ghebrehewet *et al.* 2016). However, IAV can infect the lower respiratory tract, leading to alveolar damage, necrosis of the alveolar epithelium and acute respiratory distress syndrome (ARDS) or even death (Ong *et al.* 2019). Pro-inflammatory and anti-inflammatory mechanisms following infection need to be balanced, to facilitate viral clearance with minimal damage to the host tissue (Rouse *et al.* 2010).

There is limited research investigating the long-lasting effects of IAV infection on respiratory physiology and immunology as well as their potential consequences for underlying or secondary inflammatory conditions. Kanegai *et al*. described in a mouse model extensive regions of kreatin 5 pods after infection with a sublethal dose of IAV PR8, which persist up to 200 days after infection (Kanegai *et al.* 2016). Kreatin 5-positive stem cells proliferated and formed epithelial pods in response to the infection with IAV PR8, subsequently contributing to alveolar epithelial regeneration and lung repair (Zuo *et al.* 2015). Keeler *et al*. showed that IAV replicated up to $10^6$-fold in the lung of infected mice, that chronic lung disease persisted for at least 26 weeks after infection and that IAV-specific RNA was detectable 105 days after infection. Further, they found that IL-13 production was linked to chronic lung disease after IAV infection (Keeler *et al.* 2018). In another study, an increase in alveolar macrophages (AM) was observed in the lung 28 days after IAV infection and this AM population provided

prolonged antibacterial protection mediated by IL-6 (Aegerter *et al.* 2020).

Previous work from our research group in the context of secondary bacterial infection had shown that sublethal IAV infection histologically affected the lungs and impaired the respiratory immune system over long periods of time (21 days) after infection, which in turn modulated antibacterial responses. Histologically, inflammatory lesions were observed that were characterized by an attenuation of the bronchial epithelium and an infiltration of neutrophils and macrophages within the alveoli (Sharma-Chawla *et al.* 2016). Furthermore, Wu *et al*. showed in a follow-up study that IAV infection resulted in persisting changes in the pulmonary immune cell composition over 39 days in the same mouse model. Here, moderate to severe bronchointerstitial pneumonia was detected histologically. At the same time, there was a significant increase of T cells and DC in BAL and increased B cell and macrophage numbers in the lung (Wu *et al.* 2020).

Persistent effects after IAV infections have also been observed in humans (Xie *et al.,* 2024). After ARDS caused by the H1N1 virus, a restrictive pattern was observed lung functionally after six months, but the diffuse ground-glass pattern on computed tomography (CT) improved after this time (Toufen *et al.* 2011). However, even one year after hospital discharge of H1N1 patients, mild to moderate pulmonary dysfunction was observed in the majority of patients (Liu *et al.* 2015). Similarly, survivors of severe influenza A (H7N9) showed interstitial changes and fibrosis on computed tomography six months after discharge from the hospital. Restrictive and obstructive ventilatory dysfunction persisted during a two-year follow-up (Chen *et al.* 2017).

However, there is still a lack of detailed data on the long-term effects of IAV infection on the respiratory tract and especially on the local immune system. Equally important, our understanding of the consequences of such IAV-mediated changes for late secondary inflammatory responses and the underlying mechanisms remains incomplete.

### 1.2.4 Interactions between IAV and allergic asthma

IAV has a long-term effect on the respiratory immune system (see 1.2.3). In addition to secondary infections, this can presumably also have an effect on non-infectious inflammatory processes. Although it is known that respiratory viruses such as RS viruses and RV can promote and exacerbate asthma, less is known about the links between asthma and influenza. The realization that asthma was a risk factor associated with hospitalization during the 2009 influenza pandemic raised awareness of the poor prognosis of the combination of both diseases (Skarbinski *et al.* 2011). Due to the high prevalence of asthma and respiratory viral infections, it is very likely for asthmatics to be infected with respiratory viruses, including IAV. An estimated 5 to 25 % of the German population are infected during the annual influenza season (influenza A, B and C) (RKI). Due to these considerations, also from clinical point of view, it is important to understand respiratory inflammatory responses in the context of the resolution of IAV infection and allergic asthma.

Both, IAV infection and allergic asthma are common respiratory diseases that can affect people of all ages. For this reason, the potential immunological interactions between IAV infections and allergic asthma needs further studies. While difficult to systematically address in patients, animal experiments found that influenza infection led to the accumulation of lung mast cells through the recruitment and maturation of bone marrow-derived mast cell progenitors in mice (Zarnegar *et al.* 2017). In a preceding study of the group, attenuated Th2 cell recruitment and pro-inflammatory cytokine responses were observed upon induction of OVA-AAI from 14 days after IAV infection compared to OVA-AAI alone (Wu *et al.* 2020). There is limited understanding however long-lasting effects of resolved IAV infection mechanistically affects subsequently developed AAI, which was a focus in this work.

## 1.3 Macrophages and dendritic cells in the lung

Macrophages of the innate immune system are found in almost all organs of the body, fulfilling specific functions in each organ. Lung macrophages have a high self-renewing capacity and colonize the lung during embryogenesis (Geissmann *et al.* 2010, Mass *et al.* 2016). The lung is constantly exposed to the environment *via* the breathing air and thus to many environmental factors including microorganisms. Macrophages provide a first line of defense against these microorganisms and are essential for the control of common respiratory infections (Arango Duque *et al.* 2014). In steady state, these cells are normally at rest, but can be activated by a variety of stimuli in the course of an immune response or an inflammatory process. After recognition and engulfing of microbes, macrophages present microbial antigens at the outer surface, where they will be recognized by T helper cells. Following this recognition, they release cytokines leading to the activation of B cells. These B lymphocytes further secrete antigen-specific antibodies (Arango Duque *et al.* 2014).
DC are also master regulators of the immune response and harbor the ability to capture even small amounts of antigen for presentation (Mellman 2013). Their main functions include inducing innate inflammatory responses to pathogens, priming naïve T cells, activating memory T cells and promoting B cell activation (Price *et al.* 2015). Thereby, DC efficiently bridge the innate and the adaptive immune system.

As they are both APC, macrophages and DC have been shown to cooperate and there is evidence that macrophages transfer phagocytosed antigens to DC for effective antigen presentation to enhance T cell activation (Xu *et al.* 2016). For both cell types, various subpopulations with specific tissue localization and functions have been and are still being described. Here, marker expression and cellular function can differ between mouse models and humans.

### 1.3.1 Lung macrophages in mice

Resident macrophages in the respiratory mucosa have been extensively studied over the past decades, revealing that these cells play a critical role in maintaining and restoring tissue immune homeostasis (Zaslona *et al.* 2014, Britt *et al.* 2023). The lung harbors two distinct macrophage populations: alveolar macrophages (AM) and interstitial macrophages (IM), with IM dividing into several subsets (Chakarov *et al.* 2019). AM are phagocytes usually located in the lower respiratory tract, where they fulfill different functions: the initiation of inflammation through the release of IL-1 and TNF-α, the control of inflammation through the release of inhibitors such as IL-1-receptor antagonists or soluble TNF-α receptors as well as the production of anti-inflammatory IL-10. Further, they secrete bactericidal molecules and metalloelastases, collagenases and metalloproteases (Hussell *et al.* 2014). IM are regulatory cells, which are typically located in the interstitium of the lung tissue along with DC and lymphocytes and are classified mainly based on their phenotype (Chakarov *et al.* 2019). IM can be divided into $CD11c^+$ and $CD11b^-$ IM, which are both negative for CD169. Both IM subsets are able to present antigen and stimulate the proliferation of $CD4^+$ T cells *in vitro* (Chakarov *et al.* 2019).

Over the last years, substantial research has focused on the role of macrophages during inflammation. Nonetheless, the functions of the different macrophage subpopulations in infection or inflammatory conditions is still limited. Moreover, several new macrophage populations in the lung have recently been defined, e.g. nerve- and airway-associated macrophages (NAM) (Ural *et al.* 2020) or bronchus-associated macrophages (BAM) (Tang *et al.* 2022). NAM are defined as a subset of IM that express CD169 and are morphologically and transcriptionally distinct from AM. Furthermore, NAM are lung-resident, self-renewable and yolk-sac derived, harbor regulatory functions and are primarily localized around the large bronchiolar airways adjacent to airway-associated nerves (Ural *et al.* 2020). Even though they have been well characterized by Ural *et al*., their function next to regulating inflammation in acute IAV infection remains largely unknown.

Next to resident macrophages, monocyte-derived recruited macrophages (recMac) accumulate in the lung during inflammation. RecMac are CD11b$^{+}$, MHCII$^{+}$ and CD64$^{+}$ but do not co-express MerTK and CD64, distinguishing them from AM and IM (for gating see figure 7, p. 46).

Macrophages express a variety of receptor glycoproteins and plasma membrane antigens on their surface, e.g. CD64 and CX3CR1, to recognize and respond to host, microbial and exogenous ligands in their environment (Gordon *et al.* 2020). MHCII is required for antigen-presentation, regulation of immune responses and is expressed on the surface of macrophages (Ye *et al.* 2003).

The classification of the individual subpopulations of macrophages in the lung is complex as the phenotype of macrophages differs between homoeostasis and inflammation and transitions can be dynamic (figure 4).

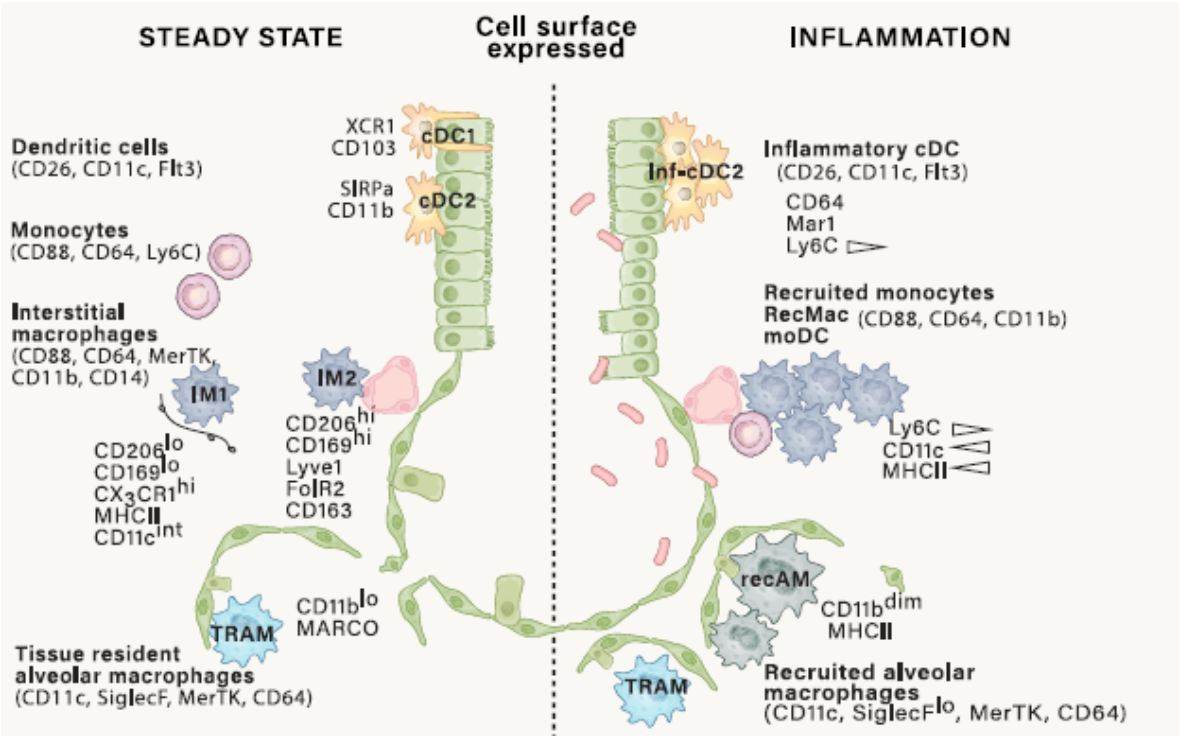

**figure 4: Cell surface proteins for the identification of mononuclear phagocytes in the mouse lung.** (taken from Aegerter *et al.* 2022)
$CD45^+$ mononuclear phagocytes represented in the figure show varying surface expression of CD11c and CD11b. Prior to defining mononuclear phagocyte cell types using protein-based approaches such as flow cytometry, other immune cell types need to be excluded using lineage markers expressed on lymphoid cells (NK1.1, CD19, and CD3), neutrophils (Ly6G) and eosinophils ($SiglecF^+$, $SSC^{hi}$, $CD11c^-$, $CD64^-$). CD88 versus CD26 distinguishes monocytes and macrophages from cDC. Activated monocytes and macrophages demonstrate high CD88 expression. AM and IM highly express MerTK and CD64 compared with recently recruited monocytes, which show low expression of MerTK, CD64 and F4/80 and varying surface expression of MHCII, CD11c and Ly6C. Ly6C expression on recruited monocytes is lost over time. IM express CD206 to a high and intermediate degree, as do cDC2s, recruited monocytes and macrophages.

### 1.3.2 Lung dendritic cells in mice

As for macrophages, DC can be divided into several subpopulations with specific functions, depending on their location (Merad *et al.* 2013). DC are critical immune cells at barrier organs, including the lung, where they play a crucial role in the initiation and regulation of adaptive immune responses against infections or commensals, among others. DC also play an important role in inducing Th2 immunity toward inhaled allergens (van Helden *et al.* 2013). DC are found throughout the lung tissue and under the epithelial layer. In response to PRR ligands, DC can rapidly produce high concentrations of proinflammatory cytokines such as IL-12, TNF-α and IL-6, thereby shaping the character of the local inflammatory environment (Mettelman *et al.* 2022).

In the murine lung, conventional DC (cDC) can be divided into $CD103^+$ and $CD11b^+$ DC (Helft *et al.* 2010). During inflammation, monocytes can differentiate into monocyte-derived DC (Vroman *et al.* 2017). In mice, cDC are reported to be essential for the migration and induction of differentiation of Th2 cells in the lung draining lymph nodes upon allergen exposure (Vroman *et al.* 2017). $CD11b^+$ cDC2 cells are thought to be key in the induction of AAI. In contrast, the role of $CD103^+$ cDC1 is less well known and their function in AAI is discussed. Available reports show conflicting data with respect to whether $CD103^+$ DC accumulate in the lung in AAI and promote or alleviate inflammation (Lajiness *et al.* 2023).

## 1.4 Aims of the study

Respiratory infections can be a trigger for developing asthma. Further, they can severely and sustainably affect local immunity. Associations between respiratory infections, their impact on local inflammatory responses and allergic asthma are of high clinical relevance, but are not well understood up to date. IAV is an acute viral respiratory infection that affects all ages and can cause mild to severe illness that can lead to death (CDC). The role of IAV infection in asthma development is unclear, and in recent years, it has been shown in mouse models to both potentially protect against or display a relevant driver of allergic inflammation in the respiratory tract.

The network of respiratory macrophages and DC as well as their involvement in respiratory inflammation of various etiologies is complex and numerous questions remain unanswered. Continuously, novel cellular subsets are being described and refined approaches for their analysis develop. Based on previous observations, this study aimed at extending the existing knowledge regarding the immunomodulatory effects of IAV on subsequently induced AAI with a focus on specialized subsets of macrophages and DC in the lung. Considering heterogeneity of allergic asthma in patients and addressing the question, whether such modulation would be generally IAV-associated or possibly model-specific with respect the allergic inflammation, two common models of AAI were analyzed. OVA-AAI induced through peripheral sensitization against the model-antigen OVA and subsequent airway challenge and HDM-AAI induced through repeated respiratory application of the natural allergen HDM were compared. A prerequisite for the analysis of IAV-mediated modulation of AAI in these two models was their characterization with respect to the target parameters, i.e. involvement of respiratory macrophages and DC. The main hypothesis followed in this thesis was, that IAV has long-lasting effects on lung macrophages and DC that relate to alterations in their accumulation and functional marker expression as well as otherwise modulated inflammation in AAI.

To address this hypothesis, the following specific aims were defined:

Aim 1: Establishing a staining panel for the analysis of lung macrophage and DC subsets (surface markers for identification and functional marker expression) next to key cellular mediators of respiratory inflammation by spectral flow cytometry. Subsequent application of the developed spectral flow cytometry approach in the comprehensive characterization of the involvement of lung macrophages and DC in OVA-AAI and HDM-AAI together with key parameters of AAI.

Aim 2: Elucidating the long-term effects of sublethal IAV infection on the local immune environment of the respiratory tract with a focus on lung macrophage and DC subsets.

Aim 3: Comprehensive analysis of the effects of a previous IAV infection on subsequently induced AAI with a focus on lung macrophage and DC subsets as well as key inflammatory markers of AAI.

# 2 Material

## 2.1 Consumables

**table 1: Consumables**

| Product | Cat.-number | Manufacturer |
|---|---|---|
| **cover film ROTILABO®** | 0954.1 | Carl Roth, Karlsruhe |
| **cannula Sterican (26G) ®** | 260091 | B. Braun Melsungen AG, Melsungen |
| **cell strainer** | | |
| **70 µm** | 542070 | Greiner Bio-One International |
| **100 µm** | 542000 | GmbH, Austria |
| **centrifuge tubes** | | |
| **15 ml** | 188271 | Greiner Bio-One International |
| **50 ml** | 227261 | GmbH, Austria |
| **FACS tubes** | 1010270 | Corning Inc., New York, USA |
| **glass capillary (20µl)** | 1041816 | Sarstedt, Nümbrecht |
| **homogenization tubes** | 60.506.001 | Sarstedt, Nümbrecht |
| **Immuno 96-well-plate** | 439454 | Fisher Scientific GmbH, Schwerte |
| **pasteur pipettes** | 8.611.171.010 | Sarstedt, Nümbrecht |
| **petri dish** | 1020586 | Paul Boettger GmbH & Co. KG, Bodenmais |
| **pipette tips** | 70.1116 | Sarstedt, Nümbrecht |
| | 70.760.012 | |
| | 70.762.010 | |
| **reaction tubes** | | |
| **0.5 ml** | 1029140 | |
| **1.5 ml** | 1012830 | Eppendorf AG, Hamburg |
| **2 ml** | 1025401 | |
| **5 ml** | 1037782 | |
| **serological pipettes** | | |
| **5 ml** | 4487 | Corning Inc., New York, USA |
| **10 ml** | 4100 | Corning Inc., New York, USA |
| **25 ml** | 94024 | |

| | | |
|---|---|---|
| | | TPP Techno Plastic Products AG, Trasadingen, Switzerland |
| **syringes** | | |
| **Omnifix ® F Solo (1 ml)** | 1020427 | B. Braun Melsungen AG, Melsungen |
| **Omnican ® 100 (1 ml)** | 9151133S | B. Braun Melsungen AG, Melsungen |
| **BD Discardit II (10 ml)** | 03626823 | BD Biosciences, Heidelberg |
| **BD Discardit II (20 ml)** | 07358756 | BD Biosciences, Heidelberg |
| | | |
| **well plates** | | |
| **6-well** | 3516 | Corning Inc., New York, USA |
| **12-well** | 353043 | Corning Inc., New York, USA |
| **24-well** | 3526 | Corning Inc., New York, USA |
| **96-well (round bottom)** | 821.582.001 | Sarstedt, Nümbrecht |

## 2.2 Chemicals and Solutions

**table 2: Chemicals and solutions**

| Product | Cat.-number | Manufacturer |
|---|---|---|
| **albumin from chicken egg white grade III** | A5378-1G | Sigma Aldrich, Missouri, USA |
| **albumin from chicken egg white grade V** | A5503-1G | Sigma Aldrich, Missouri, USA |
| **align check particles** | AE700510 | Sony Biotechnology Inc., California, USA |
| **ammonium acetate ($NH_4OAc$)** | 7869.2 | Carl Roth, Karlsruhe |
| **ammonium chloride ($NH_4Cl$)** | P726.1 | Carl Roth, Karlsruhe |
| **attune Focusing Fluid** | A24904 | Thermo Scientific, Massachusetts, USA |
| **attune shutdown solution** | A24975 | Thermo Scientific, Massachusetts, USA |
| **attune wash solution** | A24974 | Thermo Scientific, Massachusetts, USA |
| **BSA** | K45-001 | GE Healthcare |

| | | |
|---|---|---|
| **buffer RLT** | 79216 | QIAGEN GmbH, Hilden |
| **ClearFlow Sheath Fluid** | AE700592 | Sony Biotechnology Inc., California, USA |
| **coating Buffer** | 121125 | CANDOR Bioscience GmbH, Wangen |
| **collagenase D** | COLLD-RO | Roche Diagnostics, Mannheim |
| **cOmplete™ ULTRA tablets, EDTA free** | 05892791001 | Roche Diagnostics, Mannheim |
| **desoxyribunuclease (DNAse)** | D4527-10KU | QIAGEN GmbH, Hilden |
| **dimethyl sulfoxide (DMSO)** | A994.1 | Carl Roth, Karlsruhe |
| **DEPC-treated water** | 46-2224 | Thermo Scientific, Massachusetts, USA |
| **ethanol** | 9065.1 | Carl Roth, Karlsruhe |
| **ethylenediamine tetraacetic acid disodium salt ($Na_2$EDTA)** | 8043.1 | Carl Roth, Karlsruhe |
| **fetal bovine serum (FBS)** | P40-47500 | PAN-Biotech GmbH, Aidenbach |
| **house dust mite extract (*D. pteronyssinus*)** | XPB70D3A25 | Stallergenes Greer, Lenoir, USA |
| **Imject™ Alum (40 mg/ml)** | 77161 | Thermo Scientific, Massachusetts, USA |
| **Influenza A Virus PR8/A/34** | | Obtained from R. Enelow (Dartmouth Geisel School of Medicine, Hanover NH, USA), propagated in MDCK cells |
| **Iscove's Modified Dulbecco's Medium (IMDM)** | 21980065 | Thermo Scientific, Massachusetts, USA |
| **isoflurane CP 1ml/ml** | 1214 | CP-Pharma Handelsgesellschaft mbH, Burgdorf |
| **ketamine** | 3048734 | MEDISTAR Arzneimittelvertrieb GmbH, Ascheberg |
| **paraformaldehyde (PFA)** | 0335.1 | Carl Roth, Karlsruhe |
| **Percoll™** | 17-0897-02 | GE Healthcare, Illinois, USA |
| **phenylmethylsulfonyl fluoride (PMSF)** | 93482 | Sigma-Aldrich, St. Louis, Missouri, USA |
| **potassium hydrogen carbonate** | P748.1 | Carl Roth, Karlsruhe |
| **phosphate-buffered saline (PBS) tablets** | 18912014 | Thermo Scientific, Massachusetts, USA |
| **Precision Count Beads ™** | 424902 | Biolegend, San Diego, USA |
| **RNAlater** | 76106 | QIAGEN GmbH, Hilden |
| **sodium azide** | K305.1 | Carl Roth, Karlsruhe |
| **sodium chloride** | 3957.1 | Carl Roth, Karlsruhe |

| | | |
|---|---|---|
| **sodium bicarbonate** | A3590,1000 | AppliChem GmbH, Darmstadt |
| **sodium carbonate** | A135.1 | Carl Roth, Karlsruhe |
| **sulfuric acid (2N)** | X873.1 | Carl Roth, Karlsruhe |
| **tetramethylbenzidine (TMB)** | 555214 | BD Bioscience, Heidelberg |
| **triton X-100** | 3051.2 | Carl Roth, Karlsruhe |
| **tryptan blue** | 15250061 | Thermo Scientific, Massachusetts, USA |
| **Tween20** | 37470.1 | SERVA Electrophoresis GmbH, Heidelberg |
| **UltraComp eBeads compensation beads** | 01-2222-42 | Thermo Fisher Scientific Inc., Massachusetts, USA |
| **xylazine (Rompun®)** | QN05CM92 | Bayer AG, Leverkusen |
| **β-Mercaptoethanol** | 4227.1 | Carl Roth, Karlsruhe |
| **8 Peak Beads** | AE700522 | Sony Biotechnology Inc., California, USA |

## 2.3 Kits and ancillary reagents

**table 3: Kits and ancillary reagents**

| Product | Cat-.number | Manufacturer |
|---|---|---|
| **LEGENDplex™ Mouse Th Cytokine Panel (12-plex)** | 741043 | Biolegend, San Diego, USA |
| **LEGENDplex™ Mouse Cytokine Panel 2 (13-plex)** | 740134 | Biolegend, San Diego, USA |
| **Linear Polyacrylamide** | J67830.XF | Thermo Fisher Scientific Inc., Massachusetts, USA |
| **RNase-free DNase Set** | 79254 | QIAGEN GmbH, Hilden |
| **RNeasy Mini Kit** | 74104 | QIAGEN GmbH, Hilden |

## 2.4 Technical devices

**table 4: Technical devices**

| Device | Model | Manufacturer |
|---|---|---|
| **autoclave** | Systec V-150 | Systec GmbH, Linde |
| **centrifuge** | Multifuge® 3 S-R/3 L-R, Legend® RT | Kendro Laboratory Products GmbH, Hessen |

| | | |
|---|---|---|
| | Heraeus Fresco 17 Centrifuge | Fisher Scientific GmbH, Schwerte |
| | Centrifuge 5910R | Eppendorf AG, Hamburg |
| **clean bench/bio-safety cabinet** | Thermo Scientific™ Safe 2020 | Fisher Scientific GmbH, Schwerte |
| | Baker SterilGARD® III Advance | The Baker Company, Sanford, Maine, USA |
| **$CO_2$ incubator** | Heracell VIOS 160i 230V SS GS | Fisher Scientific GmbH, Schwerte |
| **disperser** | POLYTRON PT1300D | Kinematica, Schwitzerland |
| **counting chamber** | Neubauer-improved, 0.1 mm | Paul Marienfeld GmbH & Co. KG, Lauda-Königshofen |
| **dissecting tools** | | W.O. Schmidt GmbH, Braunschweig |
| **flow cytometer** | Attune NxT Flow | Thermo Fisher Scientific Inc., Massachusettes, USA |
| **magnetic stirrer** | neoMag | neolab Migge GmbH, Heidelberg |
| **microplate reader** | Infinite M Plex | Tecan Group Ltd., Switzerland |
| **microscope** | Inversmicroskop TCM400 | Labomed, Regensburg |
| **pH meter** | FE20/EL20 | Mettler-Toledo GmbH, Gießen |
| **pipettes** | PIPETMAN Classic | Gilson, Villiers-le-Bel, France |
| | Transferpette | Brandt GmbH + Co. KG, Wertheim |
| | Finnpipette | Fisher Scientific GmbH, Schwerte |
| **pipetting aid** | PIPETBOY acu 2 | INTEGRA Biosciences AG, Schwitzerland |
| **precision scale** | EMB | KERN & SOHN GmbH, Balingen-Frommern |
| **shaker** | neoLab Multi Shaker | neolab Migge GmbH, Heidelberg |
| **shaking incubator** | Corning LSE 71l | Corning Inc., New York, USA |
| **spectral flow cytometer** | ID7000™ | Sony Biotechnology Inc., California, USA |
| **suction pump** | VACUSAFE | INTEGRA Biosciences AG, Schwitzerland |
| **thermomixer** | ThermoMixer® C | Eppendorf AG, Hamburg |

| | | |
|---|---|---|
| **veterinary anesthesia machine** | combi-vet® Base Anesthesia System | Rothacher Medical GmbH, Schwitzerland |
| **vortexer** | neoVortex® Schüttler | neolab Migge GmbH, Heidelberg |
| **water bath** | WNB 7 | Memmert GmbH + Co. KG, Schwabach |

## 2.5 Antibodies

### 2.5.1 Flow cytometry panels

All antibodies listed in the following sections were titrated on murine leukocytes prior to use in order to determine the optimal staining concentration (high signal/background ratio) for the different flow cytometry panels. To assess the viability of cells, the zombie fixable viability stain was used. It is a reactive fluorescent dye that is non-permeant to live cells, but permeant to the cells with compromised membranes.

**table 5: Flow cytometry staining panel 1 (for the analysis of BAL fluid in conventional flow cytometry)**

| Detected antigen | Conjugation | Clone | Manufacturer |
|---|---|---|---|
| **CD4** | FITC | RM4-5 | Biolegend, San Diego, USA |
| **CD11b** | APC/Cy7 | M1/70 | Biolegend, San Diego, USA |
| **CD11c** | APC | N418 | Biolegend, San Diego, USA |
| **CD19** | PerCP/Cy5.5 | 1D2/CD19 | Biolegend, San Diego, USA |
| **CD8a** | PE/Cy7 | 53-6.7 | Biolegend, San Diego, USA |
| **Ly-6G** | AF700 | 1A8 | BD Bioscience, Heidelberg |
| **MHCII** | BV711 | M5/114.15.2 | Biolegend, San Diego, USA |
| **SiglecF** | PE | E50-2440 | Biolegend, San Diego, USA |
| **Zombie fixable viability stain** | Aqua | | Biolegend, San Diego, USA |

**table 6: Flow cytometry staining panel 2 (for macrophage identification in conventional flow cytometry)**

| Detected antigen | Conjugation | Clone | Manufacturer |
|---|---|---|---|
| **CD64** | BV421 | X54-5/7.1 | Biolegend, San Diego, USA |
| **CD45** | BV605 | 30-F11 | Biolegend, San Diego, USA |
| **MHCII** | BV711 | M5/114.15.2 | Biolegend, San Diego, USA |
| **CD200R** | FITC | Ox-110 | Biolegend, San Diego, USA |
| **Ly-6C** | perCP-Cy5.5 | HK1.4 | Biolegend, San Diego, USA |
| **CD169** | PE | 3D6.112 | Biolegend, San Diego, USA |
| **F4/80** | PE-Cy5 | BM8 | Biolegend, San Diego, USA |
| **MerTK** | PE-Cy7 | 2B10C42 | Biolegend, San Diego, USA |
| **CX3CR1** | APC | SA011F11 | Biolegend, San Diego, USA |
| **CD11c** | AF700 | N418 | Biolegend, San Diego, USA |
| **CD11b** | APC-Cy7 | M1/70 | Biolegend, San Diego, USA |
| **Zombie fixable viability stain** | NIR | | Biolegend, San Diego, USA |

**table 7: Flow cytometry staining panel 3 (for the analysis of macrophage, DC and key effectors of AAI by spectral flow cytometry)**

| Detected antigen | Conjugation | Clone | Manufacturer |
|---|---|---|---|
| **CD64** | BV421 | X54-5/7.1 | Biolegend, San Diego, USA |
| **CD8a** | BV510 | 53-6.7 | Biolegend, San Diego, USA |
| **CX3CR1** | BV605 | SA011F11 | Biolegend, San Diego, USA |
| **CD80** | BV650 | 16-10A1 | Biolegend, San Diego, USA |
| **MHCII** | BV711 | M5/114.15.2 | Biolegend, San Diego, USA |
| **Ly6C** | BV785 | HK1.4 | Biolegend, San Diego, USA |
| **CD4** | Kiravia Blue 520 | GK1.5 | Biolegend, San Diego, USA |
| **CD45** | Spark Blue 574 | 30-F11 | Biolegend, San Diego, USA |
| **SiglecF** | perCP-Cy5.5 | S17007L | Biolegend, San Diego, USA |
| **CD86** | PE | A17199A | Biolegend, San Diego, USA |
| **CD11b** | Spark YG593 | M1/70 | Biolegend, San Diego, USA |
| **CD169** | PE/Dazzle 594 | 3D6.112 | Biolegend, San Diego, USA |
| **F4/80** | PE/Fire 640 | QA17A29 | Biolegend, San Diego, USA |
| **CD24** | PE/Cy7 | 30-F1 | Biolegend, San Diego, USA |
| **CD11c** | PE/Fire 810 | QA18A72 | Biolegend, San Diego, USA |
| **MerTK** | APC | 2B10C42 | Biolegend, San Diego, USA |
| **CD103** | AF647 | 2E7 | Biolegend, San Diego, USA |
| **Ly6G** | AF700 | 1A8 | Biolegend, San Diego, USA |
| **Nk1.1** | APC/Fire 810 | S17016D | Biolegend, San Diego, USA |
| **CD19** | APC/Fire 810 | 6D5 | Biolegend, San Diego, USA |

| | | | |
|---|---|---|---|
| **CD3** | APC/Fire 810 | 17A2 | Biolegend, San Diego, USA |
| **Zombie fixable viability stain** | NIR | | Biolegend, San Diego, USA |

In all panels, unspecific antibody binding was blocked with TruStain FcX Plus (anti-mouse CD16/32) from BioLegend, San Diego, USA.

### 2.5.2 ELISA

**table 8: Antibodies and standard for ELISA**

| Antibody | Type | Species | Cat.-number | Manufacturer |
|---|---|---|---|---|
| **Anti-mouse IgE** | Monoclonal capture | Rat | 1130-01 | Southern Biotech |
| **Anti-mouse IgE** | Polyclonal detection, HRP conjugated | Goat | PA1-84764 | Thermo Fisher Scientific Inc., Massachusetts, USA |
| **Anti-mouse albumin** | Polyclonal | Goat | A90-134A | Biomol GmbH, Hamburg |
| **Anti-mouse albumin** | Polyclonal detection, HRP conjugated | Goat | A90-134P | Biomol GmbH, Hamburg |
| **Albumin for standard** | from mouse serum | Mouse | A3559 | Merck KGaA, Darmstadt |

## 2.6 Buffers, media and solutions

**table 9: Solutions**

| Solution | Components |
|---|---|
| **PBS solution**<br>sodium phosphate 10 mM<br>potassium chloride 2.68 mM<br>sodium chloride 140 mM | 1 PBS tablet<br>500 ml ultrapure water |
| **Paraformaldehyde (PFA) (4 %)** | 4 g PFA<br>100 ml PBS |
| **PFA (1 %)** | 3 ml PFA (4 %) |

| | |
|---|---|
| | 7 ml PBS |
| **Percoll solution**<br>**→ in ultrapure water** | 1.5 M NaCl |
| | Percoll (stock solution) |
| **final c NaCl** | 0.15 M |
| **final density (d) Percoll solution** | d = 1.041g/ml |

**table 10: Buffers**

| **Buffer** | **Composition** |
|---|---|
| **Ammonium chloride potassium lysis buffer**<br>**→ in ultrapure water** | 150 mM $NH_4Cl$<br>10 mM $KHCO_3$<br>0.1 mM $Na_2EDTA$ |
| **FACS buffer**<br>**→ in PBS** | 2 % FCS<br>2 mM EDTA<br>0.05 % sodium azide |
| **Homogenization buffer**<br>**→ in PBS** | 0.5 % Triton X-100<br>complete™ ULTRA tablets<br>pH 7.0<br>1 mM PMSF |
| **Coating buffer IgE-ELISA**<br>**→ in 1 L PBS** | 8.4 g $NaHCO_3$<br>3,56 g $Na_2CO_3$<br>pH 9.5 |
| **Wash buffer albumin and IgE-ELISA**<br>**→ in PBS** | 0.05 % Tween20 |
| **Blocking buffer IgE-ELISA**<br>**→ in PBS** | 10 % FCS |

**table 11: Media**

| Medium | Composition |
|---|---|
| **IMDM complete**<br>**→ in IMDM** | 1 % Penicillin/Streptomycin<br>10 % FCS<br>0.25 mM β-Mercaptoethanol |
| **Lung tissue enzymatic digestion medium**<br>**→ in IMDM** | 0.2 mg/ml Collagenase D<br>0.01 mg/ml DNAse<br>5 % FCS |

## 2.7 Software

**table 12: Software**

| Software | Manufacturer |
|---|---|
| **FlowJo** | Tree Star Inc., Ashland, USA |
| **GraphPad Prism 9.0** | GraphPad Software Inc., San Diego, USA |
| **i-controlTM 2.0 (TECAN)** | Tecan Group Ltd., Switzerland |
| **Attune™ NxT Software v3.1.1** | Thermo Fisher Scientific, Massachusetts, USA |
| **Sony ID7000 Software v1.2** | Sony Biotechnology Inc., California USA |
| **LEGENDplex™ Qognit** | BioLegend, San Diego, USA |
| **Python v3.9.18** | Python Software Foundation |

# 3 Methods

Parts of the following methods had previously been established in the research group and reported accordingly (Jorde *et al*., 2020, Wu *et al*., 2020).

## 3.1 Mice

Experiments were performed in female, specific-pathogen free (SPF) C57BL/6JRj mice (Janvier Labs, Saint-Berthevin, France), at an age of 7-8 weeks upon the first treatment. All mice were housed in groups of 3-5 mice in individually ventilated cages and were fed food and water *ad libitum*. All animal experiments were performed according to regional and institutional guidelines and approved by the Landesverwaltungsamt Sachsen-Anhalt (file number: 203.6.3-42502-2-1495).

## 3.2 Influenza A virus (IAV) infection

### 3.2.1 Preparation of IAV-stock inoculum and intranasal infection

For mouse infections, a Madin-Darby canine kidney (MDCK)-cell derived IAV stock solution (Stegemann *et al.* 2009) stored at -80 °C was freshly diluted in PBS: 10 µl of the stock solution were serially diluted until a dilution of 1:25,000, resulting in a dose of 0.31 $TCID_{50}$ (50 % tissue culture infectious dose) IAV in 25 µl PBS.

Mice were intranasally (*i.n*.) infected with IAV under light isoflurane anesthesia or anesthesia by intraperitoneal (*i.p*.) injection of ketamine/xylazine. For isoflurane anesthesia induction with the combi-vet® Base Anesthesia System, mice were placed in an anesthesia induction chamber, where they were anesthetized through inhalation of 5 % isoflurane supplemented with oxygen at a flow rate of 1 liter/minute in ambient air. After the induction of anesthesia, the isoflurane concentration was reduced to 2-3 %. Anesthetized animals were held in an upright position and 25 µl diluted IAV were dropwise pipetted alternately on both nostrils. After treatment, mice were kept in upright position to ensure uptake of the virus solution.

Afterwards, mice were returned to their cage and monitored until fully awake. Control mice were *i.n*. treated with 25 µl sterile PBS.

## 3.3 Ovalbumin (OVA)-mediated mouse model of allergic airway inflammation (AAI)

### 3.3.1 Preparation of OVA-stocks

OVA-stocks for grade III OVA (≥ 90 % purity) and grade V OVA (≥ 98 % purity) were prepared in PBS. Lyophilized OVA was dissolved in sterile PBS. For grade III OVA, a stock concentration of 10 mg/ml was prepared, grade V OVA was prepared likewise with a stock-concentration of 500 ng/ml. OVA-stocks were stored at -20 °C until further use.

### 3.3.2 Intraperitoneal OVA-sensitization

Mice were sensitized intraperitoneally (*i.p*.) with 10 µg OVA (grade V) in PBS containing 1 mg of the adjuvant aluminum hydroxide (40 mg/ml) (Imject™ Alum Adjuvant). For each sensitization, the OVA/aluminum hydroxide solution was freshly prepared. For each mouse, 20 µl OVA-stock (500 µg/ml; see above) were pipetted into 135 ml sterile PBS and 25 µl Imject™ Alum Adjuvant were added dropwise. The OVA/aluminum hydroxide solution was incubated for 30 minutes at room temperature on a shaker (100 rpm). Mice were sensitized *i.p.* (180 µl/mouse) three times in weekly intervals. Control animals were *i.p.* treated with 180 µl PBS containing 1 mg aluminum hydroxide (165 µl PBS + 25 µl Imject™ Alum adjuvant).

### 3.3.3 Intranasal OVA-challenge

One week after the last sensitization, mice were *i.n*. challenged under light isoflurane anesthesia on three consecutive days. For anesthesia induction, the combi-vet® Base Anesthesia System was used as described in 3.2.1. Anesthetized mice were removed from the induction chamber one by one, held in an upright position and 30 µl PBS containing 100 µg OVA (10 µl OVA-stock solution (grade III, 10 mg/ml) + 20 µl sterile PBS) were pipetted dropwise alternately on both nostrils. The solution was freshly prepared before each challenge. After *i.n*. challenge, mice were kept in upright position to ensure inhalation of the entire fluid. Subsequently, mice were returned to their cage and monitored until fully awake. Forty-eight hours after the last challenge, mice were sacrificed for analysis.

## 3.4 House dust mite (HDM)-mediated mouse model of allergic airway inflammation (AAI)

### 3.4.1 Preparation of HDM-stocks

HDM-stocks were prepared in PBS. HDM extract (159.70 mg dry weight, 29.15 mg protein/vial; Stallergenes Greer, Lenoir, USA) was dissolved in sterile PBS, so that a stock concentration of 100 µg protein/50 µl was achieved. HDM-stocks were aliquoted and stored at -20 °C until further use. For all experiments, the same batch of HDM extract was used.

### 3.4.2 Intranasal HDM-treatment

Mice were treated *i.n*. with 50 µl HDM three times in weekly intervals under light isoflurane anesthesia. For anesthesia induction, the combi-vet® Base Anesthesia System was used as described in 3.2.1. Anesthetized mice were removed from the induction chamber one by one, held in an upright position and 50 µl HDM-solution containing 100 µg HDM protein (HDM-

stock, freshly thawed) were pipetted dropwise alternately on both nostrils. After treatment, mice were held in upright position until the entire fluid was inhaled. Subsequently, mice were returned to their cage and monitored until fully awake. Control animals were sensitized with 50 µl sterile PBS. Mice were sacrificed for analysis 48 hours after the last treatment.

## 3.5 Health surveillance

All animals were closely monitored for immediate reactions right after *i.p* sensitizations as well as after *i.n*. sensitization/challenge and infection with IAV. During the entire period of the experiments, the well-being of the animals were regularly assessed with the respect to body weight loss, general condition, spontaneous behavior and clinical findings according to a score sheet. The score sheet defined clear termination criteria for all experiments.

## 3.6 Sample preparation

### 3.6.1 Preparation of serum from whole blood

Mice were anaesthetized by *i.p*. injection of ketamine/xylazine. Blood was collected through puncture of the retroorbital plexus and was incubated for 20 minutes at 37 °C and at 4 °C for 5 minutes. Subsequently, the blood was centrifuged for 10 minutes at 1500 x g and 4 °C and the serum was collected. The collected serum was aliquoted and stored at -80 °C until further analysis.

### 3.6.2 Preparation of bronchoalveolar lavage (BAL)

To obtain the bronchoalveolar lavage (BAL), the trachea was first dissected and punctured with a 20G indwelling venous cannula (Braun). Using a 1 ml syringe, the lungs were flushed

once through the cannula and trachea with 1 ml ice-cold sterile PBS and the retrieved volume of BAL fluid was documented for samples used for flow cytometry. After centrifugation of the BAL fluid (10 minutes, 4000 rpm, 4 °C), the supernatant was separated from the cell pellet, centrifuged (10 minutes, 10000 × g, 4 °C) for the removal of debris, aliquoted and stored at -80 °C until further analysis. BAL cells were resuspended in 200 µl ACK lysis buffer (see table 10, p. 33), incubated for 60 seconds and lysis was stopped by adding 1 ml PBS. After centrifugation (10 minutes, 2000 x g, 4 °C), BAL cells were resuspended in 200 µl PBS and analyzed using flow cytometry.

### 3.6.3 Preparation of lung homogenates from whole lung tissue

Lavaged lungs were perfused with 10 ml ice-cold sterile PBS through puncture of the right ventricle, excised and weighed. For homogenization, whole lungs were transferred into 5 ml reaction tubes and 1 ml homogenization buffer/100 mg lung tissue (see table 10, p. 33) was added. Lungs were homogenized on ice using a disperser (30000 rpm) and then centrifuged at 4500 rpm and 4 °C for 10 minutes. The supernatant was aliqouted and stored at -80 °C until further analysis.

## 3.7 Isolation of leukocytes from the lungs and spleens

Mouse tissues were processed depending on the subsequent analysis.

### 3.7.1 Isolation of leukocytes from lungs and spleens for flow cytometric analysis

After collection of BAL fluid, lavaged lungs were perfused with 10 ml ice-cold sterile PBS through puncture of the right ventricle, excised and minced using scissors on ice. For enzymatic digestion, 3 ml of Iscolve´s modified Dulbecco´s medium containing 0.2 mg/ml Collagenase D (Sigma-Aldrich), 0.01 mg/ml DNase (Sigma-Aldrich) and 5 % fetal calf serum

were added. Samples were incubated at 37 °C for 30 minutes using a water bath and meanwhile shortly mixed in 5-minute intervals using disposable transfer pipettes. Another 2 ml of fresh digestion medium were added and samples were incubated likewise for 15 minutes. After the addition of 60 µl 0.5 M ethylenediaminetetraacetic acid (EDTA) (5 mM final concentration) to stop the enzymatic digestion process, samples rested for 5 minutes. Suspensions were then filtered through a cell strainer (100 µm) and pelleted by centrifugation (10 minutes, 330 × g, 4 °C). For erythrocyte lysis by osmotic shock, the pellets were resuspended in 1 ml ACK-Lysis buffer (see table 10, p. 33) and incubated for 2 minutes. Lysis was stopped by adding 9 ml FACS-buffer (see table 10, p. 33). After centrifugation (10 minutes, 330 × g, 4 °C) of the samples, leukocyte enrichment was performed using a Percoll solution (GE Healthcare Life Sciences, see table 9, p. 32) and density gradient centrifugation (20 minutes, 360 × g, RT, w/o break) by forming Percoll interfaces. After centrifugation, pelleted leukocytes were resuspended in PBS and were used for flow cytometry.

Splenocytes were isolated by homogenization of spleens through a 100 µm cell strainer in PBS using a syringe plunger followed by centrifugation of the cell suspension (5 minutes, 330 × g, 4 °C). Splenocytes were resuspended in 3 ml ACK-Lysis buffer and incubated for 2 minutes. After adding 10 ml FACS-buffer, the cell suspension was filtered through a 100 µm strainer using a syringe plunger. Afterwards, the cells were centrifuged (5 min, 330 × g, 4 °C) and resuspended in 3 ml PBS/spleen cell pellet.

## 3.8 Flow cytometry

Leukocytes from BAL and lungs (see 3.7, p. 39) were incubated on a 96-well plate for blocking of Fc-receptors (anti CD16/CD36) and simultaneously stained with fixable live/dead stain (BioLegend) in PBS for 30 minutes at room temperature in the dark (100 µl volume). After washing the cells using 150 µl FACS-buffer (see table 10, p. 33) they were centrifuged (5 minutes, 1200 rpm, 4 °C) and antibody stainings were performed (see table 5, table 6 and

table 7 above). Cells and antibodies were diluted in FACS-buffer and cells were stained in 100 µl of the respective antibody cocktail. Cells and antibodies were incubated for 15 minutes, 4 °C in the dark and cells were subsequently washed using 150 µl PBS and centrifuged for 5 minutes, 1200 rpm, 4 °C. Cells were fixed by resuspension and incubation in 100 µl paraformaldehyde (1 % in PBS, see table 9, p. 32) for 20 minutes at room temperature in the dark. Following another washing step with 150 µl PBS and centrifugation (5 minutes, 1200 rpm, 4 °C), cells were resuspended in either 350 µl PBS for Attune NxT or 200 µl PBS for Sony ID7000 analysis.

Data were acquired using an Attune NxT instrument (ThermoFisher) or ID7000 spectral flow cytometer (Sony) and analyzed using the FlowJo software (Tree Star). For gating, in each experiment all samples were concatenated. Single stainings were performed for all fluorochromes for compensation using UltraComp eBeads (ThermoFisher) and fluorescence-minus-one stainings were performed on splenocytes for gating. For the calculation of absolute cell numbers from the relative population frequencies of live cells yielded by the flow cytometric analysis, 50000 fluorescent beads (Precision Count Beads, BioLegend) were added prior to antibodies to each sample. Absolute cell numbers were calculated as cells/ml BAL and cells/lung using the factor of the bead input vs. the remaining, acquired fluorescent beads. Following singlet-gating using the forward-scatter (FSC-H/FSC-A) and dead cell exclusion according to the live/dead staining, cell populations were gated as described below for the different staining approaches.

### 3.8.1 Flow cytometry staining panel 1

Flow cytometry staining panel 1 was used for the analysis of BAL cells. Leukocytes from BAL (all isolated cells/mouse; see 3.6.2, p. 38) were stained with flow cytometry staining panel 1 (see table 5, p. 30; Jorde *et al*., 2020). Leukocytes and fluorescent beads (see 3.8) were separately gated. Further, leukocyte doublets were excluded. Live, single cells were gated for

CD11c$^+$, CD11b$^+$/CD11c$^-$ and CD11b$^-$/CD11c$^-$ cells. CD11c$^+$ cells were further divided into macrophages (gated as CD11c$^+$/SiglecF$^+$) and SiglecF$^-$ cells from which DC (CD11c$^+$/SiglecF$^-$/MHCII$^+$) were gated using MHCII as a marker. CD11b$^+$/CD11c$^-$ cells were further gated for the Ly6G and SiglecF markers. Neutrophils were gated as CD11b$^+$/CD11c$^-$/Ly6G$^+$ cells and eosinophils as CD11b$^+$/CD11c$^-$/Ly6G$^-$/SiglecF$^+$ cells. CD4$^+$ T cells were gated as CD11b$^-$/CD11c$^-$/CD8$^-$/CD4$^+$ and CD8$^+$ T cells as CD11b$^-$/CD11c$^-$/CD4$^-$/CD8$^+$ cells.

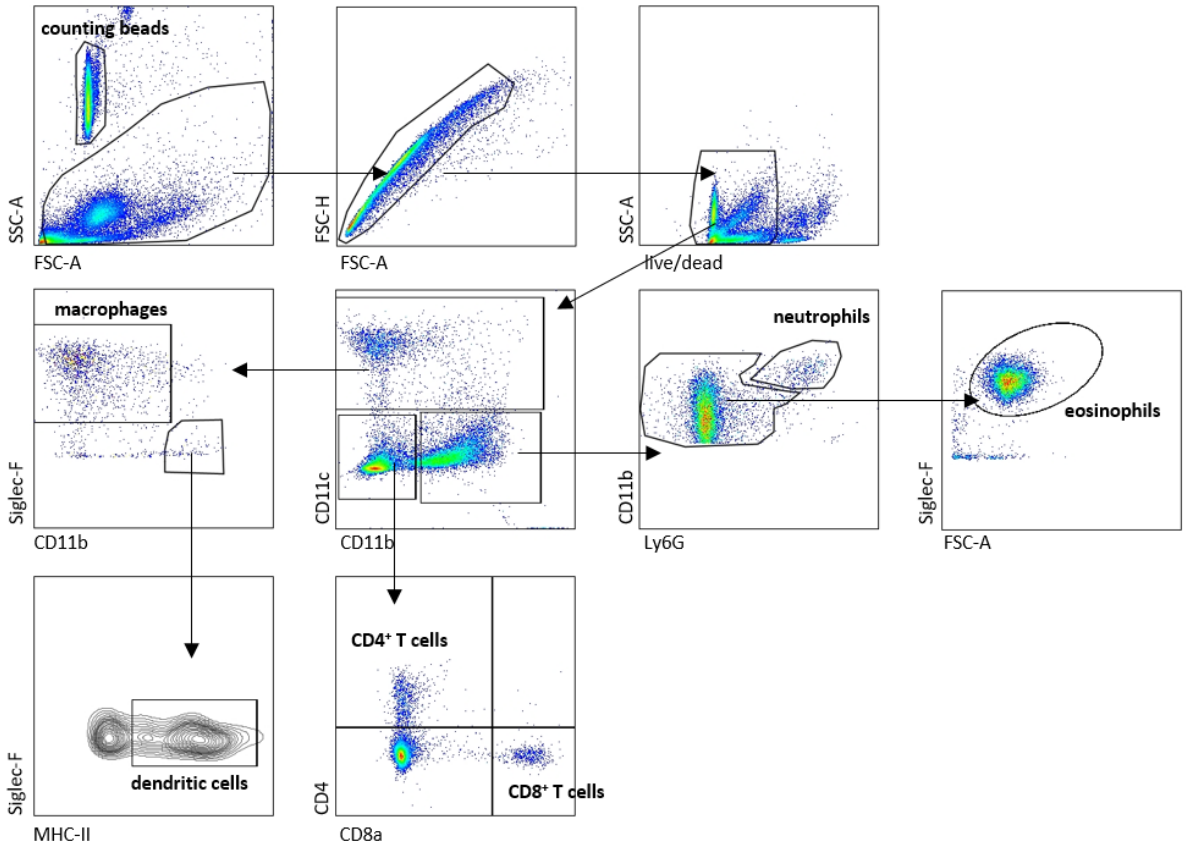


**figure 5: Gating strategy flow cytometry staining panel 1.**
After the exclusion of doublets and dead cells, cells were gated for CD11c$^+$, CD11b$^+$/CD11c$^-$ and CD11b$^-$/CD11c$^-$ cells. CD11c$^+$ cells were further gated for macrophages (CD11c$^+$/SiglecF$^+$) and SiglecF$^-$ cells from which DC (CD11c$^+$/SiglecF$^-$/MHCII$^+$) were gated using MHCII as a marker. CD11b$^+$/CD11c$^-$ cells were further gated for the Ly6G and SiglecF markers. Neutrophils were gated as CD11b$^+$/CD11c$^-$/Ly6G$^+$ cells and eosinophils as CD11b$^+$/CD11c$^-$/Ly6G$^-$/SiglecF$^+$ cells. CD4$^+$ T cells were gated as CD11b$^-$/CD11c$^-$/CD8$^-$/CD4$^+$ and CD8$^+$ T cells as CD11b$^-$/CD11c$^-$/CD4$^-$/CD8$^+$ cells. Displayed here are concatenated samples of all analyzed groups from one representative experiment. Cells were analyzed at an Attune NxT instrument.

### 3.8.2 Flow cytometry staining panel 2

Leukocytes from the lung (complete lungs) (see 3.7, p. 39) were stained with flow cytometry panel 2 (see table **6**, p. 31). Live, single cells were gated for CD45$^+$ cells, which were further gated for MerTK$^+$/CD64$^+$ cells. MerTK$^+$/CD64$^+$ cells were gated for F4/80$^{high}$/Ly6C$^{low}$ cells that were further gated for alveolar macrophages (CD11c$^+$/CD169$^+$) and remaining cells. From those cells, which were not identified as AM, IM (CX3CR1$^+$) were gated.

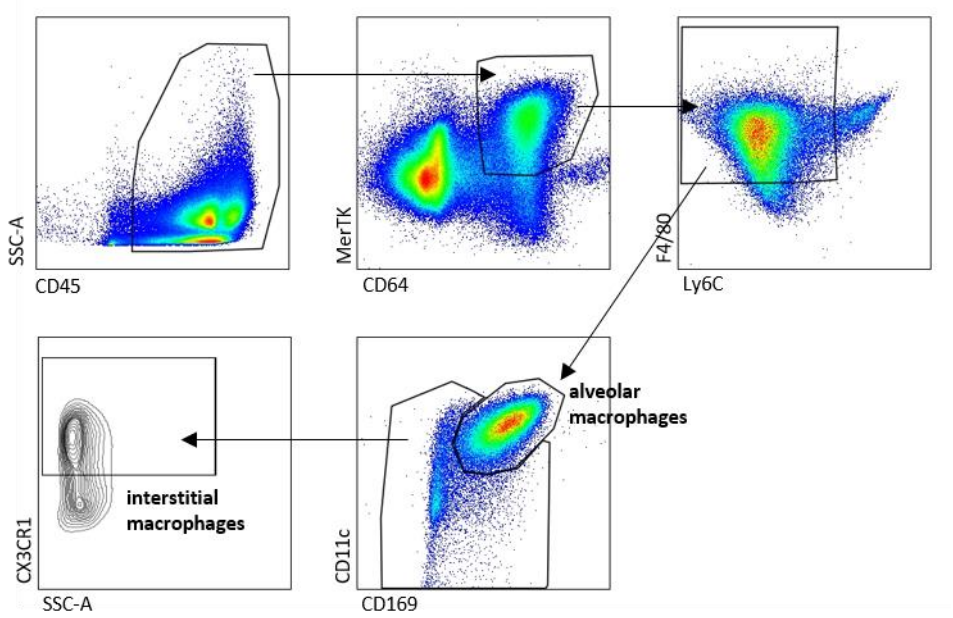


**figure 6: Gating strategy flow cytometry staining panel 2.**
After the exclusion of doublets and dead cells, cell populations were gated as follows: Live single CD45$^+$ cells were gated for MerTK$^+$/CD64$^+$ cells. MerTK$^+$/CD64$^+$ cells were further gated for F4/80$^{high}$/Ly6C$^{low}$ cells. These cells were divided into alveolar macrophages (CD11c$^+$/CD169$^+$) and interstitial macrophages (CX3CR1$^+$). Displayed here are concatenated samples of all analyzed groups from one representative experiment. Cells were analyzed at an Attune NxT instrument.

### 3.8.3 Flow cytometry staining panel 3

Leukocytes from the lung (all isolated leukocytes/mouse lung) (see 3.7, p. 39) were stained with flow cytometry panel 3 for the identification of macrophages, DC and effectors of AAI (see table 7, p. 31). Live, single, $CD45^+$ cells were gated for $MerTK^+/CD64^+$ cells. $MerTK^+/CD64^+$ cells were further gated for AM ($CD11c^+/CD169^+/Ly6C^-/SiglecF^+$), $CD11c^+$ IM ($CD11c^+/CD169^-/CX3CR1^+$), $CD11c^-$ IM ($CD11c^{low}/CD169^-/CX3CR1^+$) and $CD11c^-/CD11c^{low}$ NAM ($CD11c^-/CD169^{high}/CX3CR1^+$). Remaining cells from the CD64/MerTK gating were gated for $CD103^+$ DC ($CD11c^+/CD11b^-/CD103^+/CD24^+$), neutrophils ($CD11b^+/Ly6G^+$) and eosinophils ($CD11b^+/CD11c^-/Ly6G^-/SiglecF^+$). Further, recMac were gated as $CD11b^+/MHCII^+$ and $CD11b^+$ DC as $CD64^-/MHCII^+/CD11b^+$. Monocytes were gated as $MHCII^-/CD11b^{high}/CD64^-$ and were further gated as $Ly6C^+$ monocytes and the remaining cells. Remaining cells were gated for $CX3CR1^+/Ly6C^-$ cells and were identified as $Ly6C^-$ monocytes. T cells were gated as $CD11b^-/CD11c^-/CD24^-/MHCII^-$ and B cells were gated as $CD11b^-/CD11c^-/MHCII^+/CD24^{low/+}$.

Prior to gating the cells, spectral unmixing was performed. The spectral unmixing and substraction of autofluorescence signals, using an unstained sample of lung, spleen or lymph node, were performed using the Sony ID7000™ software. Unmixed FCS files were exported and analyzed using the FlowJo software (Tree Star).

# Methods

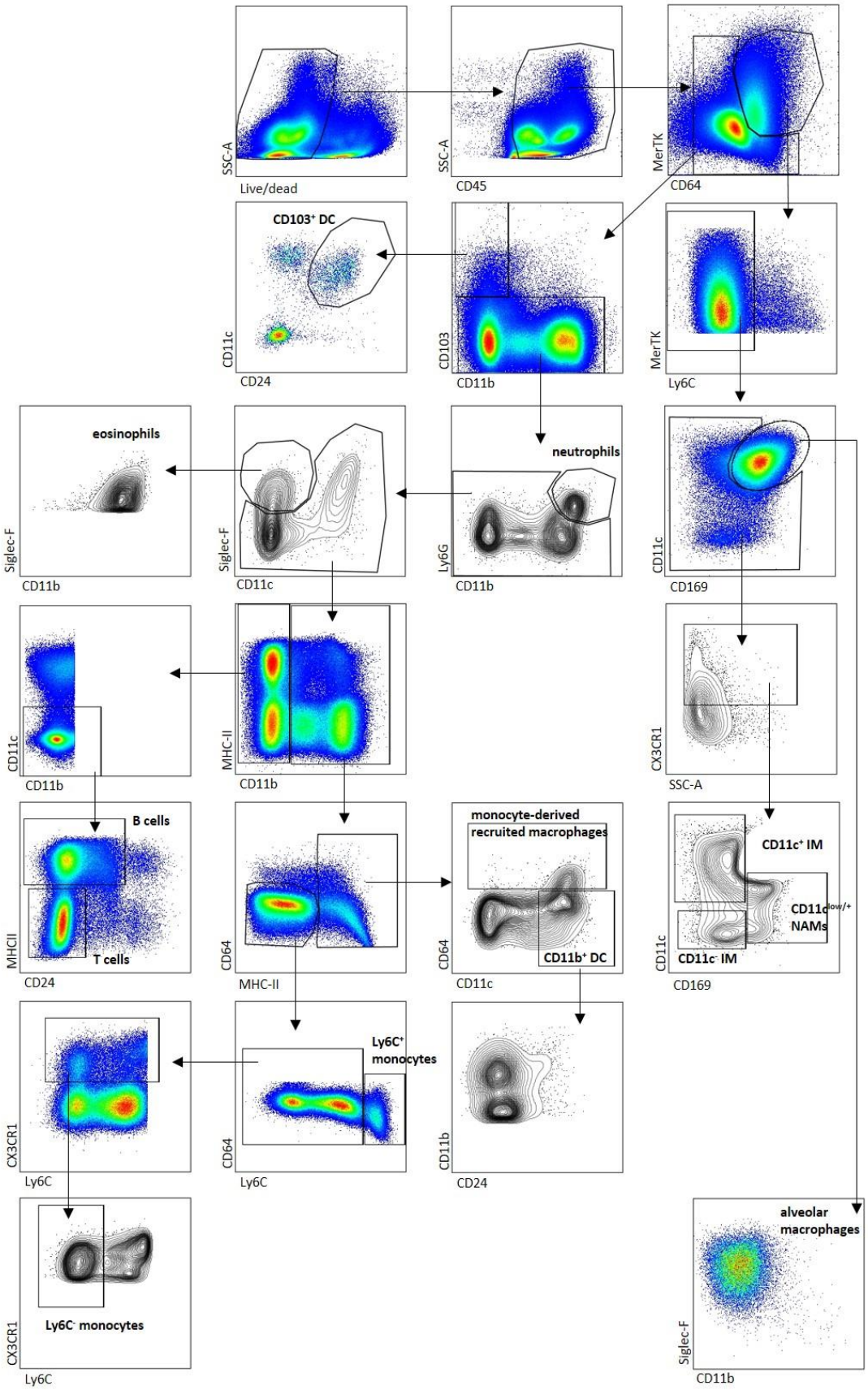
SSC-A
Live/dead
SSC-A
CD45
MerTK
CD64
CD103⁺ DC
CD11c
CD24
CD103
CD11b
MerTK
Ly6C
eosinophils
Siglec-F
CD11b
Siglec-F
CD11c
neutrophils
Ly6G
CD11b
CD11c
CD169
CD11c
CD11b
MHC-II
CD11b
CX3CR1
SSC-A
B cells
MHCII
T cells
CD24
CD64
MHC-II
monocyte-derived
recruited macrophages
CD64
CD11b⁺ DC
CD11c
CD11c⁺ IM
CD11c^low/+
NAMs
CD11c⁻ IM
CD11c
CD169
CX3CR1
Ly6C
Ly6C⁺
monocytes
CD64
Ly6C
CD11b
CD24
alveolar
macrophages
Siglec-F
CD11b
Ly6C⁻ monocytes
CX3CR1
Ly6C

**figure 7: Gating strategy flow cytometry staining panel 3.**
After the exclusion of doublets and dead cells, $CD45^+$ cell populations were gated as follows: Live, single and $CD45^+$ cells were gated for $MerTK^+/CD64^+$ cells. $MerTK^+/CD64^+$ cells were further gated for $Ly6C^-$ cells and these then divided into AM ($CD11c^+/CD169^+$) and remaining cells. From the remaining cells, $CD11c^+$ IM ($CD11c^+/CD169^-/CX3CR1^+$), $CD11c^-$ IM ($CD11c^{low}/CD169^-/CX3CR1^+$) and $CD11c^{low/+}$ NAM ($CD11c^{-/low}/CD169^{high}/CX3CR1^+$) were gated. Remaining cells from the CD64/MerTK gating were further gated into $CD103^+$ DC ($CD11c^+/CD11b^-/CD103^+/CD24^+$), neutrophils ($CD11b^+/Ly6G^+$) and eosinophils ($CD11b^+/CD11c^-/Ly6G^-/SiglecF^+$). Remaining cells from the SiglecF/CD11c gating that were not eosinophils were gated for $CD11b^{+/high}$ cells. From these, $MHCII^+$ cells were gated. From the $CD11b^{+/high}/MHCII^+$ cells, monocyte-derived recruited macrophages ($CD11b^{+/high}/MHCII^+$) and $CD11b^+$ DC ($CD11b^{+/high}/MHCII^+/CD64^-$) were gated. Monocytes were gated as $MHCII^-/CD11b^{high}/CD64^-$ and were further gated as $Ly6C^+$ monocytes and the remaining cells. Remaining cells were gated for $CX3CR1^+/Ly6C^-$ cells and were identified as $Ly6C^-$ monocytes. T cells were gated as $CD11b^-/CD11c^-/CD24^-/MHCII^-$ and B cells were gated as $CD11b^-/CD11c^-/MHCII^+/CD24^{low/+}$. Displayed here are concatenated samples of all analyzed groups from one representative experiment. Cells were analyzed at a Sony ID7000 spectral analyzer.

## 3.9 Enzyme-linked immunosorbent assay (ELISA)

### 3.9.1 ELISA for the detection of serum albumin

Serum albumin was quantified in BAL samples by a specific ELISA. A 96-well plate was coated with 100 µl/well of the capture antibody (final c = 10 µg/ml) (see table 8, p. 32) over night at 4 °C. The wells were washed five times with 200 µl/well wash buffer (see table 10, p. 33) to remove unbound antibody and blocked with 100 µl/well blocking buffer (see table 10, p. 33) for 1 hour at room temperature on a plate shaker (180 rpm). After blocking, the plate was washed again. A volume of 100 µl/well sample and standard were added in duplicate (negative control: blocking buffer), incubated for 1 hour at room temperature on a plate shaker (180 rpm) and washed again. Subsequently, 100 µl/well (final c = 33,3 ng/ml) of the secondary antibody (HRP-conjugated) (see table 8, p. 32) were added, incubated for 1 hour at room temperature on a plate shaker (180 rpm) and the wells were washed again. For detection, the TMB substrate was mixed according to the manufacturer´s instructions (BD Bioscience). A volume of 100 µl/well substrate was added and the enzymatic reaction was stopped directly by adding 100 µl/well sulfuric acid (2N). The optical density (OD) was measured on a plate reader at 450 nm for all wells. For the analysis, a standard curve was generated using the absorbance of the standard wells and their known concentrations (500 ng/ml, 250 ng/ml, 125

ng/ml, 62.5 ng/ml, 31.25 ng/ml, 15.625 ng/ml, 7.8125 ng/ml, 0 ng/ml). The concentration (ng/ml) of serum albumin in the sample wells was determined from the acquired absorbance and the standard curve.

### 3.9.2 ELISA for the detection of total IgE

Relative levels of murine IgE were measured by ELISA in the serum. A 96-well plate was coated with 100 µl/well of the capture antibody (final c = 2 µg/ml; see table 8, p. 32) over night at 4 °C. The wells were washed four times with 200 µl/well wash buffer (see table 10, p. 33) to remove unbound antibody and blocked with 100 µl/well blocking buffer (see table 10, p. 33) for 1 hour at room temperature on a plate shaker (180 rpm). After blocking, the plate was washed again. A volume of 100 µl sample (1:10 dilution)/well were added in duplicate ($OD_1$ and $OD_2$; negative control: blocking buffer), incubated for 2 hours at room temperature on a plate shaker (180 rpm) and wells were washed again. Subsequently, 100 µl/well of the secondary antibody (final c = 1 µg/ml; HRP-conjugated) (see table 8, p. 32) were added, incubated for 1 hour at room temperature on a plate shaker (180 rpm) and washed again. For detection, the TMB substrate was mixed according to the manufacturer´s instructions. A volume of 100 µl/well substrate was added to all wells and incubated for 10 minutes in the dark. The enzymatic reaction was stopped by adding 100 µl/well sulfuric acid (2N). The optical density (OD) was measured on a plate reader at 450 nm and 570 nm for all wells. The values were used to calculate the relative levels of the target substance (equation (1)-(3)).

$$(1)\ OD_{corr.} = OD_{450} - OD_{570}$$

$$(2)\ OD = \frac{OD_{1,corr.} + OD_{2,corr.}}{2}$$

$$(3)\ \text{Relative amount of target immunoglobulin:} = OD_{sample} - OD_{control}$$

## 3.10 Multiplex quantification of cytokines in bronchoalveolar lavage (BAL) and lung homogenates

Concentrations of different cytokines were simultaneously detected in the supernatant of the BAL or in lung homogenates (see 3.6.2, p. 38) using a cytometric bead array according to the manufacturer´s recommendations (LEGENDplex™, BioLegend). First, 12.5 µl assay buffer was added to the wells of the included 96-well v-bottom plate. For generating a standard curve, the top standard was diluted six times in 1:4 steps and 12.5 µl of each standard dilution were added to the standard wells in duplicate. At the same time, 12.5 µl undiluted BAL samples or supernatant of lung homogenates was added in duplicates into the sample wells, respectively. Next, 12.5 µl of the provided bead-mix was added to each well and the plate was incubated over night at 4 °C shaking on a plate shaker (200 rpm). After a centrifugation step (5 minutes, 1050 rpm, 4 °C), the supernatant was discarded and the beads were washed twice using 200 µl/well washing buffer. Next, 12.5 µl of the detection antibody were added to the wells and incubated for 1 hour at room temperature while shaking (200 rpm). Further, 12.5 µl of the provided streptavidin R-Phycoerythrin solution was added to the wells and incubated for 30 minutes at room temperature, shaking at 200 rpm. The plates were centrifuged (5 minutes, 1050 rpm, 4 °C), the supernatant was discarded and the beads were washed using 200 µl washing buffer. Beads were transferred into acquisition tubes and data were acquired using an Attune NxT flow cytometer and analyzed using the LEGENDplex™ Qognit software (BioLegend). Cytokine concentration that were below the detection limit were evaluated as zero.

## 3.11 Statistical analysis

All statistical analysis was performed using the GraphPad Prism software version 9 (GraphPad Software).

To assess the induction of AAI, a comparison of the AAI group to the respective control group

was performed (OVA-AAI control vs. OVA-AAI, HDM-AAI control vs. HDM-AAI). OVA-AAI and HDM-AAI were directly compared in independent calculations. To assess the effects of IAV infection on AAI, comparisons between AAI with and without previous IAV infection, were performed (AAI vs. IAV + AAI). Data for all experimental groups were tested for normality using the Shapiro-Wilk normality test. An unpaired two-sided t-test was performed in case of Gaussian distribution and an unpaired two-sided Mann-Whitney test in case of non-Gaussian distribution of the data. $P \leq 0.05$ was considered indicative of statistical significance (*$p < 0.05$, ** $p < 0.01$, *** $p < 0.005$, **** $p < 0.0001$).

Individual fold changes were calculated for all animals with respect to the effect of IAV infection on AAI. For the accumulation and functional marker expression of cells in IAV + OVA-AAI and IAV + HDM-AAI, these individual fold changes were calculated as the ratio of individual data of mice from the IAV + AAI group over the median of the respective AAI only group of the respective experiment (fold change = individual IAV + AAI value / AAI only group median). Samples for cytokine, IgE and serum albumin levels were collected in individual experiments, stored and simultaneously analyzed in the respective assays. Here, the individual ratios of each IAV + AAI sample over the median of all analyzed AAI only samples were calculated.

For UMAP plots, manually gated populations from FACS data were exported into a combined master fcs file with 27384 events/sample and a population label for each event. Data in each fluorescence channel were transformed with the Yeo–Johnson algorithm (Yeo *et al.* 2000) followed by an heuristic negative-peak detection algorithm. Z-scores in reference to the peak center of each channel's negative peak were calculated in order to normalize fluorescence channels. Dimension reduction was performed using UMAP algorithm (McInnes *et al.* 2018) (n_neighbors = 30 and min_dist = 0.2). Population assignment of manually gated events was color-coded. All calculations were performed using a Python script (cooperation with Dr. A. Jeron, Helmholtz Centre for Infection Research, Braunschweig).

# 4 Results

## 4.1 Comparative characterization of allergic airway inflammation in two common mouse models with a focus on the macrophage and dendritic cell compartment

In the OVA-mediated mouse model of AAI employed in this study, mice were sensitized three times against the model-antigen OVA in combination with alum in weekly intervals (*i.p*. injection). One week after the last sensitization, mice were challenged with OVA alone on three consecutive days (*i.n.* application) and sacrificed forty-eight hours after the last challenge (figure 8, p. 51). In the HDM-model, mice were treated three times in weekly intervals with the allergen HDM (*i.n*. application) and sacrificed forty-eight hours after the last sensitization (figure 8, p. 51). As a measure of the reduction of experimental animal use, the animals reported here for AAI alone served as control groups in those experiments with prior IAV infection and were *i.n*. treated with 25 µl PBS once before the induction of AAI.

For any experimental setup and animal model, it is of crucial importance to assess the efficiency and specificity of any treatment with appropriate control groups. Due to different timelines and treatments of the control animals in the models, the induction of OVA-AAI and HDM-AAI as such was separately evaluated in relation to a corresponding control group. Further, OVA-AAI and HDM-AAI were directly compared.

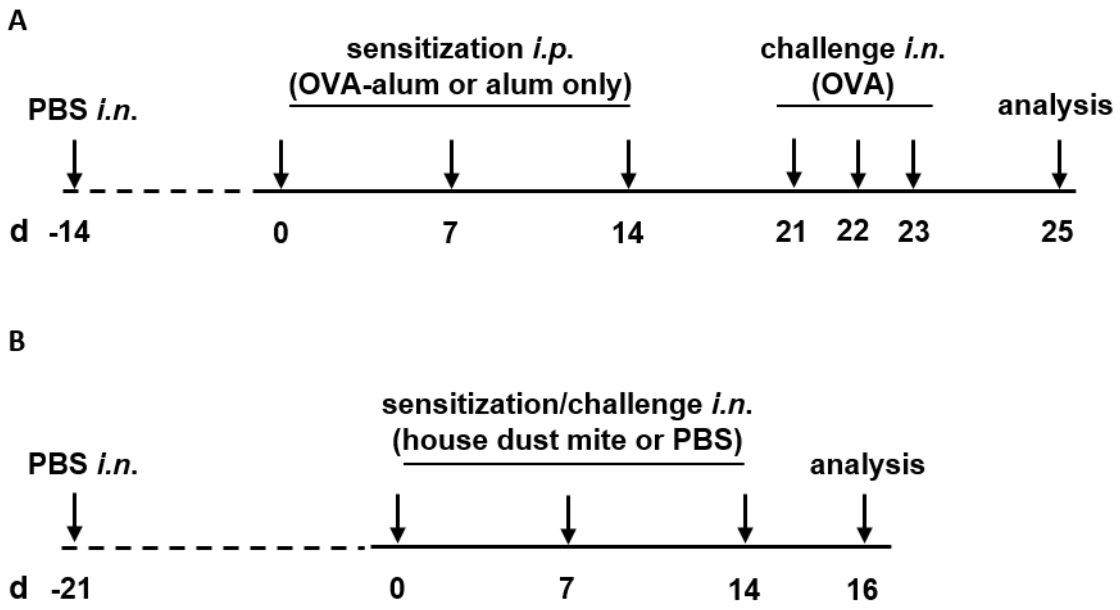


**figure 8: Timelines of the experimental setups for the induction of allergic airway inflammation (AAI).**
(A) For the induction of ovalbumin (OVA)-mediated AAI, mice were sensitized three times intraperitoneally (*i.p.*) with 10 µg ovalbumin (OVA) and 1 mg aluminum hydroxide (alum) in weekly intervals (d 0, 7, 14). One week after the last sensitization they were intranasally (*i.n.)* challenged with 100 µg OVA alone on three consecutive days (d 21, 22, 23). (B) For the induction of house dust mite (HDM)-mediated AAI, mice were sensitized/challenged three times *i.n*. with 100 µg HDM-extract in weekly intervals (d 0, 7, 14). Control mice were sensitized with alum only instead of OVA/alum or treated with PBS instead of HDM. All mice were *i.n*. treated with PBS prior to sensitization/challenge. Forty-eight hours after the last treatment (day 25 in the OVA model, day 16 in the HDM model), mice were sacrificed for analysis.

To monitor whether sensitization and the induction of AAI affected the health status of the mice, they were weighted and their general condition was closely observed on a regular basis according to an experiment-specific score sheet (see 3.5, p. 38). No severe weight loss or increased severity score was observed in either AAI model.

### 4.1.1 Basic characterization of allergic inflammation in OVA-AAI and HDM-AAI

To analyze and compare the induction of AAI in both models, key inflammatory parameters such as immune cell influx to the respiratory tract, airway cytokines and the production of IgE antibodies were quantified in OVA-AAI and HDM-AAI. This comparative characterization served as a basis for the subsequent analysis of IAV-mediated modulation of AAI. The local cellular inflammatory response was evaluated as the influx of eosinophils, neutrophils, T cells and B cells into the airways (figure 9, p. 53). For a characterization of the humoral immune response, the concentrations of total IgE-antibodies were measured in serum (figure 10, p. 54), serum albumin was measured in BAL (figure 12, p. 58) and different cytokines were measured in the BAL (figure 11, p. 56).

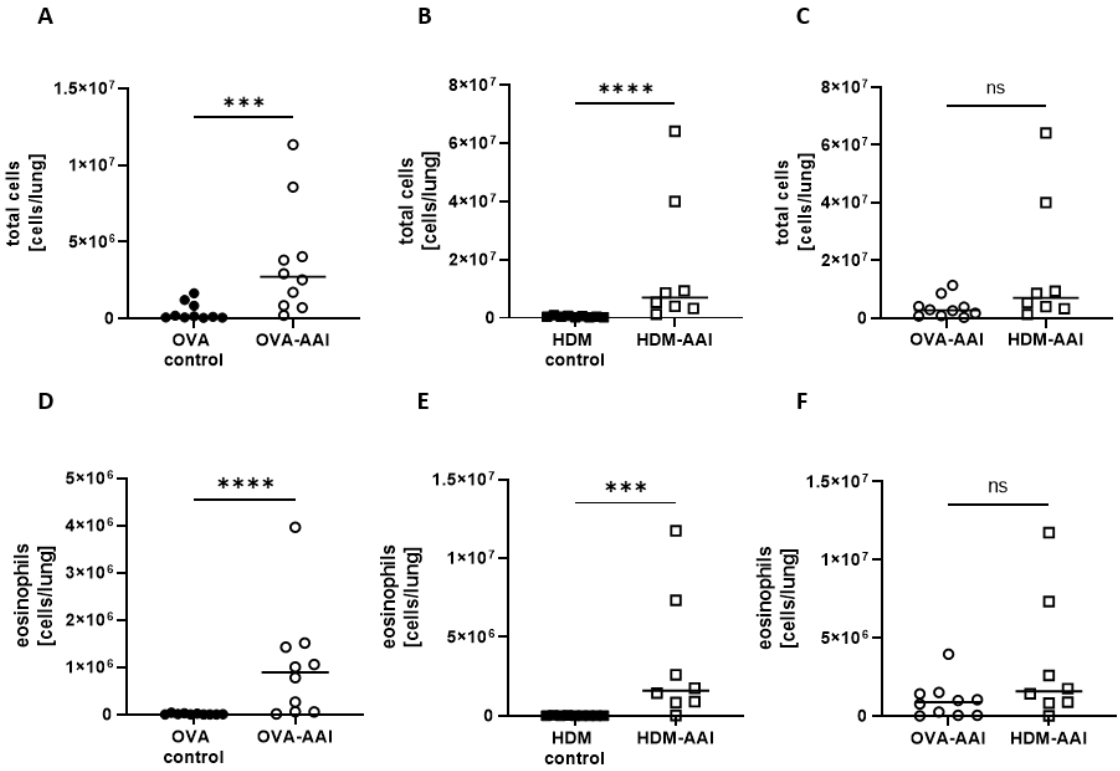


Figure continued on the next page.

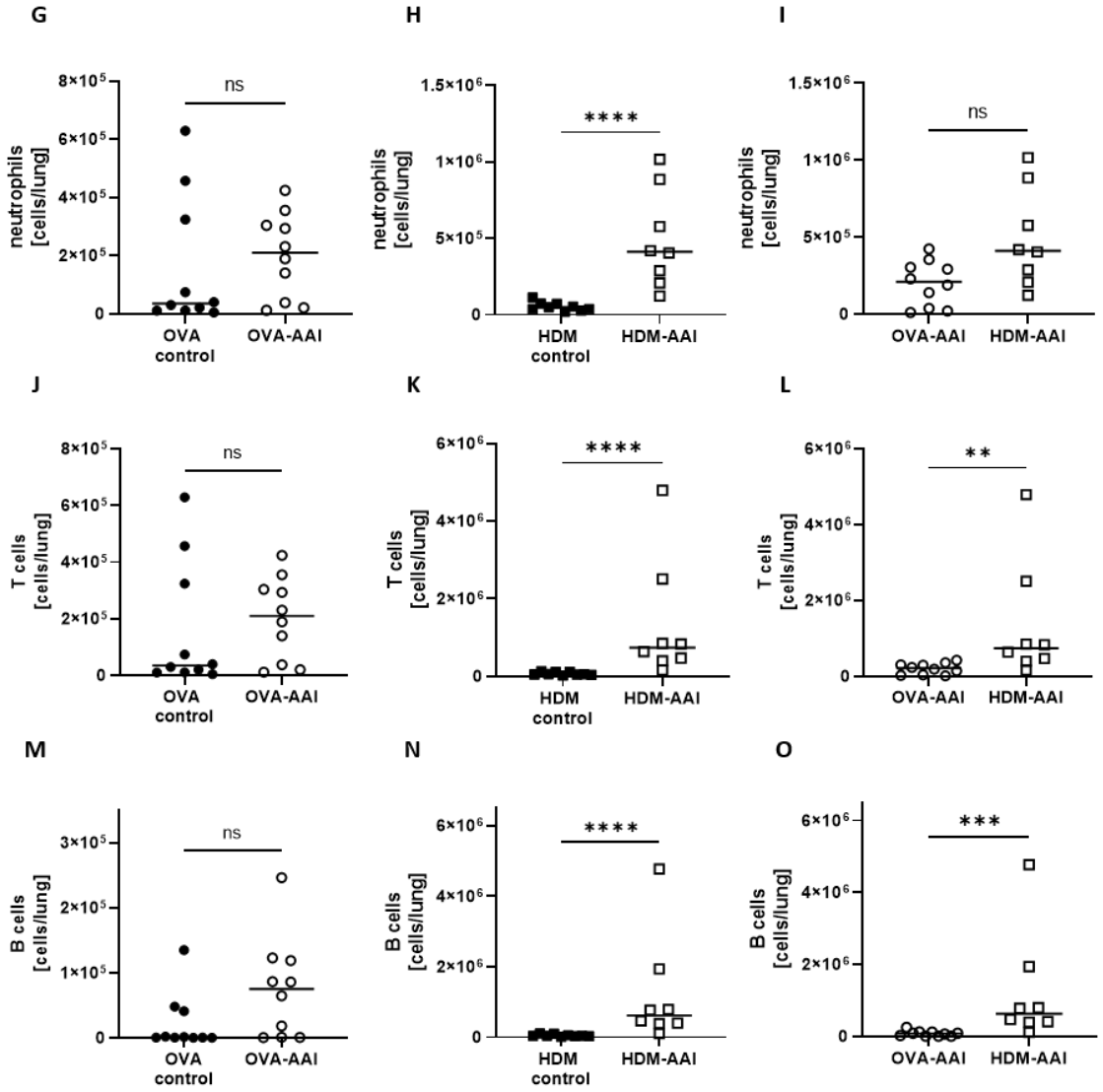


**figure 9: OVA-AAI and HDM-AAI led to distinct accumulation of leukocytes in the lung.**
For the induction of allergic airway inflammation (AAI), mice were treated with ovalbumin (OVA) (and aluminum hydroxide (alum) for sensitization) or house dust mite extract (HDM) as described. Control mice were mock-treated with alum or PBS only. Lung leukocytes were analyzed for total cell counts (A-C), eosinophil numbers (D-F), neutrophil numbers (G-I), T cell numbers (J-L) and B cell numbers (M-O) by spectral flow cytometry. Data compiled from at least three independent experiments are shown for individual mice with the median. $^{**}p < 0.01$, $^{***}p < 0.005$, $^{****}p < 0.0001$, ns = not significant.

Both, in OVA-AAI and HDM-AAI, a significant increase in total leukocyte numbers in the lung as compared to control-treated mice was observed. The median lung absolute cell number in

HDM-AAI was slightly higher as compared to OVA-AAI, although without statistical significance (figure 9 A, B, C). Eosinophils are key players in allergic asthma and neutrophilic inflammation occurs to a varying extent. The numbers of lung eosinophils were significantly elevated in both OVA-AAI (figure 9 D) and HDM-AAI (figure 9 E) as compared to the respective control group. Eosinophil numbers did not differ significantly between both models (figure 9 F). At the same time there was a significant increase of lung neutrophils following treatment with HDM but not with OVA (figure 9 G, H), with no significant difference between both models (figure 9 I). The used antibody panel also allowed the identification of pan T cell and B cell numbers (see 3.8.3). The median T cell number in the lung was elevated in OVA-AAI without statistical significance (figure 9 J) and significantly elevated in HDM-AAI (figure 9 K), with a significant increase in HDM-AAI over OVA-AAI (figure 9 L). The analysis of lung B cells showed similar results as for T cells with elevated numbers in OVA-AAI, significantly increased numbers in HDM-AAI (figure 9 M, N) and a significant increase in HDM-AAI over OVA-AAI (figure 9 O).

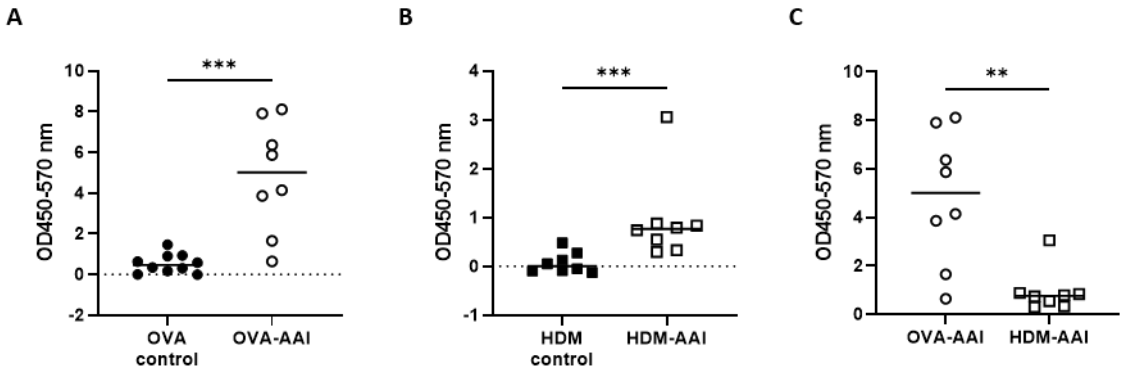


**figure 10: OVA-AAI and HDM-AAI led to significantly increased serum IgE-levels with model-specific differences.**
For the induction of allergic airway inflammation (AAI), mice were treated with ovalbumin (OVA) (and aluminum hydroxide (alum) for sensitization) or house dust mite extract (HDM) as described. Control mice were mock-treated with alum or PBS only. Total IgE-levels were assessed in the serum**.** AAI groups were compared with the respective control group (A, B) and between the models (C). Data compiled from at least three independent experiments are shown for individual mice with the median. $^{**}p < 0.01$, $^{***}p < 0.005$.

Elevated levels of serum IgE display a hallmark characteristic of allergic asthma that likewise occurs in mouse models. Indeed, total serum IgE was significantly elevated in OVA-AAI as well as in HDM-AAI (figure 10 A, B). A comparison between median serum IgE levels in both models revealed, that serum IgE levels were significantly higher in OVA-AAI as compared to HDM-AAI (5-fold; figure 10 C).

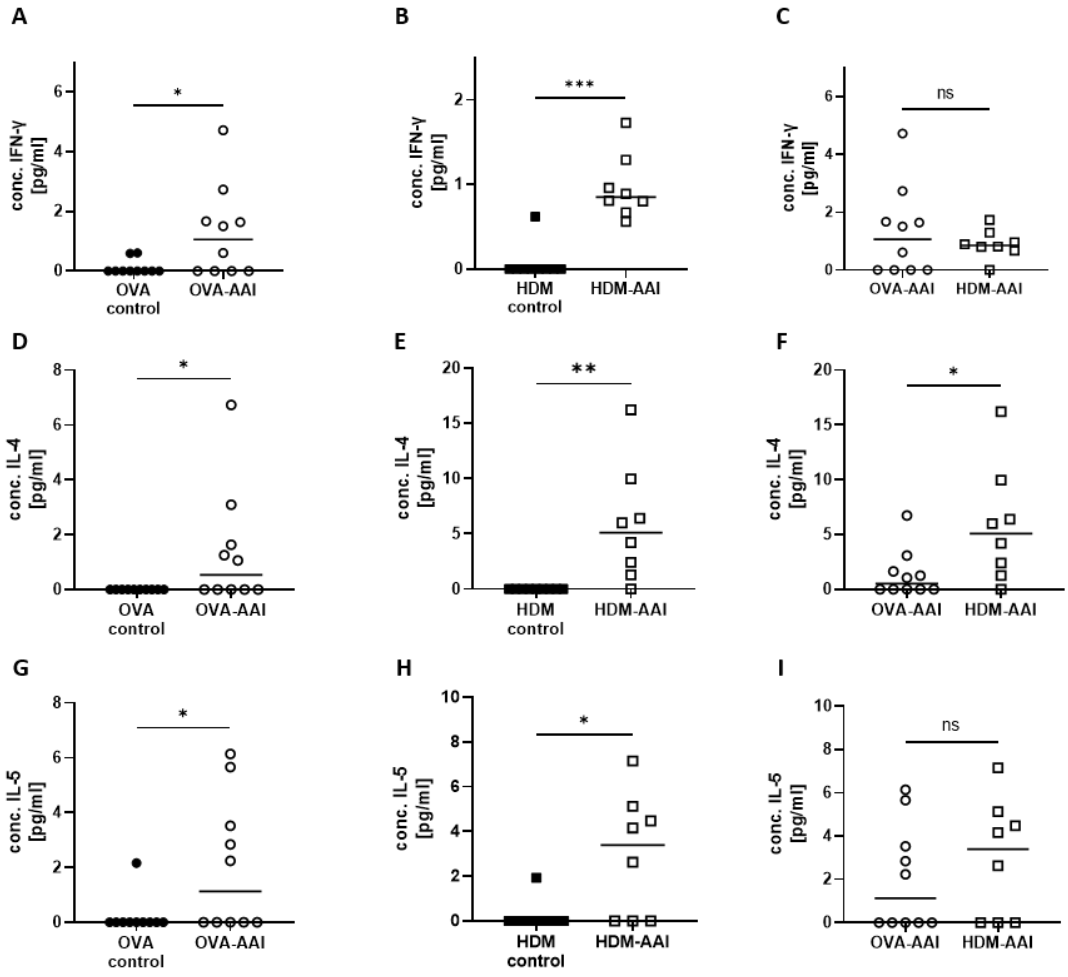


Figure continued on the next page.

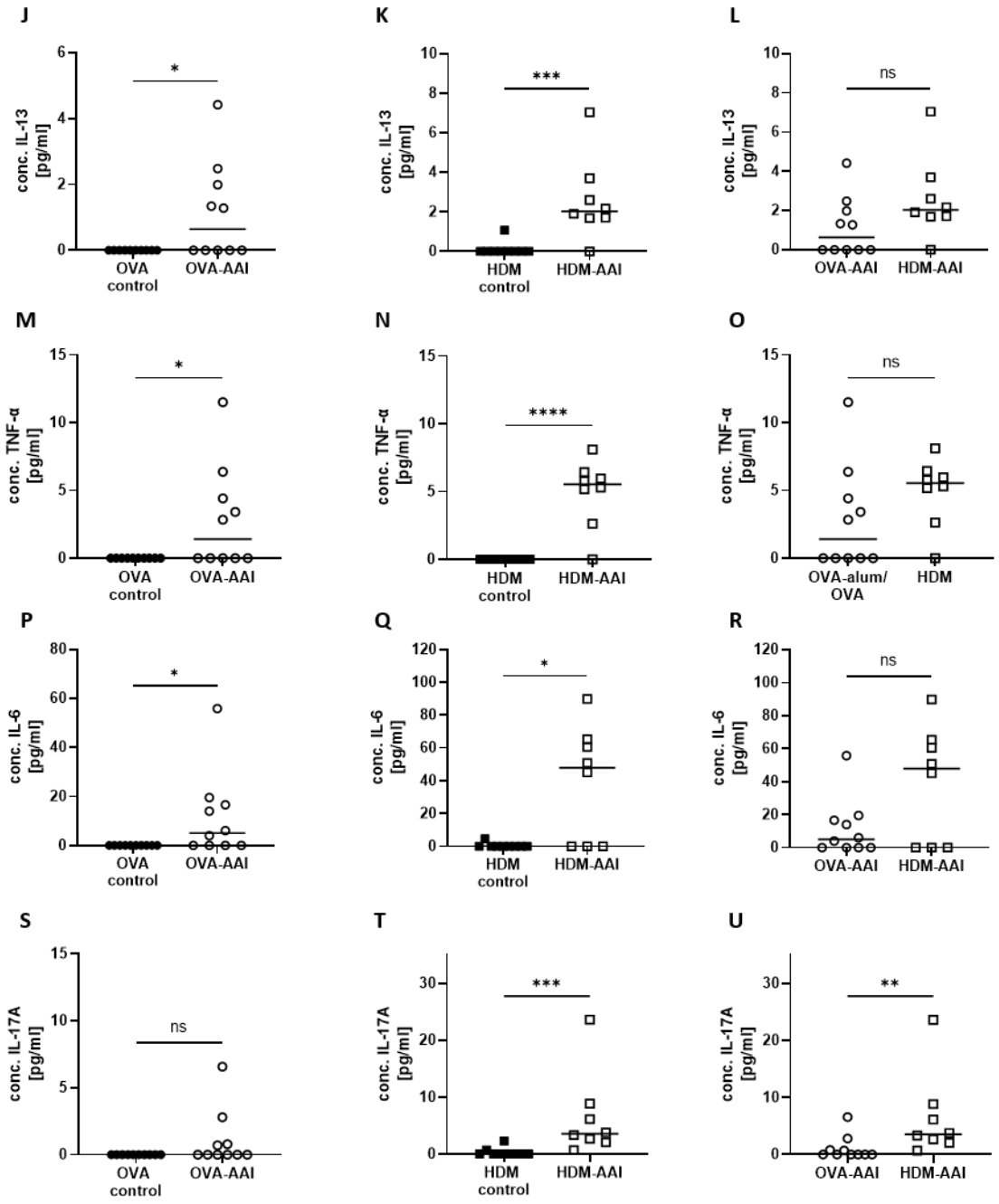


**figure 11: OVA-AAI and HDM-AAI led to distinct, partly model-specific cytokine production in the respiratory tract.**

For the induction of allergic airway inflammation (AAI), mice were treated with ovalbumin (OVA) (and aluminum hydroxide (alum) for sensitization) or house dust mite extract (HDM). Control mice were mock-treated with alum or PBS only. BAL was analyzed for concentrations of interferon (IFN)-γ (A-C), interleukin (IL)-4 (D-F), IL-5 (G-I), IL-13 (J-L), tumor necrosis factor (TNF)-α (M-O), IL-6 (P-R) and IL-17A (S-U). AAI groups were compared with the

respective control group and with each other. Data compiled from at least three independent experiments are shown for individual mice with the median. *$p < 0.05$, **$p < 0.01$, ***$p < 0.005$, ****$p < 0.0001$, ns = not significant.

Cellular responses in respiratory inflammation are associated with the release of cytokines. In order to further characterize the lung inflammatory micromillieu in OVA-AAI and HDM-AAI, cytokine levels (IL-2, IL-4, IL-5, IL-6, IL-9, IL-10, IL-13, IL-17A, IL-17F, IL-22, IFN-γ and TNF-α) were measured in the BAL. Concentrations below LOD were evaluated as zero.

There was a statistically significant increase in the mean concentration of the Th1 cytokine IFN-γ in OVA-AAI and HDM-AAI as compared to the mock-sensitized control group (figure 11 A, B). The mean concentration of IFN-γ did not significantly differ between both models (figure 11 C). The Th2 cytokines IL-4, IL-5 and IL-13 were significantly increased in both OVA-AAI and HDM-AAI as compared to the respective control groups (figure 11 D, E, G, H, J, K). In all cases, mean cytokine levels were higher in HDM-AAI as compared to OVA-AAI (figure 11 F, I, L), reaching statistical significance in case of IL-4. In addition, the respiratory concentrations of the pro-inflammatory cytokines TNF-α and IL-6 were clearly and significantly increased in both AAI models as compared to the controls (figure 11 M, N, P, Q). Again, there was an increase, however not statistically significant, in HDM-AAI as compared to OVA-AAI (figure 11 O, R). The mean levels of IL-17A were significantly increased in HDM-AAI as compared to the respective control group (figure 11 T), but not in OVA-AAI as compared to the control (figure 11 S). There was a statistically significant difference in IL-17A levels between the models, with higher concentrations in HDM-AAI as compared to OVA-AAI (figure 11 U). The analysis of the cytokines IL-2 and IL-9 did not show any differences, neither between the control and AAI groups nor between both AAI models (data not shown). For IL-10, IL-17F and IL-22 all cytokine levels were below the limit of detection for all samples in all groups (data not shown).

Altogether, both models of AAI were associated with a significant cytokine response in the airways and that recapitulated important aspects of human allergic asthma. Further, these

results obtained so far indicated that HDM-AAI induced a stronger local inflammatory response as compared to OVA-AAI.

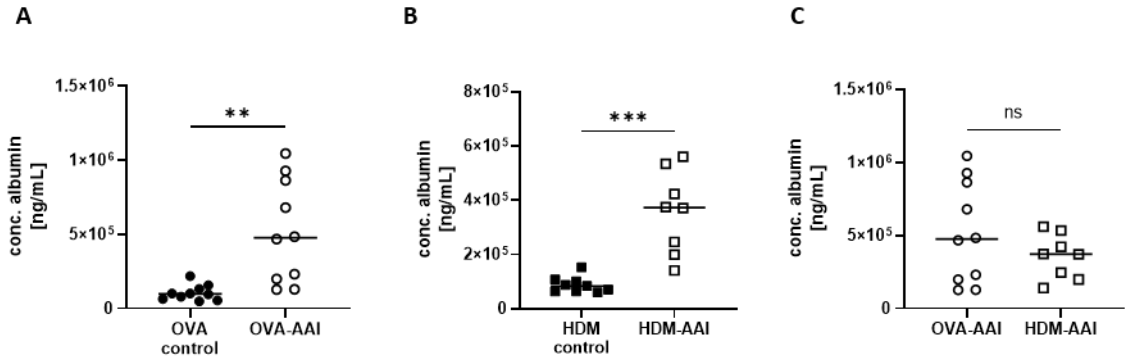


**figure 12: OVA-AAI and HDM-AAI led to a similar, significant increase in the concentration of serum albumin in bronchoalveolar lavage (BAL).**
For the induction of allergic airway inflammation (AAI), mice were treated with ovalbumin (OVA) (and aluminum hydroxide (alum) for sensitization) or house dust mite extract (HDM) as described. Control mice were mock-treated with alum or PBS only. The concentration of serum albumin in BAL was assessed by ELISA. AAI groups were compared with the respective control group (A, B) and between each other (C). Data compiled from at least three independent experiments are shown for individual mice with the median. $**p < 0.01$, $*** p < 0.005$, ns = not significant.

Respiratory infections and inflammatory diseases, such as asthma, can lead to reduced pulmonary function and increased capillary permeability, causing serum albumin to leak from the circulation into tissue fluid or to escape into the alveolar space (Yoshikawa *et al.* 2004, Kantrow *et al.* 2009). To assess capillary leakage to the airways in experimental AAI, the concentration of serum albumin was analyzed in BAL fluid. In both OVA-AAI and HDM-AAI, a significant increase in the concentration of serum albumin in BAL, as compared to the respective control group was observed (figure 12 A, B). Furthermore, the serum albumin concentrations in BAL were marginally, however not significantly, reduced in HDM-AAI as compared to OVA-AAI (figure 12 C).

Taken together, hallmark features of AAI with respect to absolute leukocyte numbers isolated

from the lungs, eosinophil and neutrophil accumulation, IgE-production and respiratory cytokine and serum albumin concentrations were detected in both models. These parameters at times significantly varied in intensity between OVA-AAI and HDM-AAI. The direction of these model-specific differences however was not uniform, with by trend higher cell numbers and cytokine levels, significantly increased T and B cell numbers, BAL IL-4 and IL-17A and at the same time significantly reduced serum IgE levels in HDM-AAI as compared to OVA-AAI.

With regard to the hypothesis of this thesis, the involvement of the lung macrophage and DC cellular compartment in OVA-AAI and HDM-AAI was analyzed in detail. Spectral analysis enables high-parameter flow cytometry and thereby the collection of comprehensive information about heterogeneous cellular compartments with a high sensitivity to detect rare populations. It further enables the handling of autofluorescence, which plays a particularly important role in macrophages in the lung (Wanner *et al.* 2022). Here, it enabled the parallel analysis of several different macrophage and dendritic cell populations. Next to the comparative and detailed analysis of macrophages and DC in OVA-AAI and HDM-AAI, this approach was followed for IAV infection alone to assess IAV-mediated changes to the lung macrophage and DC pool with increased subset resolution (figure 13). In recent years, novel macrophage populations, distinct from known populations, have been identified in the lung. Two distinct DC populations ($CD103^+$ and $CD11b^+$ DC) and five distinct macrophage populations of the lung were analyzed, comparing the two AAI-models: alveolar macrophages (AM), two subpopulations of interstitial macrophages (IM), nerve- and airway-associated macrophages (NAM) and monocyte-derived recruited macrophages (recMac) (table 13, p. 61).

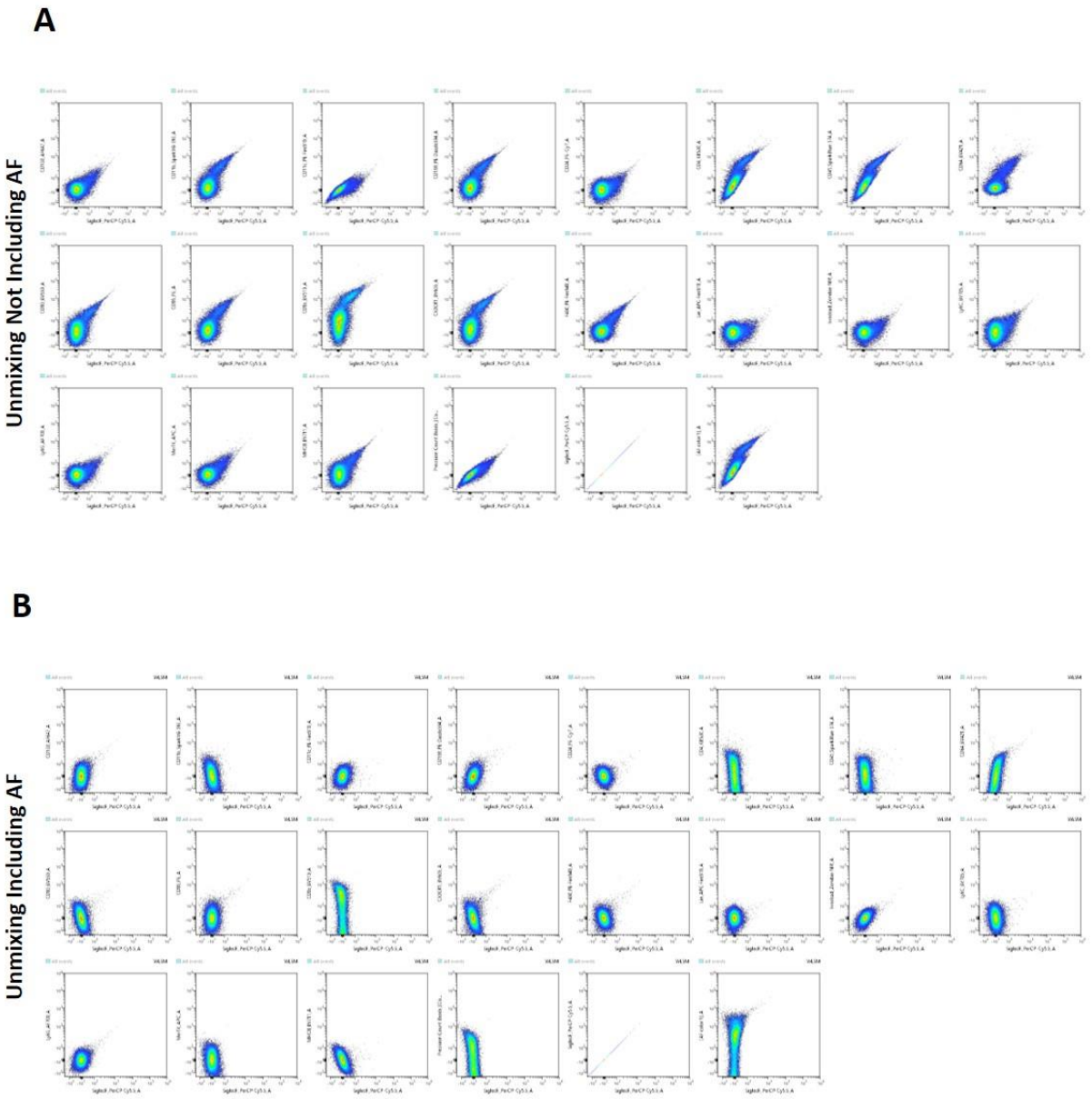


**figure 13: Unmixing of spectral flow cytometry data with and without autofluorescence (AF) handling.**
There is improved resolution of the unstained sample with AF included in unmixing. The unstained lung cell sample is representatively displayed in dot plots for perCP-Cy5.5 (SiglecF) vs. every fluorophore of the staining panel. (A) shows results for unmixing applied without including the AF population in the unmixing. (B) shows results for unmixing with including the AF population, as it was performed for data analysis.

**table 13: Cell surface marker expression of analyzed cell populations in the lung (spectral flow cytometry)**

| Population | Cell Surface Marker |
|---|---|
| Alveolar macrophages (AM) | $MerTK^+/CD64^+/Ly6C^-/CD11c^+/CD169^+/SiglecF^+/CD11b^-$ |
| $CD11c^+$ interstitial macrophages (IM) | $MerTK^+/CD64^+/Ly6C^-/CX3CR1^+/CD169^-/CD11c^+$ |
| $CD11c^-$ interstitial macrophages (IM) | $MerTK^+/CD64^+/Ly6C^-/CX3CR1^+/CD169^-/CD11c^-$ |
| Nerve- and airway-associated macrophages (NAM) | $MerTK^+/CD64^+/Ly6C/CX3CR1^+/CD169^+/CD11c^{+/low}$ |
| Monocyte-derived recruited macrophages (recMac) | $CD64^+/CD11b^+$ |
| $CD103^+$ dendritic cells (DC) | $CD11c^+/MHCII^+/CD11b^-/CD24^+/CD103^+$ |
| $CD11b^+$ dendritic cells (DC) | $CD11c^+/MHCII^+/CD24^-/CD103^-/CD11b^+$ |
| $Ly6C^+$ monocytes | $SiglecF^-/CD11c^-/CD11b^+/MHCII^-/CD64^-/Ly6C^+$ |
| $Ly6C^-$ monocytes | $SiglecF/CD11c/CD11b^+/MHCII/CD64/CX3CR1^+/Ly6C^-$ |
| Eosinophils | $Ly6G^-/SiglecF^+/CD11c^-/CD64^-$ |
| Neutrophils | $Ly6G^+/CD11b^+/CD64^-$ |
| T cells | $CD11b^-/MHCII^-/CD24^-$ |
| B cells | $CD11b^-/MHCII^+/CD24^{low/+}$ |

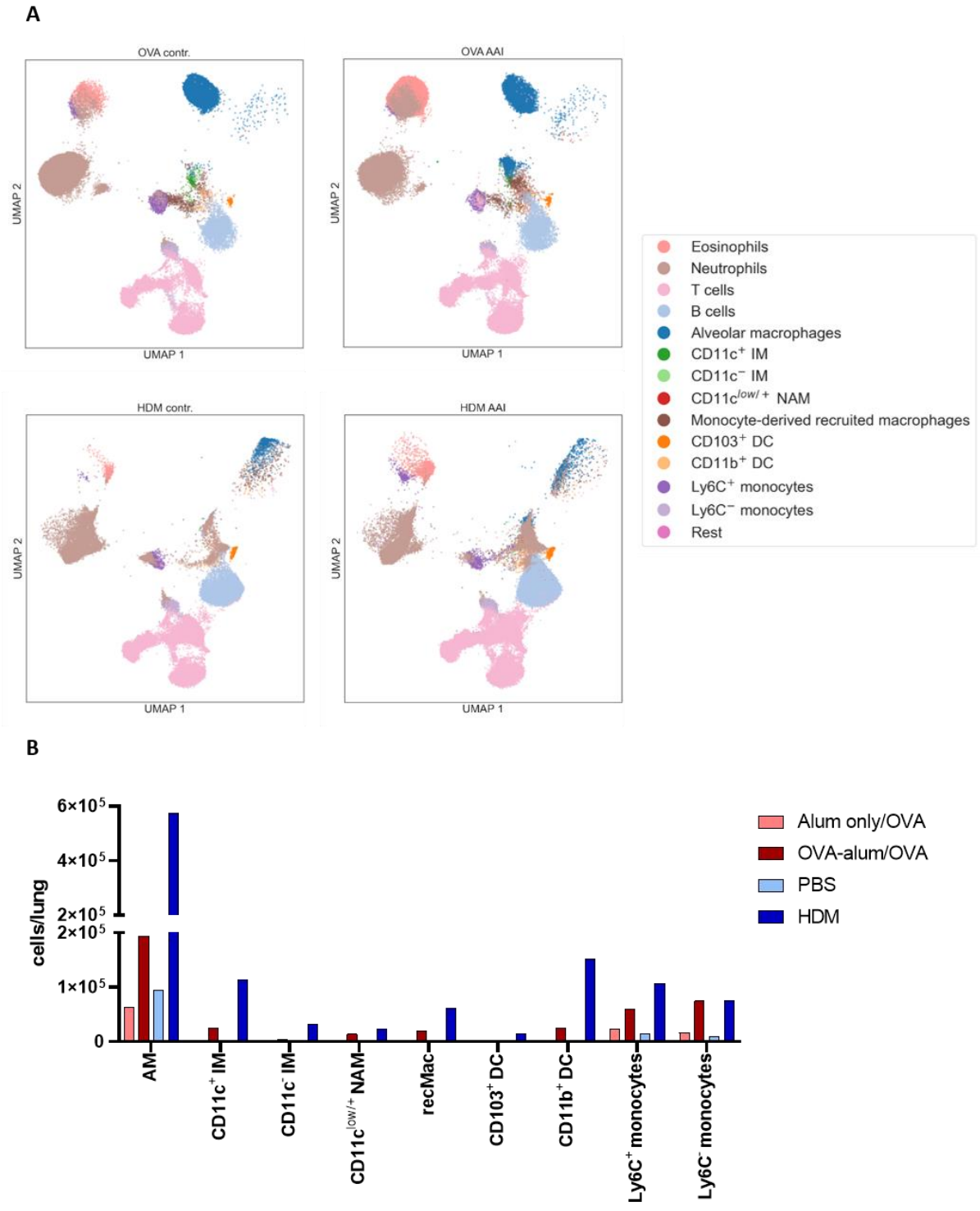


**figure 14: Representative UMAP plots and mean absolute cell numbers of the analyzed macrophage and DC subsets.**

For the induction of allergic airway inflammation (AAI), mice were treated with ovalbumin (OVA) (and aluminum hydroxide (alum) for sensitization) or house dust mite extract (HDM) as described. Control mice were mock-sensitized with alum only (OVA-AAI) or treated with PBS only (HDM-AAI). Clustering of immune cell subsets was performed by UMAP and cell subsets were identified and color-coded based on manual gating. Representative UMAP plots for all four analysed conditions (A). Overview of median absolute numbers of the indicated immune cells compiled from all experiments (B). Individual data for these populations are shown in figures 15 to 21.

For an overview of the involved immune cells, manually gated populations from FACS data were used for UMAP embedding of the analyzed cell subsets (figure 14 A). UMAP plotting revealed substantial differences between both AAI models, with a model-specific accumulation of different macrophage, DC and monocyte subsets in the lung (figure 14 B).

### 4.1.2 Accumulation and MHCII expression of lung macrophage subsets in AAI

AM, CD11c$^{+}$ and CD11c$^{-}$ IM, NAM and recMac were analyzed and compared between OVA-AAI and HDM-AAI.

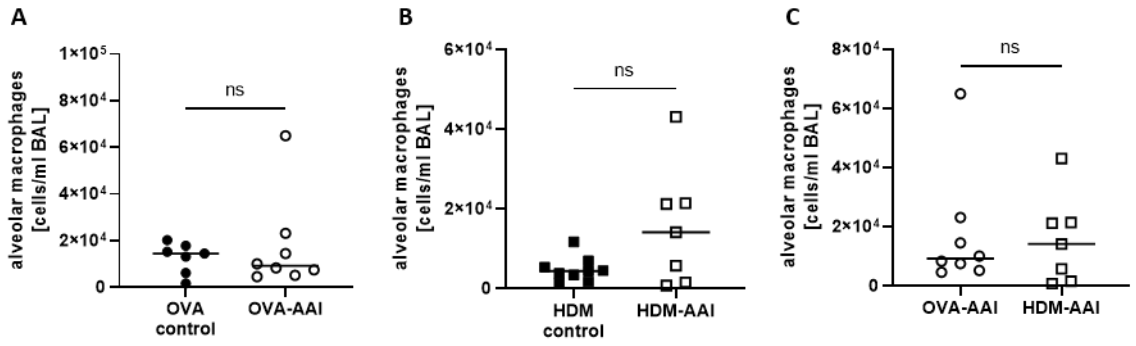


Figure continued on the next page.

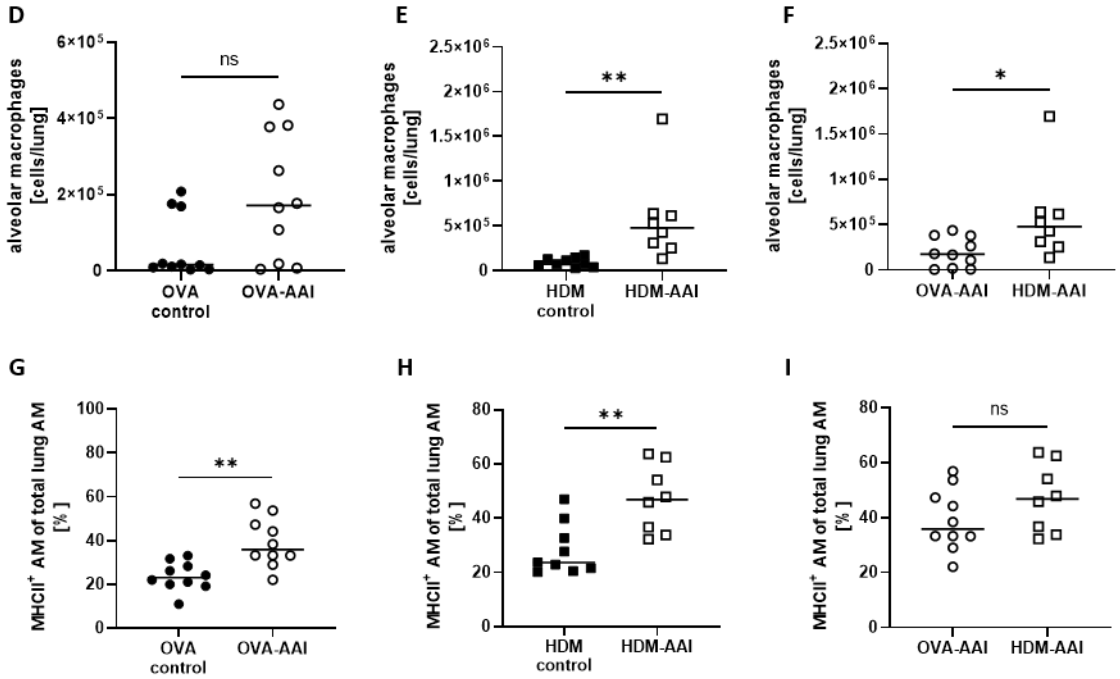


**figure 15: Alveolar macrophages in the respiratory tract in OVA-AAI and HDM-AAI.**
For the induction of allergic airway inflammation (AAI), mice were treated with ovalbumin (OVA) (and aluminum hydroxide (alum) for sensitization) or house dust mite extract (HDM) as described. Control mice were mock-treated with alum or PBS only. Bronchoalveolar lavage (BAL) (A-C) and lung (D-F) leukocytes were analyzed for absolute numbers of alveolar macrophages. Lung alveolar macrophages were also analyzed for their MHCII expression (G-I). AAI groups were compared to the respective control group and between each other. Data compiled from at least three independent experiments are shown for individual mice with the median. *$p < 0.05$, **$p < 0.01$, ns = not significant.

In the BAL, neither OVA-AAI nor HDM-AAI led to a significant increase of AM ($CD11c^+/SiglecF^+$) detected by conventional flow cytometry as compared to control groups (figure 15 A-B). BAL AM numbers also did not differ significantly between both models (figure 15 C). While lung AM ($MerTK^+/CD64^+/Ly6C^-/CD11c^+/CD169^+/SiglecF^+/CD11b^-$) accumulated to some extent in OVA-AAI, their absolute numbers were not significantly elevated as compared to the control group (figure 15 D). In HDM-AAI, AM revealed a stronger and significant increase as compared to controls (figure 15 E) and the mean AM count in HDM-AAI was significantly increased as compared to OVA-AAI (3-fold) (figure 15 F). Despite the difference in AM numbers between the models, the frequency of $MHCII^+$ cells within the lung AM pool significantly increased to

similar extents in OVA-AAI and HDM-AAI as compared to the respective controls (figure 15 G, H). The frequency of MHCII expression on AM did not differ significantly between both models (figure 15 I).

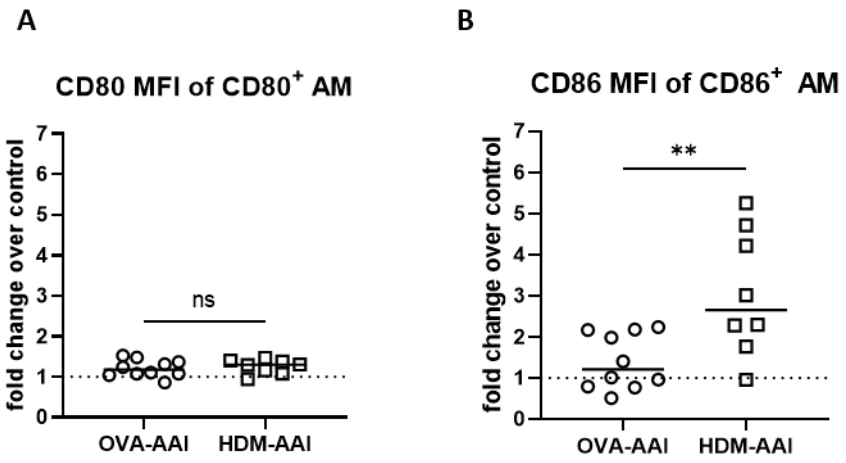


**figure 16: Mean fluorescence intensity (MFI) of the staining for the markers CD80 and CD86 on AM comparing OVA-AAI and HDM-AAI.**
For the induction of allergic airway inflammation (AAI), mice were treated with ovalbumin (OVA) (and aluminum hydroxide (alum) for sensitization) or house dust mite extract (HDM) as described. The mean fluorescence intensity (MFI) of alveolar macrophages (AM) for the respective marker was averaged for the control group for each separate experiment. Corresponding individual MFI-values of samples in the OVA-AAI or HDM-AAI group were compared to the median of the respective control samples, resulting in the fold change over control shown. (A) Fold change over control of the CD80 MFI of $CD80^+$ AM in OVA-AAI and HDM-AAI. (B) Fold change over the control of the CD86 MFI of $CD86^+$ AM in OVA-AAI and HDM-AAI. Data compiled from at least three independent experiments are shown for individual AAI mice with the median. $^{**}p < 0.01$, ns = not significant.

There are implications for AM CD80 and CD86 expression in allergic asthma (Burastero *et al.* 1999, Balbo *et al.* 2001). The mean fluorescence intensity (MFI) of the CD80 staining on $CD80^+$ AM was nearly unchanged in OVA-AAI and HDM-AAI as compared to the controls (figure 16 A). In contrast, CD86 expression (MFI) on $CD86^+$ AM was increased 3.1-fold in HDM-AAI as compared to 1.4-fold in OVA-AAI (figure 16 B).

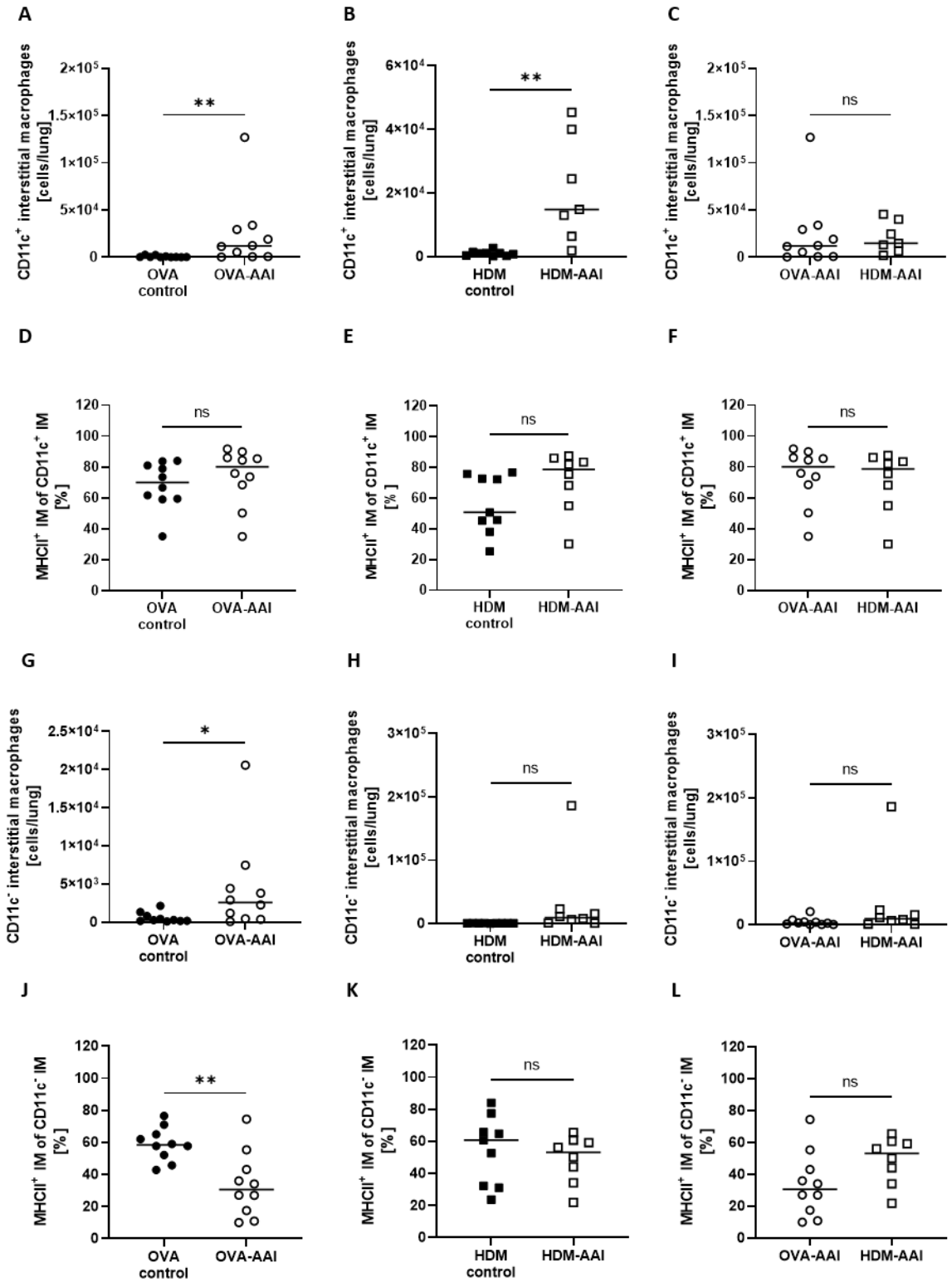
A
CD11c+ interstitial macrophages [cells/lung]
2×10^5
1.5×10^5
1×10^5
5×10^4
0
**
OVA control
OVA-AAI
B
CD11c+ interstitial macrophages [cells/lung]
6×10^4
4×10^4
2×10^4
0
**
HDM control
HDM-AAI
C
CD11c+ interstitial macrophages [cells/lung]
2×10^5
1.5×10^5
1×10^5
5×10^4
0
ns
OVA-AAI
HDM-AAI
D
MHCII+ IM of CD11c+ IM [%]
120
100
80
60
40
20
0
ns
OVA control
OVA-AAI
E
MHCII+ IM of CD11c+ IM [%]
120
100
80
60
40
20
0
ns
HDM control
HDM-AAI
F
MHCII+ IM of CD11c+ IM [%]
120
100
80
60
40
20
0
ns
OVA-AAI
HDM-AAI
G
CD11c- interstitial macrophages [cells/lung]
2.5×10^4
2×10^4
1.5×10^4
1×10^4
5×10^3
0
*
OVA control
OVA-AAI
H
CD11c- interstitial macrophages [cells/lung]
3×10^5
2×10^5
1×10^5
0
ns
HDM control
HDM-AAI
I
CD11c- interstitial macrophages [cells/lung]
3×10^5
2×10^5
1×10^5
0
ns
OVA-AAI
HDM-AAI
J
MHCII+ IM of CD11c- IM [%]
120
100
80
60
40
20
0
**
OVA control
OVA-AAI
K
MHCII+ IM of CD11c- IM [%]
120
100
80
60
40
20
0
ns
HDM control
HDM-AAI
L
MHCII+ IM of CD11c- IM [%]
120
100
80
60
40
20
0
ns
OVA-AAI
HDM-AAI

**figure 17: Populations of interstitial macrophages in the lung comparing OVA-AAI and HDM-AAI.**
For the induction of allergic airway inflammation (AAI), mice were treated with ovalbumin (OVA) (and aluminum hydroxide (alum) for sensitization) or house dust mite extract (HDM) as described. Control mice were mock-treated with alum or PBS only. Lung leukocytes were analyzed for (A-C) cell numbers of $CD11c^+$ interstitial macrophages, (D-F) the frequency of their MHCII expression, (G-I) cell numbers of $CD11c^-$ interstitial macrophages and (J-L) the frequency of their MHCII expression. Data compiled from at least three independent experiments are shown for individual mice with the median. $*p < 0.05$, $**p < 0.01$, ns = not significant.

Lung IM have been classified into two or more distinct populations, mainly based on their phenotype (Chakarov *et al.* 2019). Detailed knowledge with respect to the function of IM subpopulations during homeostasis, inflammation and infection is still limited. According to published studies, IM were analyzed for $CD11c^+$ IM, $CD11c^-$ IM and NAM (Gibbings *et al.* 2017, Schyns *et al.* 2018, Ural *et al.* 2020). A significant increase of absolute numbers of $CD11c^+$ IM was detected in OVA-AAI and HDM-AAI and the number of $CD11c^+$ IM did not differ between the two models of AAI (figure 17 A-C). In contrast to the significant increase in MHCII-expressing AM, significantly altered frequency of $MHCII^+$ $CD11c^+$ IM was neither observed in OVA-AAI nor HDM-AAI (figure 17 D-F).

As opposed to $CD11c^+$ IM, $CD11c^-$ IM numbers were significantly elevated only following the induction of OVA-AAI but not HDM-AAI (figure 17 G, H). There was however no significant difference in the number of $CD11c^-$ IM between the models (figure 17 I). The frequency of $MHCII^+$ $CD11c^-$ IM significantly decreased in OVA-AAI, but not in HDM-AAI as compared to the respective controls (figure 17 J, K). Even though not statistically significant, as a consequence the frequency of MHCII expression of $CD11c^-$ IM was higher in HDM-AAI as compared to OVA-AAI (figure 17 L).

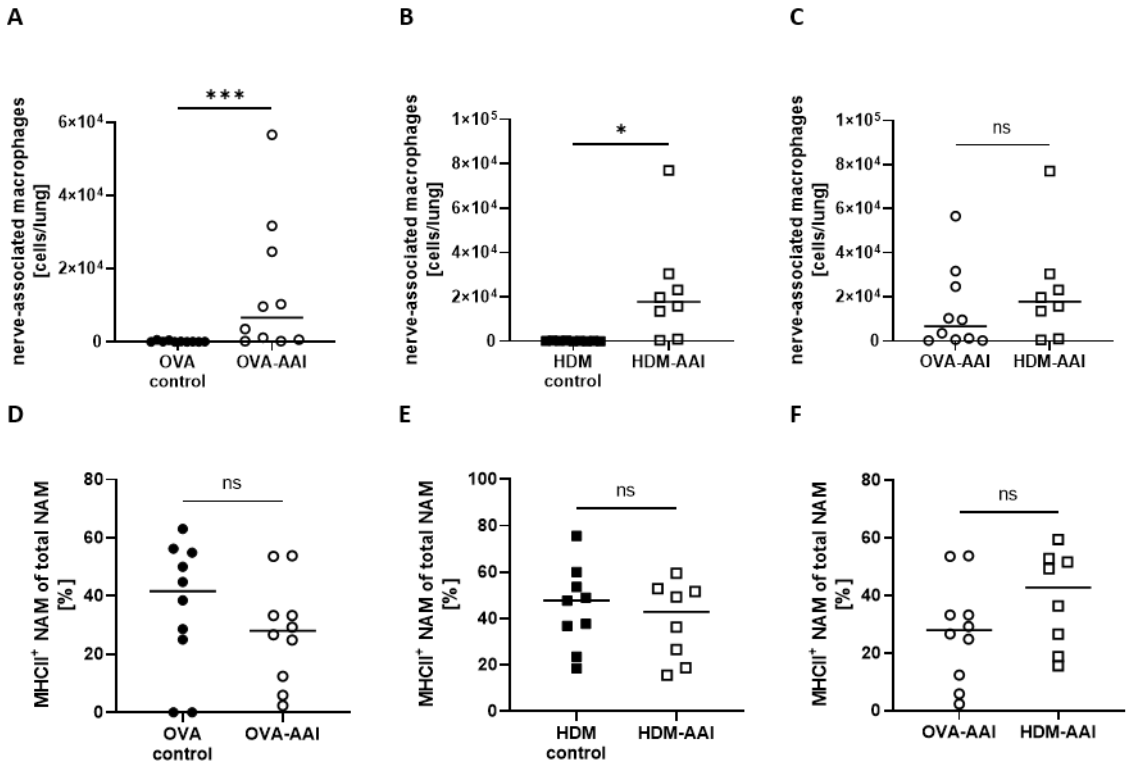


**figure 18: Nerve- and airway-associated macrophages (NAM) in the lung comparing OVA-AAI and HDM-AAI.** For the induction of allergic airway inflammation (AAI), mice were treated with ovalbumin (OVA) (and aluminum hydroxide (alum) for sensitization) or house dust mite extract (HDM) as described. Control mice were mock-treated with alum or PBS only. Lung leukocytes were analyzed for (A-C) absolute numbers of NAM and (D-F) their frequency of MHCII expression. Data compiled from at least three independent experiments are shown for individual mice with the median. *$p < 0.05$, ***$p < 0.005$, ns = not significant.

Nerve- and airway-associated macrophages (NAM) are lung-resident macrophages that are primarily localized around the large bronchiolar airways and adjacent to airway-associated nerves (Ural *et al.* 2020) and this recently described, specialized subset of IM was included in the analyses. Indeed, a significant increase of NAM was observed in OVA-AAI as well as HDM-AAI (figure 18 A, B). The median NAM number was 1.6-fold higher in HDM-AAI as compared to OVA-AAI, even though this increase did not reach statistical significance. As opposed to other macrophage subsets, the frequency of MHCII$^+$ NAM was not altered in either model of AAI as compared to the respective controls or between models (figure 18 D, E, F).

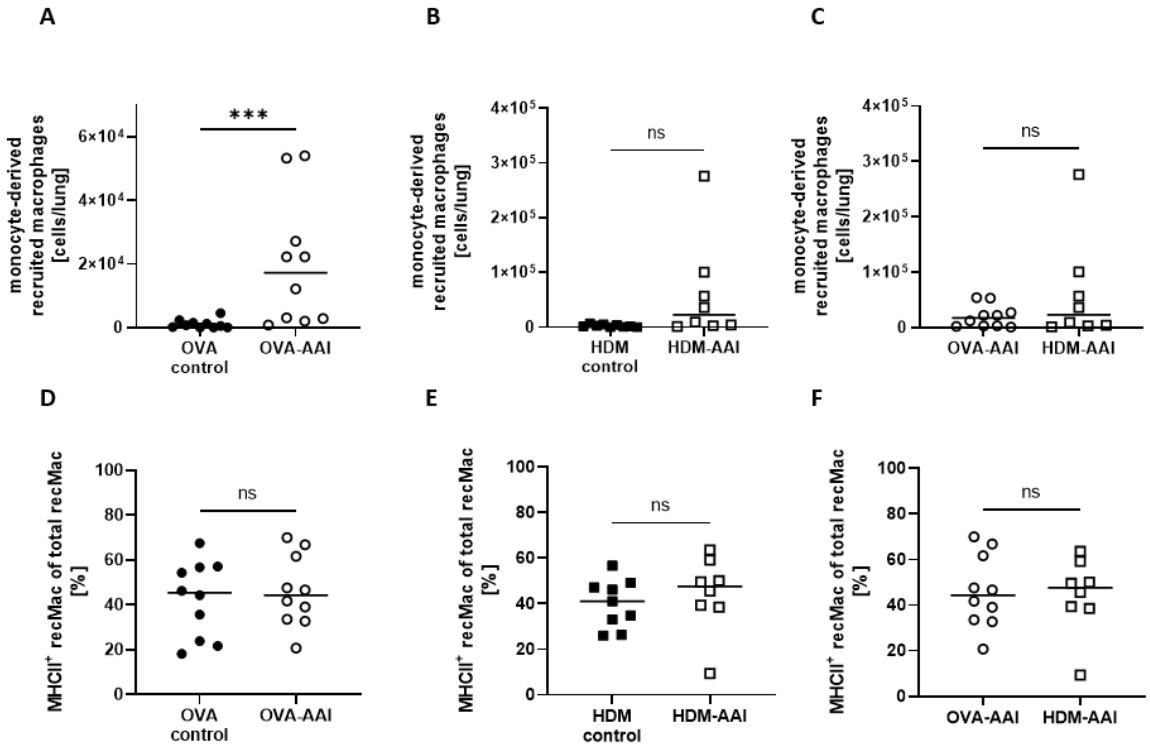


**figure 19: Absolute numbers and frequency of MHCII expressing monocyte-derived recruited macrophages (recMac) in the lung comparing OVA-AAI and HDM-AAI.**
For the induction of allergic airway inflammation (AAI), mice were treated with ovalbumin (OVA) (and aluminum hydroxide (alum) for sensitization) or house dust mite extract (HDM) as described. Control mice were mock-treated with alum or PBS only. Lung leukocytes were analyzed for (A-C) absolute numbers of recMac and (D-F) the frequency of their MHCII expression. Data compiled from at least three independent experiments are shown for individual mice with the median. ***$p < 0.005$, ns = not significant.

During inflammation, also monocyte-derived recruited macrophages (recMac), distinct from IMs (see 3.8.3, p. 44), accumulate in the lung. In OVA-AAI but not HDM-AAI a significant increase in the number of recMac in the lung was observed as compared to the respective control group (figure 19 A, B), without a significant difference between both AAI models (figure 19 C). The median frequency of MHCII$^+$ recMac was not altered in AAI as compared to controls (figure 19 D, E, F).

In conclusion, these analyses revealed substantial alterations to the respiratory macrophage compartment in AAI that were not only macrophage subset- but also model-specific. For two of the analyzed macrophage populations, $CD11c^+$ IM and NAM, a significant increase in cell numbers in the lung in OVA-AAI and HDM-AAI was observed. For AM, such significant increase was only observed in HDM-AAI, resulting in a significant difference in AM numbers comparing both models. The numbers of $CD11c^-$ IM and recMac were only significantly increased in OVA-AAI and not in HDM-AAI as compared to the respective controls. A significant effect of AAI on the frequency of MHCII expression within macrophage subsets was detected for AM in both models and for $CD11c^-$ IM in OVA-AAI and was not significantly altered between HDM- and OVA-AAI. These results show that AAI harbors model-specific characteristics in the accumulation of different macrophage subsets in the lung.

### 4.1.3 Accumulation and functional marker expression of lung dendritic cell subsets in AAI

Given their central role in inducing and shaping allergic responses in the airways, DC populations were analyzed in the lungs in OVA-AAI and HDM-AAI using spectral flow cytometry. Lung DC were discriminated into $CD103^+$ and $CD11b^+$ DC.

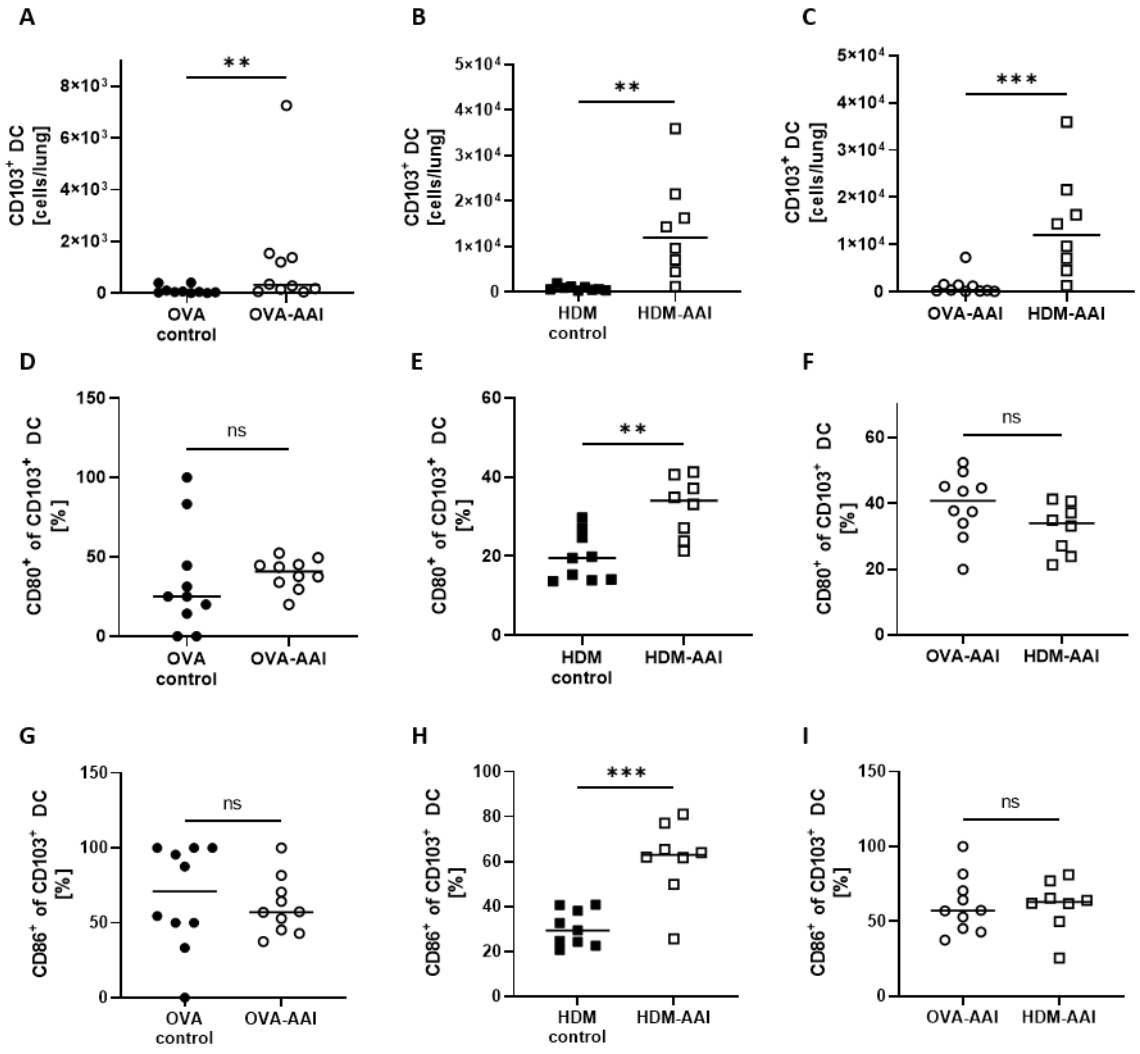


Figure continued on the next page.

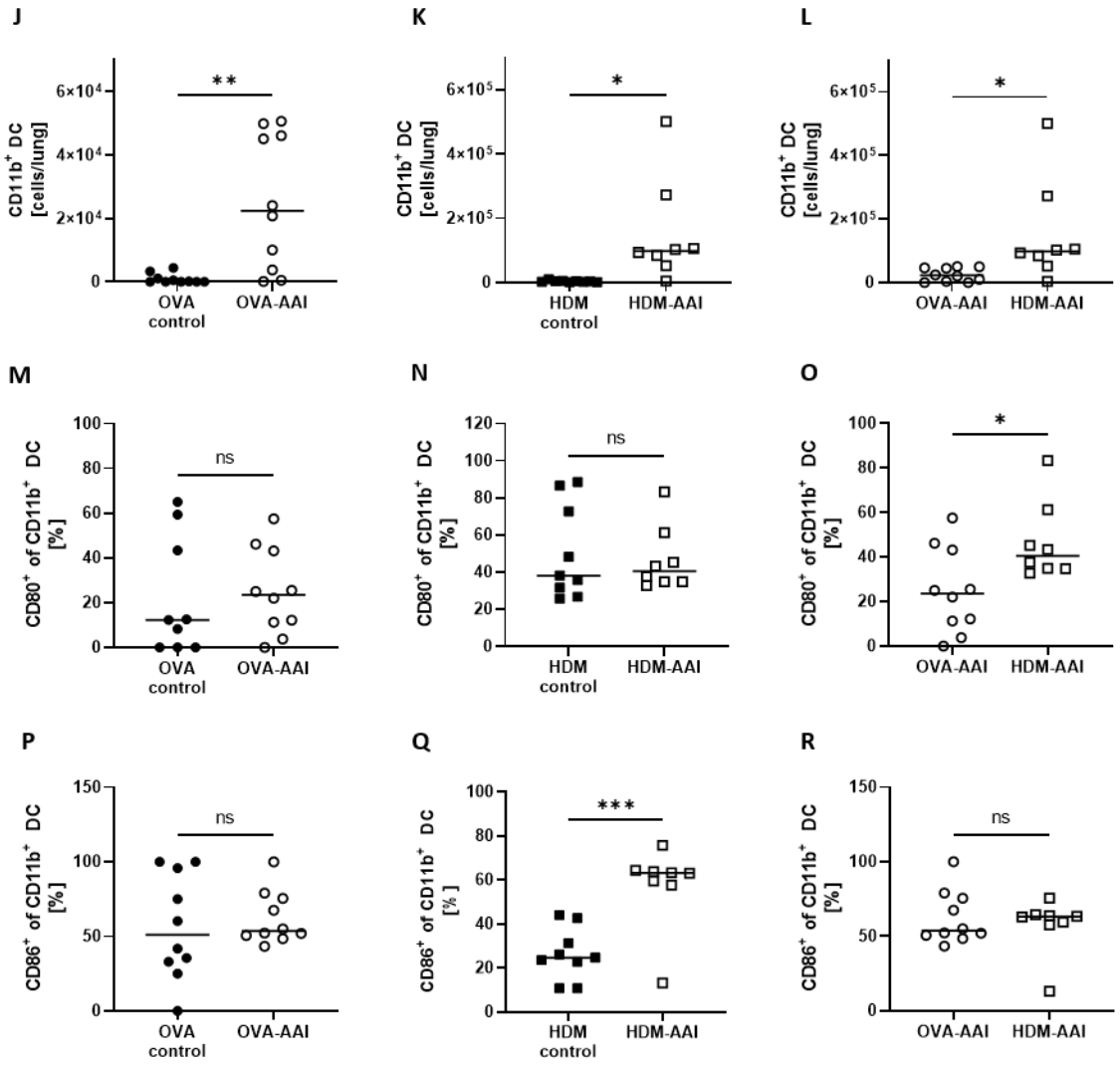


**figure 20: OVA- and HDM-AAI led to an accumulation of CD103$^+$ and CD11b$^+$ dendritic cells (DC) in the lung with subset- and model model-specific effects on cell numbers, CD80- and CD86-expression.**
For the induction of allergic airway inflammation (AAI), mice were treated with ovalbumin (OVA) (and aluminum hydroxide (alum) for sensitization) or house dust mite extract (HDM) as described. Control mice were mock-treated with alum or PBS only. Lung leukocytes were analyzed for (A-C) cell numbers of CD103$^+$ DC and the frequency of their expression of the activation markers (D-F) CD80 and (G-I) CD86. Furthermore, (J-L) cell numbers of CD11b$^+$ DC and the frequency of their expression of the activation markers (M-O) CD80 and (P-R) CD86 were analyzed. Data compiled from at least three independent experiments are shown for individual mice with the median. *$p < 0.05$, **$p < 0.01$, ***$p < 0.005$, ns = not significant.

Lung CD103$^+$ DC numbers were significantly elevated in both AAI models as compared to the respective controls (figure 20 A, B). Comparing both models revealed the number of CD103$^+$ DC to be strongly and significantly increased in HDM-AAI as compared to OVA-AAI (11-fold; figure 20 C). Interestingly, a significant increase of the expression of the activation markers CD80 and CD86 in terms of the frequency of marker-expressing CD103$^+$ DC was observed only in HDM-AAI but not OVA-AAI as compared to their respective control groups (figure 20 D, E, G, H). In OVA-AAI, a slight increase in CD80$^+$ CD103$^+$ DC was observed, although this increase was not statistically significant (figure 20 D). The frequency of CD80$^+$ and CD86$^+$ CD103$^+$ was however unchanged between OVA-AAI and HDM-AAI (figure 20 F, I).

As CD103$^+$ DC, also lung CD11b$^+$ DC showed significantly increased numbers in both models of AAI (figure 20 J, K). Further, also the overall number of CD11b$^+$ DC was significantly higher in HDM-AAI as compared to OVA-AAI (6-fold; figure 20 L) which was consistent with the results for CD103$^+$ DC. While the frequency of CD11b$^+$ DC expressing the activation marker CD80 was not significantly changed in both AAI models as compared to their controls (figure 20 M, N), the frequency of CD86-expressing CD11b$^+$ DC was clearly and significantly elevated in HDM-AAI but not in OVA-AAI (figure 20 P, Q). At the same time, the frequency of CD80$^+$ CD11b$^+$ DC was significantly higher in HDM-AAI (figure 20 O) while the percentage of CD86$^+$ CD11b$^+$ DC was unchanged between the models (figure 20 R).

Taken together, a clear increase of CD103$^+$ DC and CD11b$^+$ DC was observed after induction of AAI with both OVA and HDM. For both DC populations, DC numbers in the lung were significantly higher in HDM-AAI as compared to OVA-AAI. With respect to the activation status of both DC populations, model- as well as marker-specific results were observed. Whereas in CD103$^+$ DC, activation comprised CD80- and CD86-expression and was restricted to HDM-AAI, in CD11b$^+$ DC, activation was restricted to CD86-expression that was also detectable exclusively in HDM-AAI.

### 4.1.4 Accumulation of lung monocyte subsets in AAI

As monocytes can differentiate into populations of macrophages and monocyte-derived DC in the tissue and as clear effects on the respiratory myeloid cell compartment in AAI were detected, the accumulation of two distinct monocyte populations within the leukocytes isolated from the lung was also analyzed (Ly6C$^+$ and Ly6C$^-$).

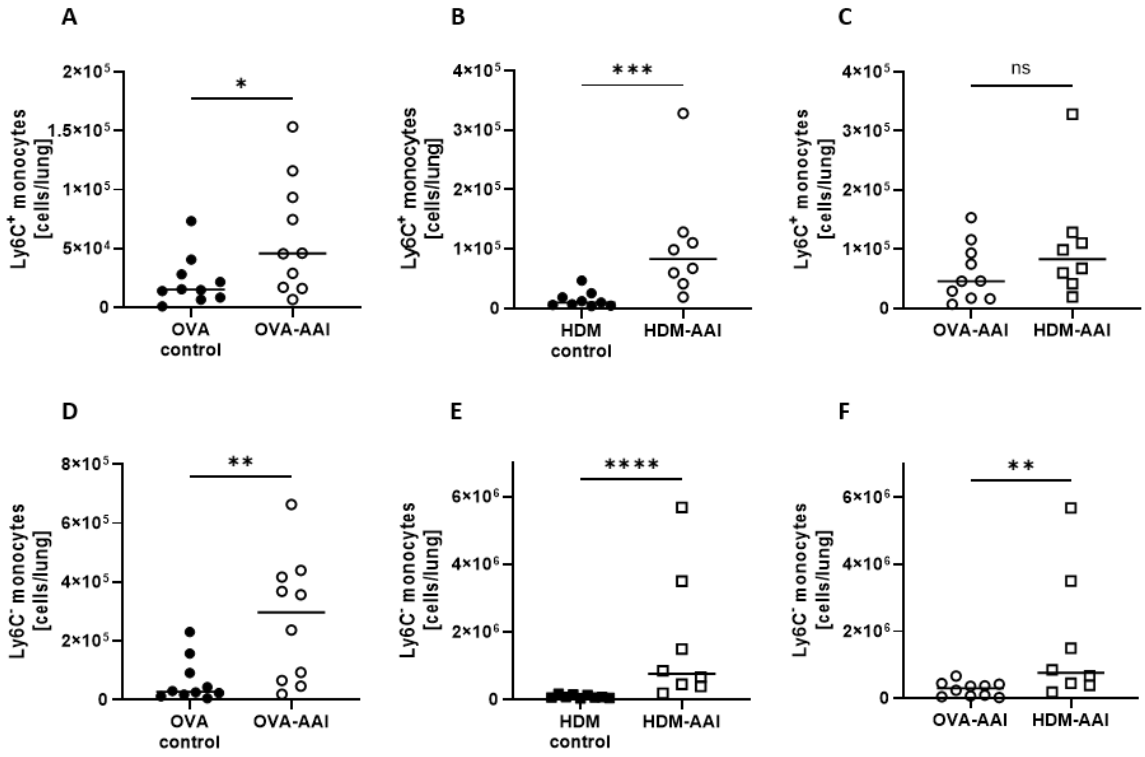


**figure 21: OVA- and HDM-AAI led to a significant increase of Ly6C$^+$ and Ly6C$^-$ monocytes in the lung with model-specific differences in Ly6C$^-$ monocytes.**
For the induction of allergic airway inflammation (AAI), mice were treated with ovalbumin (OVA) (and aluminum hydroxide (alum) for sensitization) or house dust mite extract (HDM) as described. Control mice were mock-sensitized with alum only (OVA-AAI) or treated with PBS only (HDM-AAI). Lung leukocytes were analyzed for absolute numbers of (A-C) Ly6C$^+$ monocytes and (D-F) Ly6C$^-$ monocytes and compared between the models. Data compiled from at least three independent experiments are shown for individual mice with the median. *$p < 0.05$, **$p < 0.01$, ***$p < 0.005$, ****$p < 0.0001$, ns = not significant.

Indeed, a significant increase in lung Ly6C$^+$ and Ly6C$^-$ monocytes was observed in both models of AAI (figure 21 A-D). The median absolute number of Ly6C$^+$ monocytes was slightly higher in HDM-AAI as compared to OVA-AAI (1.8-fold), but this increase did not reach statistical significance (figure 21 C). For Ly6C$^-$ monocytes, significantly higher numbers (1.3-fold increase) were observed in HDM-AAI as compared to OVA-AAI (figure 21 F).

In summary, next to a significant increase in lung Ly6C$^+$ and Ly6C$^-$ monocytes irrespective of the analyzed model, the intensity of monocyte accumulation in AAI partly depended on the experimental model.

The results from 4.1 were summarized in figure 22 with respect to significant differences detected between OVA-AAI and HDM-AAI.

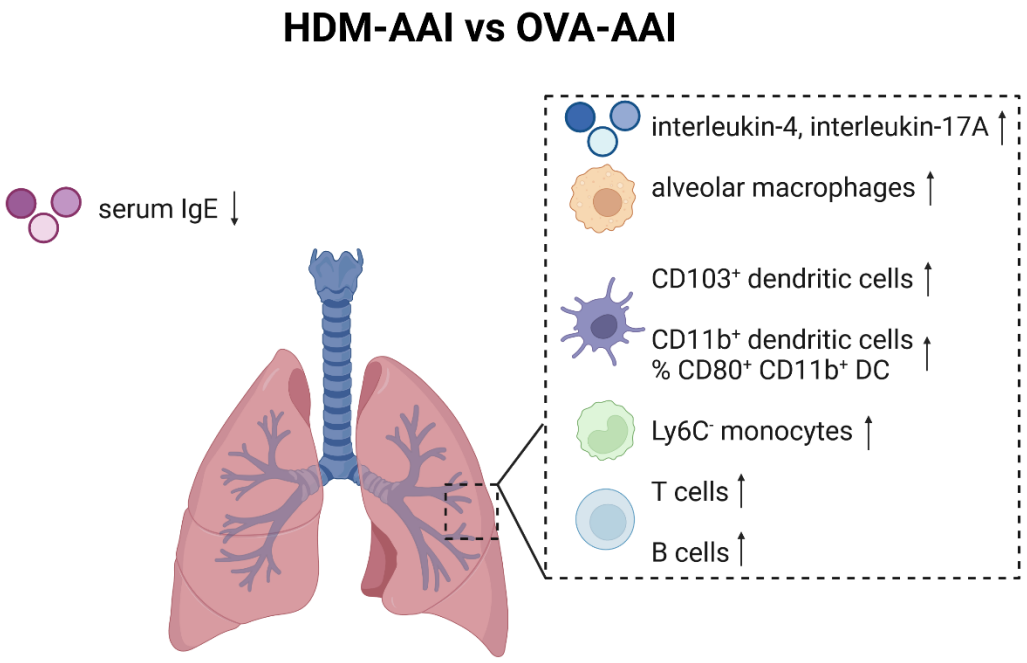


**figure 22: Graphical summary of significant changes between HDM-AAI and OVA-AAI.**

Significant increases comparing HDM-AAI to OVA-AAI are displayed with an upward arrow, significant decreases with a downward arrow. IMs, interstitial macrophages; DC, dendritic cells; IgE, immunoglobulin E. Created in BioRender.com.

## 4.2 Analysis of the effects of resolved influenza A virus (IAV) infection on lung immune homeostasis and subsequently induced AAI with a focus on pulmonary macrophages and DC

Based on preliminary data and on the detailed characterization of macrophages and DC in OVA-AAI and HDM-AAI, the effect of a resolved IAV infection on the lung immune homeostasis, especially with respect to the macrophage and DC compartment, and possible changes in their involvement in AAI was analyzed.

Mice were infected *i.n*. with a sublethal dose of IAV A/PR/8/34 (H1N1) (see 3.2.1, p. 35). The animals reported here for IAV-mediated changes served as only IAV infected control group in the experiments addressing IAV-mediated changes in AAI. Therefore, they were *i.p.* mock-sensitized with alum only (d 14, 21, 28) and *i.n*. challenged three times with OVA (d 35, 36, 37) after recovery of infection. Control mice (PBS) and mice with IAV infection alone were sacrificed at day 39 after infection (table 14, p. 76; figure 23 A, p. 77). Mice treated with PBS instead of HDM-extract from day 21 after IAV infection served as the respective IAV only group in the IAV + HDM model and were sacrificed on day 37 post infection.

**table 14: Treatment regimen for all analyzed groups**

| **Group OVA-model** | **Treatment (infection/sensitization/challenge)** | **Group HDM-model** | **Treatment (infection/*i.n.* allergen)** |
|---|---|---|---|
| OVA control | PBS/alum only/OVA | HDM control | PBS/PBS |
| IAV | IAV/alum only/OVA | IAV | IAV/PBS |

| | | | |
|---|---|---|---|
| OVA-AAI | PBS/OVA-alum/OVA | HDM-AAI | PBS/HDM |
| IAV + OVA-AAI | IAV/OVA-alum/OVA | IAV + HDM-AAI | IAV/HDM |

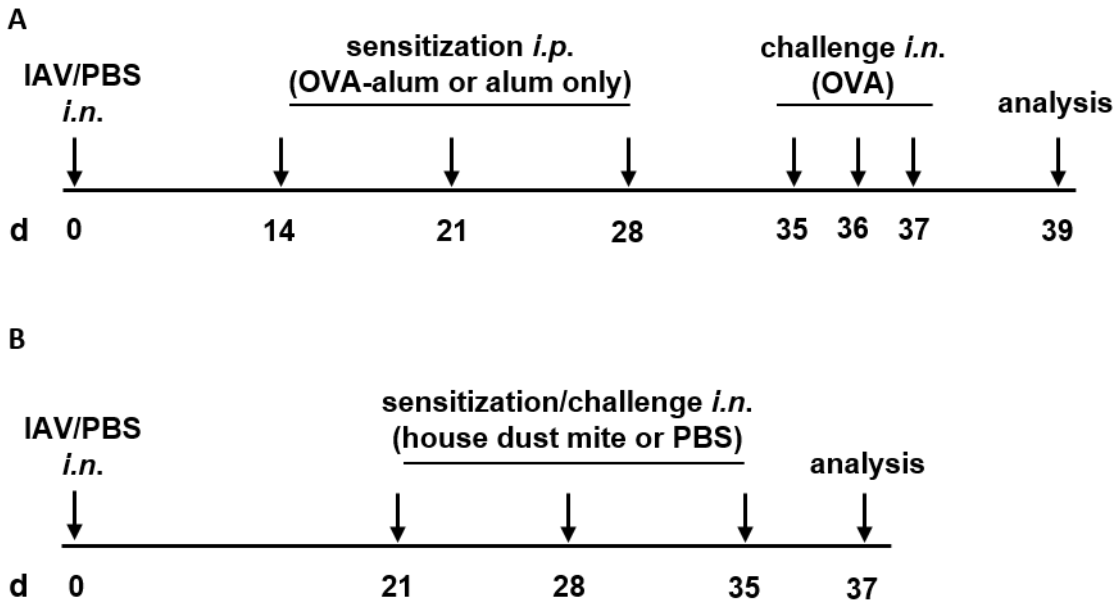


**figure 23: Timelines of the experimental setups for the analysis of AAI induced following IAV infection.**
(A) Mice were infected with a sublethal dose of IAV or treated with PBS (d 0). For the induction of allergic airway inflammation (AAI), mice were sensitized 14 days after infection three times intraperitoneally (*i.p.*) with 10 µg ovalbumin (OVA) and 1 mg aluminum hydroxide (alum) in weekly intervals (d 14, 21, 28). One week after the last sensitization all mice were intranasally (*i.n.*) challenged with 100 µg OVA alone on three consecutive days (d 35, 36, 37). (B) For house dust mite-mediated (HDM)-AAI, mice were infected with IAV (d 0) and then treated three times *i.n.* with 100 µg HDM-extract or PBS in weekly intervals (d21, 28, 35) from day 21 after infection. Control mice were mock-infected with PBS and sensitized with alum only or treated with PBS instead of OVA and HDM. Forty-eight hours after the last treatment (day 39 in the OVA model, day 37 in the HDM model), mice were sacrificed for analysis.

### 4.2.1 Long-term effects of IAV infection in the lung with a focus on pulmonary macrophages and DC

On day 39 after IAV infection, uninfected control mice and IAV infected mice were compared with respect to serum albumin and cytokine levels in the BAL as well as the accumulation of leukocytes in the respiratory tract.

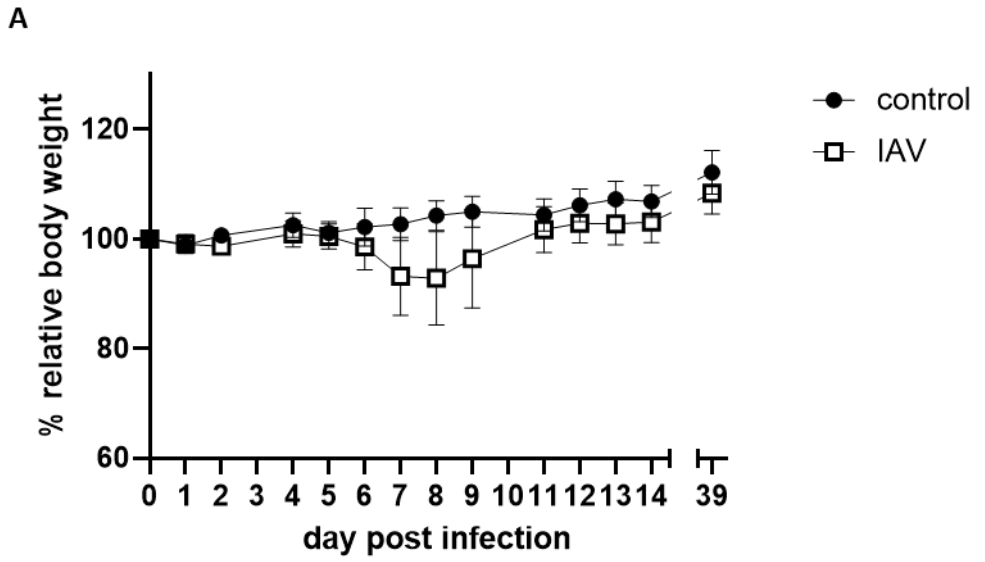


**figure 24: Influenza A virus infection leads to transient body weight loss.**
(A) Body weight was monitored regularly following the infection. Relative body weights are shown as the mean ± SD of n = 14 controls (PBS/alum only/OVA) and *n* = 14 IAV infected mice (IAV/alum only/OVA) for days 0 to 14 and day 39 compiled from three experiments.

The body weight and health status of the animals was monitored throughout the experiment. A transient weight reduction was observed in the IAV-infected animals from day 6 after infection. The maximum weight loss was reached on day 8, with a weight loss of approximately 10 to 20 % of the starting weight. Mice recovered to their starting weight by day 14 post infection and by day 39 post infection, mice had further gained body weight (figure 24).

Previous studies had shown, that in this model for IAV infection, the virus is cleared from the lung by day 9 to 14 after infection (Stegemann *et al.* 2009, Sharma-Chawla *et al.* 2016).

#### 4.2.1.1 Accumulation of macrophages and DC in the lung after resolution of IAV infection

In previous experiments of the group using the same experimental setup, the sustained accumulation of a $CD11c^+$/$SiglecF^+$ macrophage population in the lung following resolution of IAV infection along with significant changes to OVA-AAI had been observed (Wu *et al.* 2020). To further characterize the lung immune milieu in resolved IAV infection with respect to AM and IM, first an extended (conventional) flow cytometry staining panel was established (see table 6, p. 31 and figure 6, p. 43) and applied to lung leukocytes isolated following resolution of IAV infection (day 39). It enabled the differentiation between AM ($CD64^+$/$MerTK^+$/$CD11c^+$/$CD169^+$) and overall IM ($CD64^+$/$MerTK^+$/$CX3CR1^+$) and was based on findings of Ural *et al*. (Ural *et al.* 2020).

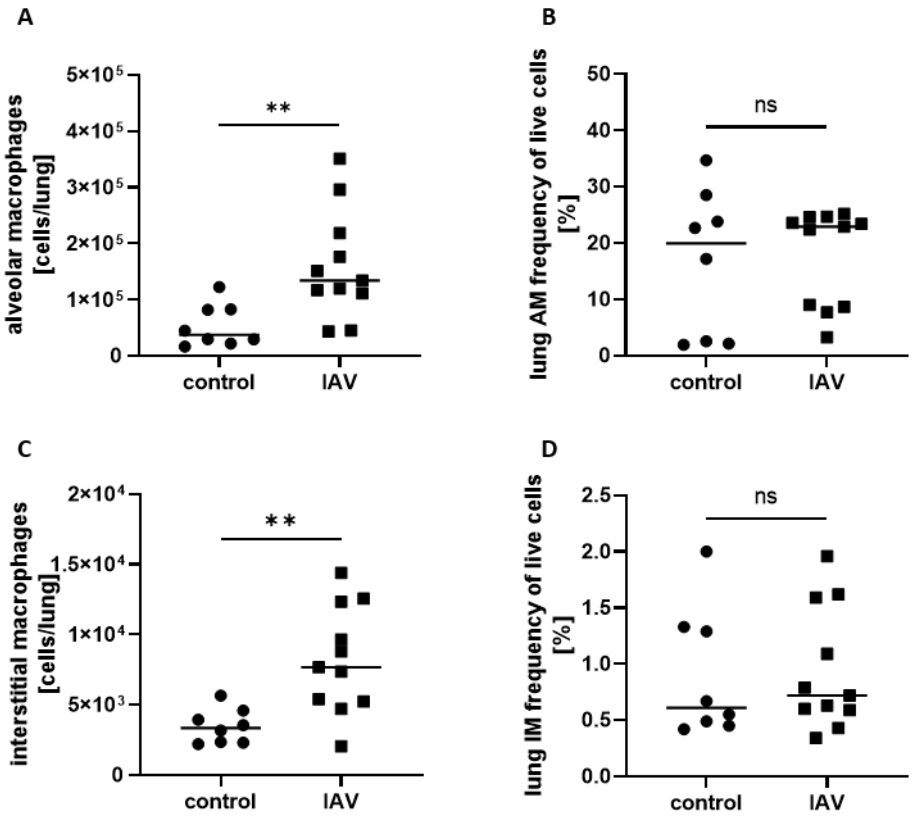


**figure 25: IAV infection led to a sustained accumulation of alveolar and interstitial macrophages in the lung.** Mice were infected with a sublethal dose of IAV and the control group was treated with PBS (for full treatment regimen see figure 23). Lung leukocytes were analyzed for (A, C) absolute cell numbers and (B, D) the frequencies of live cells (in %) for alveolar macrophages and interstitial macrophages. Data compiled from at least three independent experiments are shown for individual mice with the median. $^{**}p < 0.01$, ns = not significant.

In these analyses, a significant increase of the absolute numbers of lung AM and IM was observed 39 days after IAV infection as compared to PBS-treated mice (figure 25 A, C). The frequency of AM and IM within the isolated leukocytes (live cells) was not increased after IAV infection as compared to controls (figure 25 B, D). Nevertheless, the frequency gives an impression of the distribution of these two macrophage subpopulations in the lung. While AM made up to 20 %, only about 0.5 to 1.0 % of the isolated cells were IM.

Taken together, in line with previous studies, a significant increase of AM and IM in the lung long after IAV infection was observed in this thesis and provided the basis for a more detailed

analysis of macrophages, DC and monocytes in resolved IAV infection alone and in AAI induced after IAV infection. To this end, the spectral flow cytometry staining panel and analysis established in this thesis was employed.

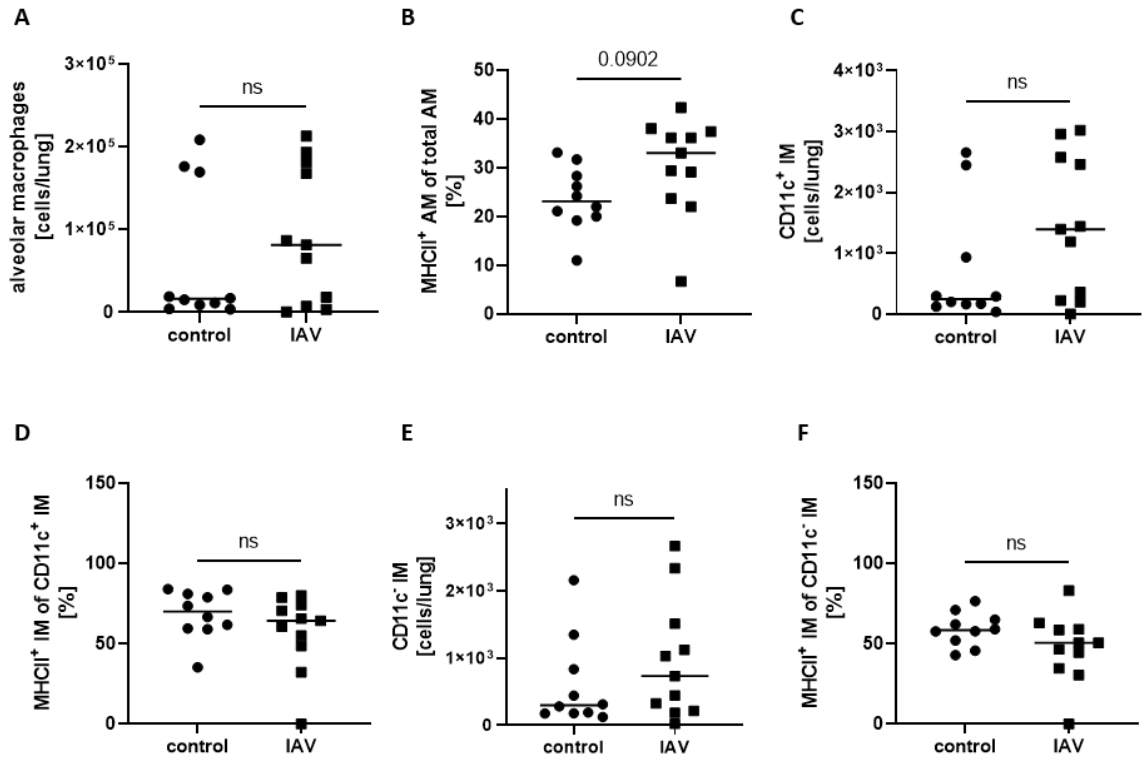


Figure continued on the next page.

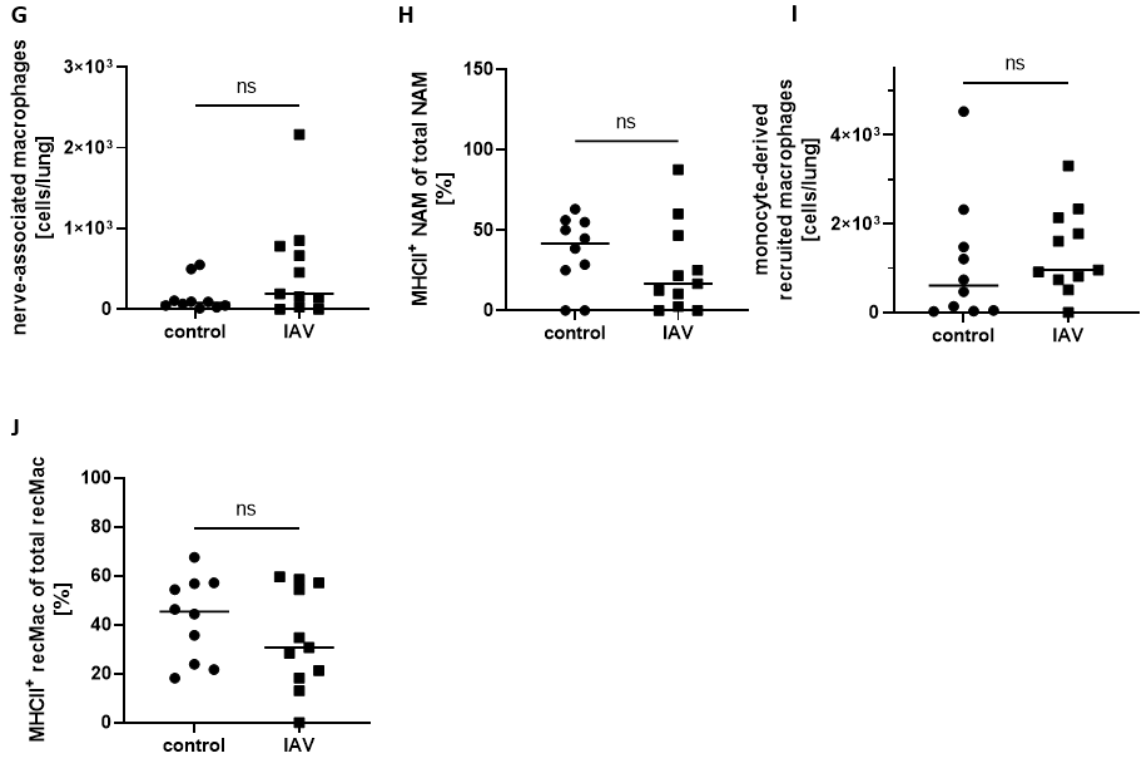


**figure 26: Absolute numbers and frequency of MHCII expression of different macrophage subsets in the lung after resolution of IAV infection yielded by spectral flow cytometric analysis.**
Mice were infected with a sublethal dose of IAV and the control group was treated with PBS (for full treatment regimen see figure 23). Lung leukocytes were analyzed for absolute numbers of (A) alveolar macrophages (AM), (C) $CD11c^+$ interstitial macrophages (IM), (E) $CD11c^-$ IM, (G) nerve-associated macrophages (NAM) and (I) monocyte-derived recruited macrophages (recMac). In (B, D, F, H, J) the MHCII expression of these macrophage subsets was analyzed (frequency of $MHCII^+$ cells within the population). Data compiled from at least three independent experiments are shown for individual mice with the median. ns = not significant.

Here, analysis of the different macrophage subsets in the lung revealed an increase in AM (1.46-fold), $CD11c^+$ (1.96-fold) and $CD11c^-$ IM (1.59-fold), NAM (3.26-fold) and recMac (1.25-fold) median cell numbers after resolution of IAV infection as compared to the control group. However, none of these increases reached statistical significance (figure 26 A, C, E, G, I). While the frequency of MHCII expression differed between the macrophage subsets, no significant differences in the frequency of $MHCII^+$ cells in these populations were observed in resolved

IAV infection as compared to the control group (figure 26 B, D, F, H, J). Nevertheless, there was a clear trend for increased MHCII expression after IAV infection for AM, while there was rather a decrease for NAM and recMac.

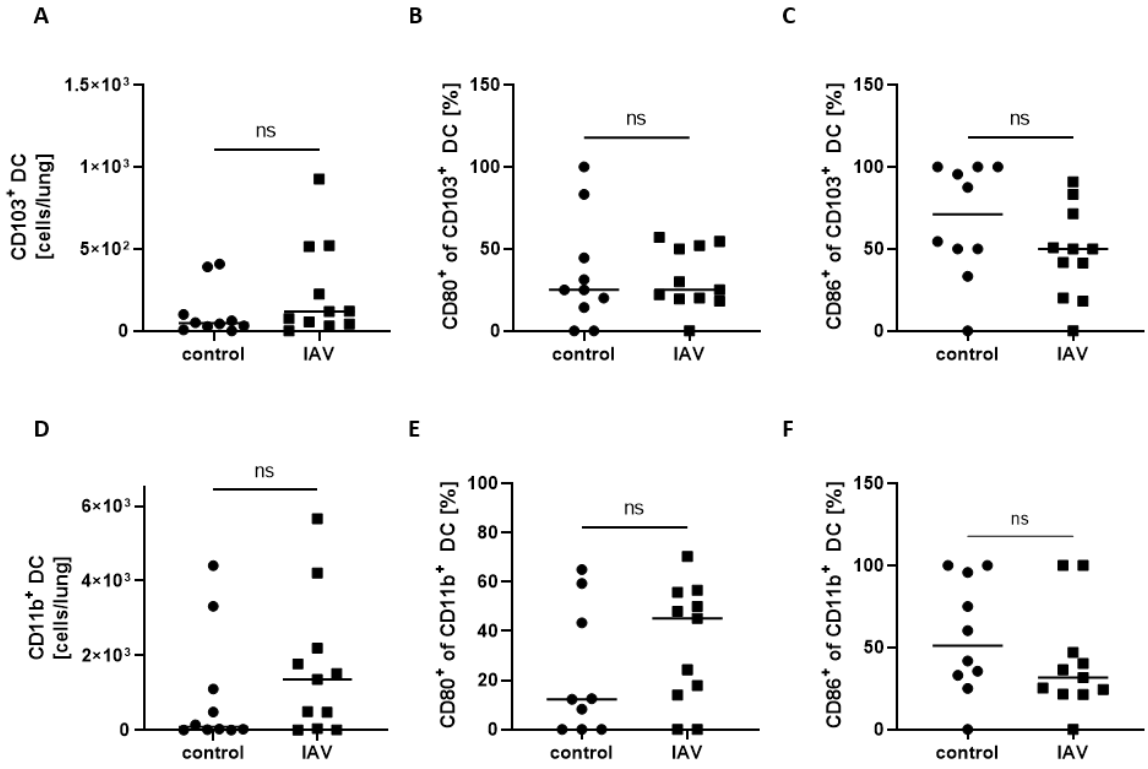


**figure 27: Accumulation and expression of activation markers of DC in the lung following IAV infection.**
Mice were infected with a sublethal dose of IAV and the control group was treated with PBS (for full treatment regimen see figure 23). Lung leukocytes were analyzed for cell numbers of (A) $CD103^+$ dendritic cells (DC) and (D) $CD11b^+$ DC. The activation status of these DC subsets was analyzed using the activation markers (B, E) CD80 and (C, F) CD86 (frequency of marker-expressing cells within the respective population). Data compiled from at least three independent experiments are shown for individual mice with the median. ns = not significant.

$CD103^+$ and $CD11b^+$ DC numbers in the lung showed a slight increase in resolved IAV infection, although this observation did not reach statistical significance (figure 27 A, D). There were no significant changes to the activation status (frequency of CD80 and CD86 expression) of DC

following IAV infection. However, for CD80 an increase in marker expressing CD11b$^+$ DC could be observed (figure 27 B, E), whereas for CD86 there was a trend for a decrease in marker expressing CD103$^+$ and CD11b$^+$ DC (figure 27 C, F).

Taken together, these analyses provided evidence for an impact of resolved IAV infection mainly on lung macrophages and possibly also on lung DC. Using conventional flow cytometry, a significant increase of AM and IM was detected. In the subsequent, more detailed analysis using spectral flow cytometry a slight, varying increase for AM, CD11c$^+$ and CD11c$^-$ IM, NAM, recMac as well CD103$^+$ and CD11b$^+$ DC numbers was observed 39 days after IAV infection, even though these effects did not reach statistical significance. Potential effects of resolved IAV on the frequency of MHCII expression of macrophages was strongest for AM, however overall without significant alterations. In DC, potential activation in resolved IAV infection was restricted to increased CD80-expression of CD11b$^+$ DC, albeit likewise without statistical significance.

Parts of the analysis of only IAV infected and otherwise control-treated mice was also performed within the treatment regimen of the HDM-mediated mouse model of AAI (see figure 23 B). Here, analysis of macrophage and DC in resolved IAV infection by spectral flow cytometry yielded similar results as for the OVA treatment regimen (data not shown).

#### 4.2.1.2 Long-term effects of IAV infection on cytokine and serum albumin levels in the respiratory tract

Based on the changes detected mainly in macrophages and partly in DC long after IAV infection, levels of the cytokines IL-1α, IL-1β, IL-3, IL-12p40 and IL-12p70, IL-23, IL-7, IL-11, IL-27, IL-33, IFN-β, GM-CSF and TSLP were measured in lung homogenates. This set of cytokines was chosen due to associations with the respiratory epithelium (IL-33, TSLP) and macrophages (GM-CSF, IL-33) next to general inflammation. Of note, IL-33 and GM-CSF had

been shown to be associated with polynucleation and polyploidy of AM in AAI (Quell *et al.* 2020), which we had previously also observed in this experiment model (Wu *et al.* 2020). Furthermore, the cytokines IFN-γ, IL-5, TNF-α, IL-2, IL-6, IL-4, IL-9, IL-10, IL-17A, IL-17F, IL-22 and IL-13 were measured at the supernatant of the BAL using a multiplex-based immunoassay to assess effects on the local cytokine milieu with respect to type 1, 2 and 3 inflammation (see 3.10, p. 48).

As described before (see 4.1.1), respiratory infections can also lead to reduced pulmonary function in increased capillary leakage. Therefore, the concentration of serum albumin in the BAL was also determined after resolution of IAV infection to assess sustained changes to barrier integrity.

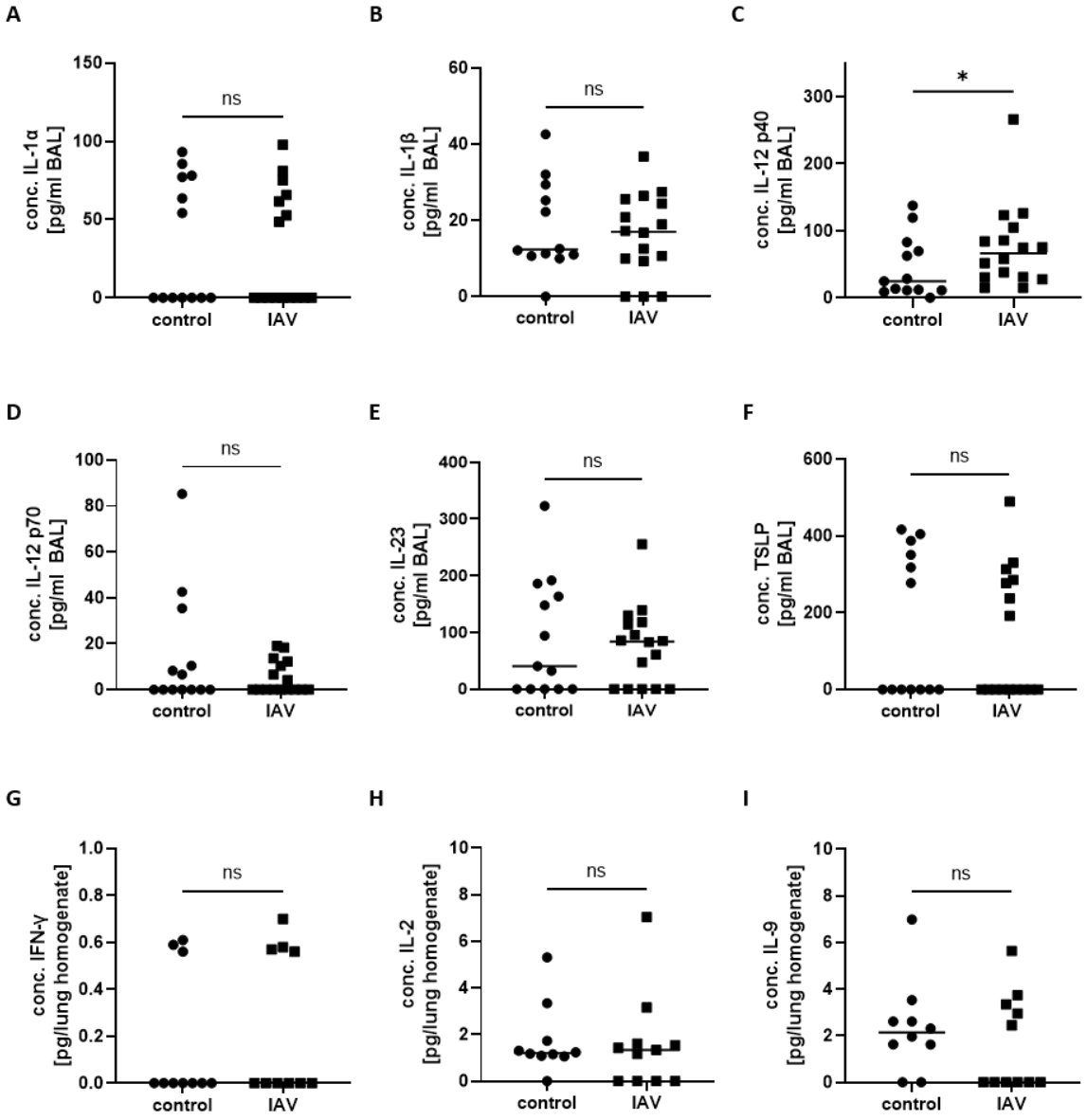


**figure 28: Cytokine levels in lung homogenates and BAL 39 days after *i.n*. IAV infection.**
Mice were infected with a sublethal dose of IAV and the control group was treated with PBS (for full treatment regimen see figure 23). On day 39, lung homogenates and bronchoalveolar lavage (BAL) were prepared for analysis. The concentrations of (A) IL-1α, (B) IL-1β, (C) IL-12p40, (D) IL-12p70, (E) IL-23 and (F) TSLP were analyzed in lung homogenates. The concentrations of (G) IFN-γ, (H) IL-2 and (I) IL-9 were obtained from BAL samples. Data are shown for individual mice with the median. *$p < 0.05$, ns = not significant.

For the analyzed cytokines IL-3, IL-7, IL-11, IL-27, IL-33, IFN-β, GM-CSF, IL-6, IL-4, IL-10, IL-17A, IL-17F, IL-22, IL-13, IL-5 and TNF-α almost all samples yielded concentrations below the detection limit for the control group and samples from mice after IAV infection (data not shown).

On day 39 after IAV infection, a significant increase was observed for IL-12p40 in lung homogenates as compared to the control group in the OVA treatment regimen (figure 28 C). Concentrations of all other cytokines were not significantly changed following resolution of IAV infection and alterations were only marginal and without statistical significance (figure 28 A, B, D-I). However, the significant increase in IL-12p40 further supported sustained IAV-mediated effects on the lung immune micromillieu.

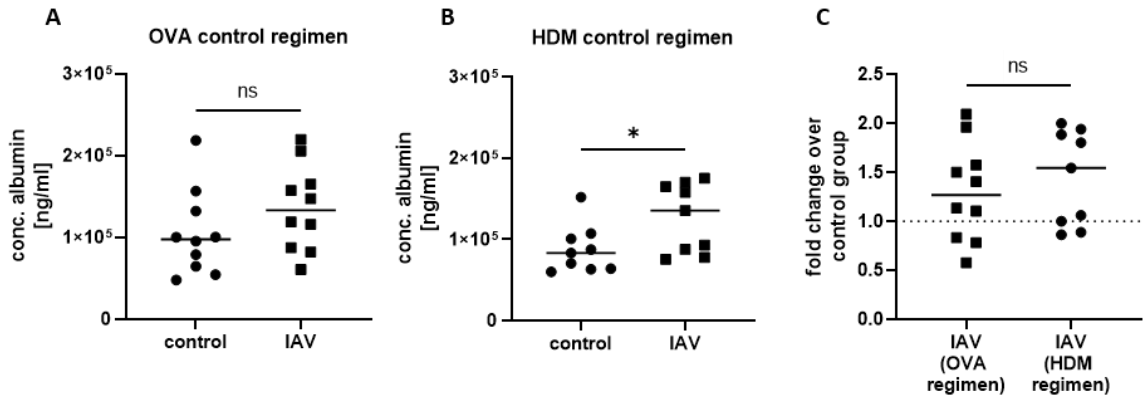


**figure 29: Concentrations of serum albumin in the BAL after IAV infection.**
Mice were infected with a sublethal dose of IAV and the control group was treated with PBS (for full treatment regimen see figure 23). On day 39 (OVA model) and day 37 (HDM model), respectively, bronchoalveolar lavage (BAL) were harvested to determine (A, B) the concentrations of serum albumin. (C) The fold changes of IAV infected mice over the respective control group were calculated for both regimen. Data compiled from at least three independent experiments are shown for individual mice with the median. *$p < 0.05$, ns = not significant.

In both control treatment regimen, an increase in the median concentration of serum albumin in BAL as compared to the respective uninfected control group was observed (figure 29 A-C),

which was statistically significant for mice treated according to the HDM regimen. Comparing the IAV only infected group of the OVA treatment regimen to the IAV only infected group of the HDM treatment regimen with respect to the fold change in serum albumin levels over the control, this was slightly higher in the HDM regimen as compared to the OVA regimen, although it did not reach statistical significance (figure 29 C).

In summary, resolved IAV infection had only marginal effects on the analyzed respiratory tract cytokine levels. Nevertheless, the statistically significant increase of IL-12p40, a well-known inducer for the Th1 response (Wang *et al.* 1999) and the increase in serum albumin in the BAL, as an indicator for capillary leakage, indeed pointed at sustained IAV-associated changes to the respiratory (immune) micromillieu. Together with the significantly increased numbers of AM and IM detected in conventional flow cytometry, these IAV-mediated changes laid the basis for exploring IAV-mediated effects in subsequently induced AAI.

### 4.2.2 Effects of resolved IAV infection on subsequently induced OVA-AAI and HDM-AAI

The analyses in this study had so far shown a clear and partly model-specific involvement of macrophages and DC in OVA-AAI and HDM-AAI as well as changes in macrophages, partly in DC and on cytokine and serum albumin levels in the BAL in resolved IAV infection. The extent to which IAV affects subsequent AAI was then investigated in both models of AAI.

To analyze the influence of a previous and resolved IAV infection on subsequently induced AAI, mice were sensitized against OVA or treated with HDM after recovery from the infection (see figure 23). As in the previous experiments analyzing IAV-mediated effects on the local (immune) micromillieu, mice were *i.n.* infected with a sublethal dose of 0.31 $TCID_{50}$ IAV A/PR/8/34 (H1N1). From two or three weeks after the IAV infection, respectively, OVA-AAI or HDM-AAI was induced as described. Here, AAI alone (as shown above for the comparison of

the models) and AAI following IAV infection were compared for both models with respect to serum IgE and BAL serum albumin levels, respiratory immune cell accumulation and phenotypic alterations as well as cytokines. Fold changes in these parameters (IAV + AAI over AAI only) were compared between OVA-AAI and HDM-AAI. For the detailed analysis of macrophage and DC subsets, as well as monocytes, spectral flow cytometry was performed as described above.

#### 4.2.2.1 Long-term effects of IAV infection on lung key cellular effectors, respiratory tract cytokines and serum albumin levels as well as serum IgE levels in OVA-AAI and HDM-AAI

Comparing AAI without and with previous IAV infection, no significant differences were observed regarding the absolute number of leukocytes in the lung in OVA-AAI or HDM-AAI (figure 30 A, B). Similar results were found for the numbers of eosinophils and neutrophils in the lung. Neither IAV + OVA-AAI nor IAV + HDM-AAI showed significant differences as compared to AAI alone (figure 30 D, E, G, H). Of note however, mean cell numbers for overall leukocytes, eosinophils and neutrophils were generally lower in IAV + AAI as compared to AAI alone. Comparing the fold change in cell numbers between IAV + AAI and AAI between both models revealed this reduction to be more pronounced in HDM-AAI as compared to OVA-AAI (figure 30 C, F, I). However, these differences in fold change reduction between the models did not reach statistical significance.

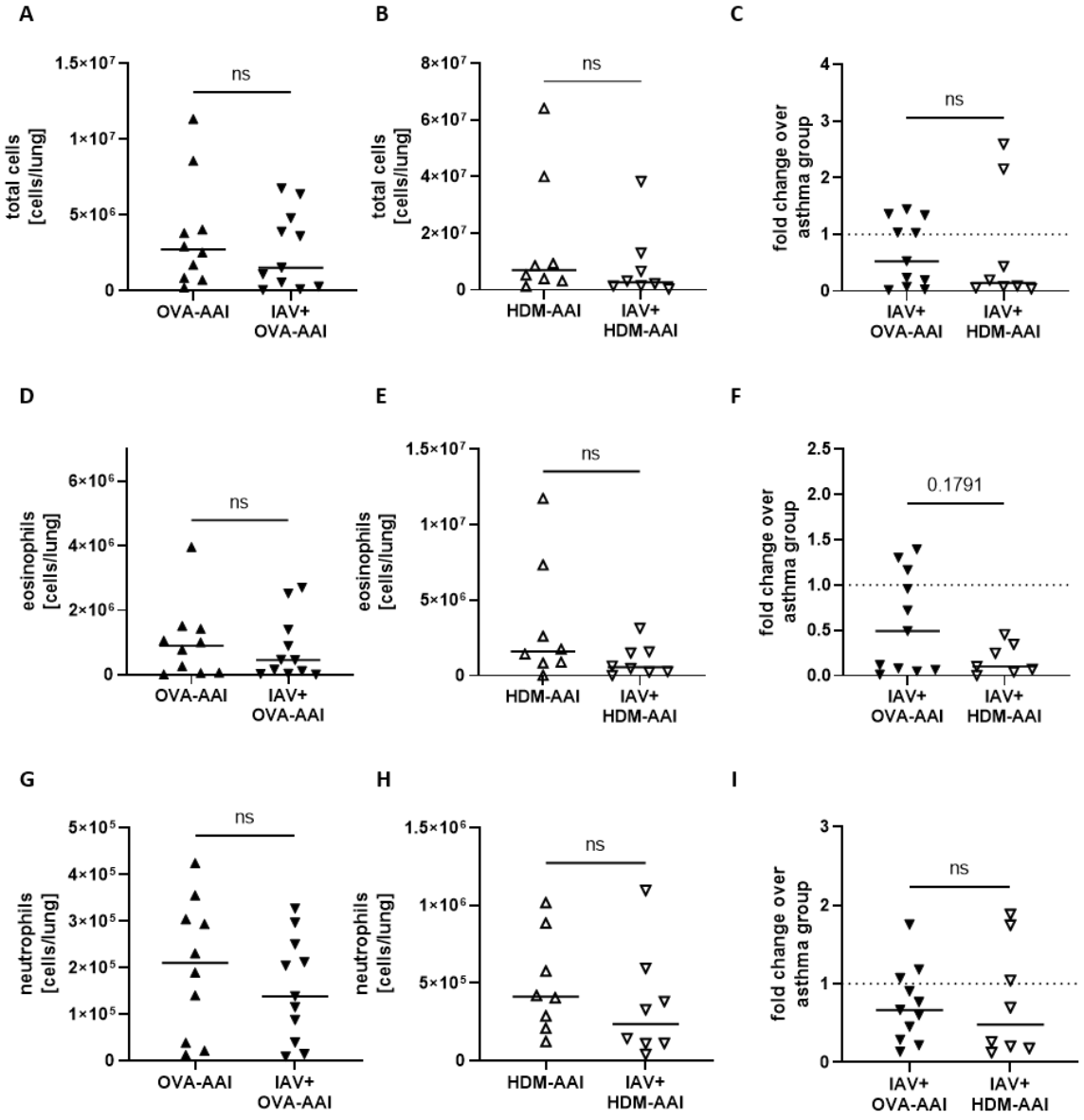


**figure 30: Resolved IAV infection did not lead to significant changes in overall leukocyte, eosinophil or neutrophil recruitment to the lung in OVA-AAI or HDM-AAI.**
Mice were infected with a sublethal dose of IAV or treated with PBS. For the induction of allergic airway inflammation (AAI), mice were treated with ovalbumin (OVA) (and aluminum hydroxide (alum) for sensitization) or house dust mite extract (HDM) as described. Lung leukocytes were analyzed for total cell counts (A-C), eosinophil numbers (D-F) and neutrophil numbers (G-I). Data compiled from at least three independent experiments are shown for individual mice with the median. ns = not significant.

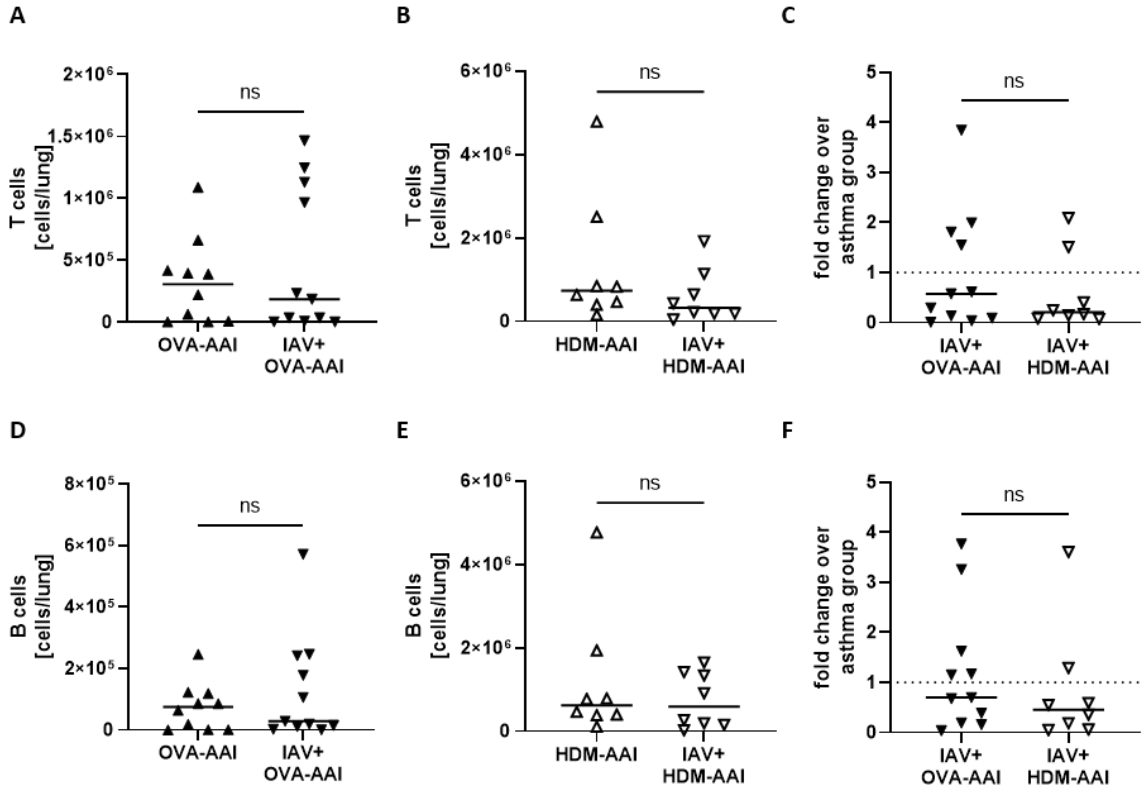


**figure 31: Resolved IAV infection did not led to significant changes in overall T cell or B cell accumulation in the lung in OVA-AAI or HDM-AAI.**
Mice were infected with a sublethal dose of IAV or treated with PBS. For the induction of allergic airway inflammation (AAI), mice were treated with ovalbumin (OVA) (and aluminum hydroxide (alum) for sensitization) or house dust mite extract (HDM) as described. Lung leukocytes were analyzed for T cell (A-C) and B cell (D-F) numbers. Data compiled from at least three independent experiments are shown for individual mice with the median. ns = not significant.

T and B cell numbers in the lung were not significantly changed in IAV + OVA-AAI and IAV + HDM-AAI as compared to the respective AAI group (figure 31 A, B, D ,E). Comparing the fold changes in T and B cell numbers between IAV + AAI and AAI between both models, no significant differences could be observed while fold change reduction over AAI only was stronger in IAV + HDM-AAI as compared to IAV + OVA-AAI in both cases (figure 31 C, F).

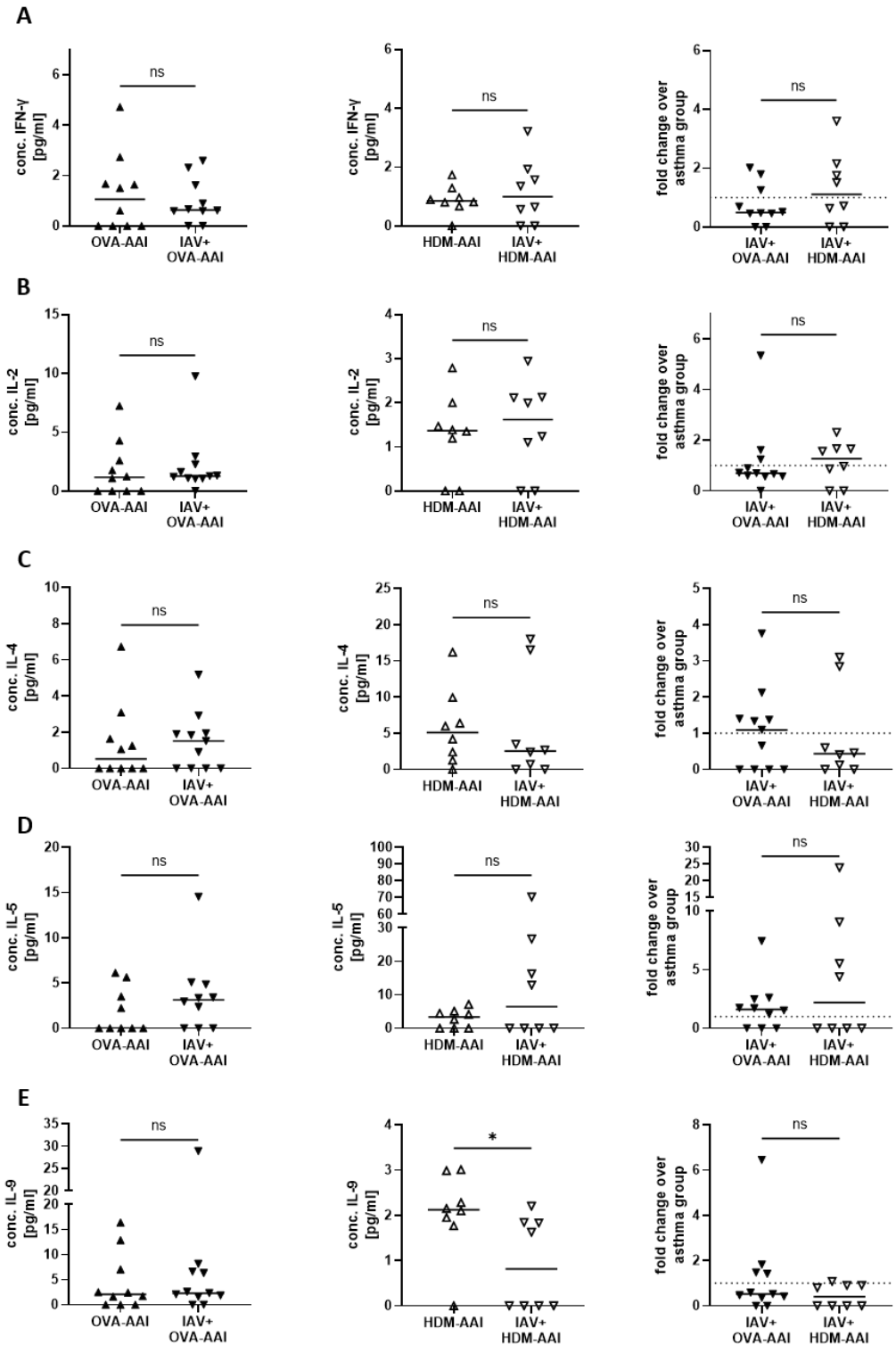


Figure continued on the next page.

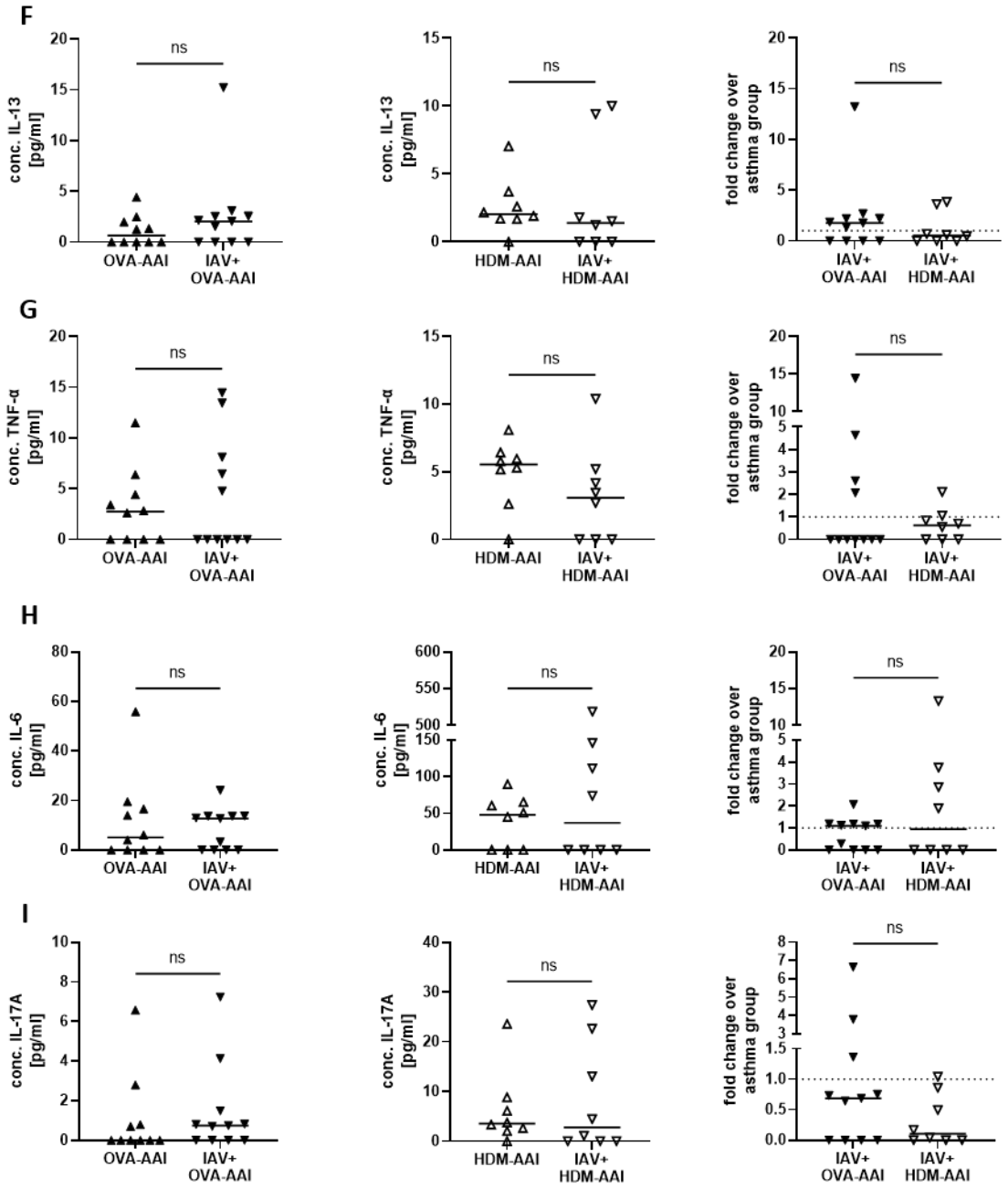


**figure 32: Previous, resolved IAV infection led to significantly reduced BAL IL-9 concentrations in HDM-AAI while not significantly affecting other cytokines.**

Mice were infected with a sublethal dose of IAV or treated with PBS. For the induction of allergic airway inflammation (AAI), mice were treated with ovalbumin (OVA) (and aluminum hydroxide (alum) for sensitization) or house dust mite extract (HDM) as described. On day 39 (OVA model) and day 37 (HDM model), respectively, BAL was analyzed for concentrations of interferon (IFN)-γ (A), interleukin 2 (IL-2) (B), IL-4 (C), IL-5 (D), IL-9 (E),

IL-13 (F), tumor necrosis factor (TNF)-α (G), IL-6 (H) and IL-17A (I)**.** Data compiled from at least three independent experiments are shown for individual mice with the median. *$p < 0.05$, ns = not significant.

The cytokines IFN-γ, IL-5, TNF-α, IL-2, IL-6, IL-4, IL-9, IL-10, IL-17A, IL-17F, IL-22 and IL-13 were quantified in the BAL to assess effects of resolved IAV infection on the local cytokine milieu in AAI (see 3.10, p. 48). For IL-10, IL-17F and IL-22 the cytokine levels were below the LOD for all samples (data not shown).

The median concentrations of the Th1 cytokines IFN-γ and IL-2 were nearly unchanged between all experimental groups. While IFN-γ was rather reduced in IAV + OVA-AAI as compared to OVA-AAI alone, there were nevertheless no prominent or significant differences in the fold change over AAI alone between IAV + OVA-AAI and IAV + HDM-AAI (figure 32 A, B). IL-4 concentrations were also not significantly changed in either model, but a trend for decreased IL-4 was present in IAV + HDM-AAI as compared to HDM-AAI alone. This also became apparent from the fold changes over AAI that was < 1 for IAV + HDM-AAI but not IAV + OVA-AAI (figure 32 C). For IL-5, concentrations in the BAL were marginally higher in IAV + AAI as compared to AAI alone in both models, however without statistical significance (figure 32 D). IL-9 was significantly decreased in IAV + HDM-AAI as compared to HDM-AAI, while the median IL-9 level remained unchanged in OVA-AAI after resolved IAV infection as compared to OVA-AAI alone (figure 32 E). For IL-13, the median concentrations were nearly unchanged in both AAI models after resolution of IAV infection as compared to the respective AAI group (figure 32 F). The proinflammatory cytokine TNF-α was reduced in IAV + AAI as compared to AAI alone in both models, albeit without statistical significance (figure 32 G). IL-6 and IL-17A levels were also not significantly changed in IAV + AAI as compared to the respective AAI group, neither was the fold change between both models (figure 32 H, I).

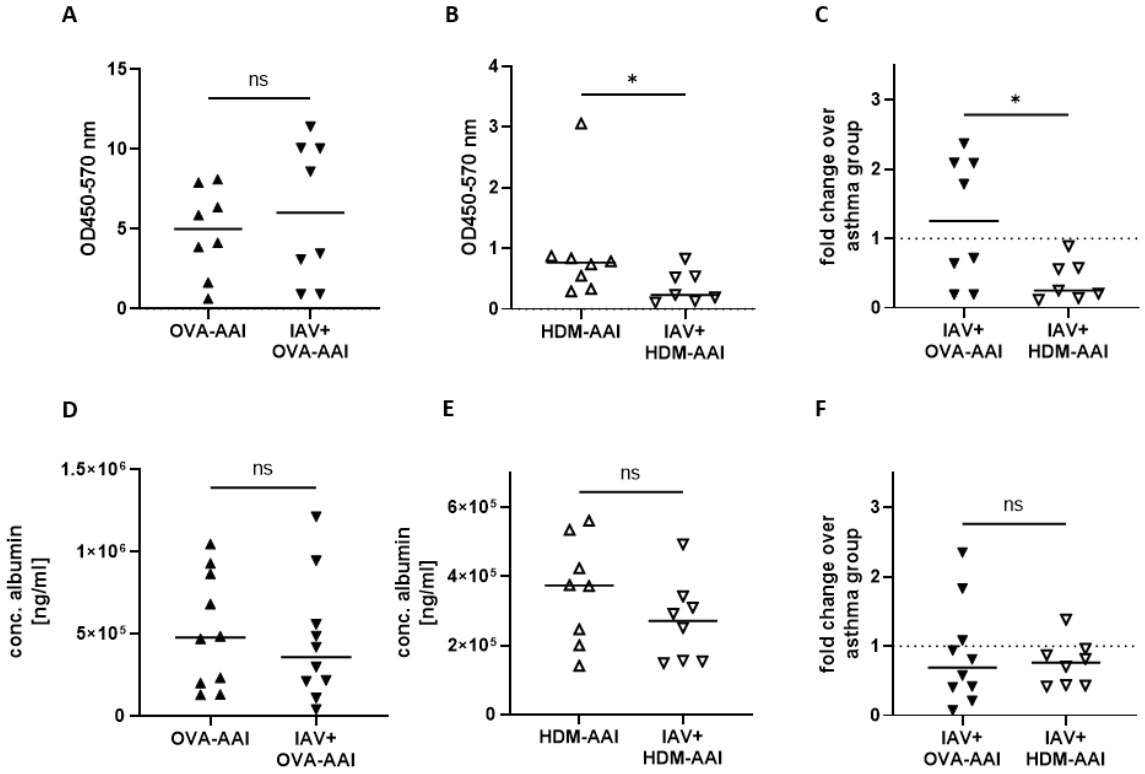


**figure 33: Total IgE levels in the serum and serum albumin concentrations in the BAL in OVA-AAI and HDM-AAI without and with previous IAV infection.**
Mice were *i.n*. infected with IAV or treated with PBS. After recovery, allergic airway inflammation (AAI) was induced. Mice were treated with ovalbumin (OVA) (and aluminum hydroxide (alum) for sensitization) or house dust mite extract (HDM) as described. On day 39 (OVA model) and day 37 (HDM model), respectively, (A-C) total IgE-levels were assessed in the serum and (D-F) serum albumin concentrations were assessed in the BAL**.** Data compiled from at least three independent experiments are shown for individual mice with the median. *$p < 0.05$, ns = not significant.

Interestingly, the effect of previous IAV infection on serum IgE levels significantly differed between OVA-AAI and HDM-AAI induced following resolved IAV infection. In IAV + OVA-AAI a slight, but not significant increase in total serum IgE was observed as compared to OVA-AAI alone (figure 33 A). In contrast, in IAV + HDM-AAI serum IgE levels were significantly reduced as compared to HDM-AAI alone (figure 33 B). Comparing the fold change in IgE levels between IAV + AAI and AAI between both models, the reduction was significantly more pronounced in HDM-AAI as compared to OVA-AAI (figure 33 C).

To evaluate, to which extent resolved IAV infection affected capillary permeability as it was detected in AAI alone (see 4.1.1), the concentration of serum albumin in BAL was analyzed. In OVA-AAI and HDM-AAI, resolved infection with IAV to a similar extent led to slightly, although not significantly, reduced concentrations of serum albumin in the BAL as compared to AAI alone (figure 33 D-F).

Taken together, modulation of AAI though a previous, resolved IAV infection was marginal in most of these parameters. Overall, IAV infection nevertheless seemed to rather attenuate than aggravate AAI. IAV infection led to a slight decrease in absolute cell numbers as well as numbers of eosinophils and neutrophils in the lungs in AAI as compared to OVA-AAI and HDM-AAI alone. Moreover, total IgE levels and IL-9 concentrations were significantly decreased in IAV + HDM-AAI as compared to AAI alone, supporting attenuation of AAI by previous IAV infection and highlighting the need to consider model-specific characteristics.

#### 4.2.2.2 Effects on the lung macrophage compartment in AAI induced after resolution of IAV infection

Based on their strong involvement shown in the characterization of OVA-AAI and HDM-AAI alone, the five distinct macrophage populations in the lung defined above were analyzed by spectral flow cytometry, combining the two AAI-models with previous IAV infection: AM, $CD11c^+$ and $CD11c^-$ IM, NAM and recMac.

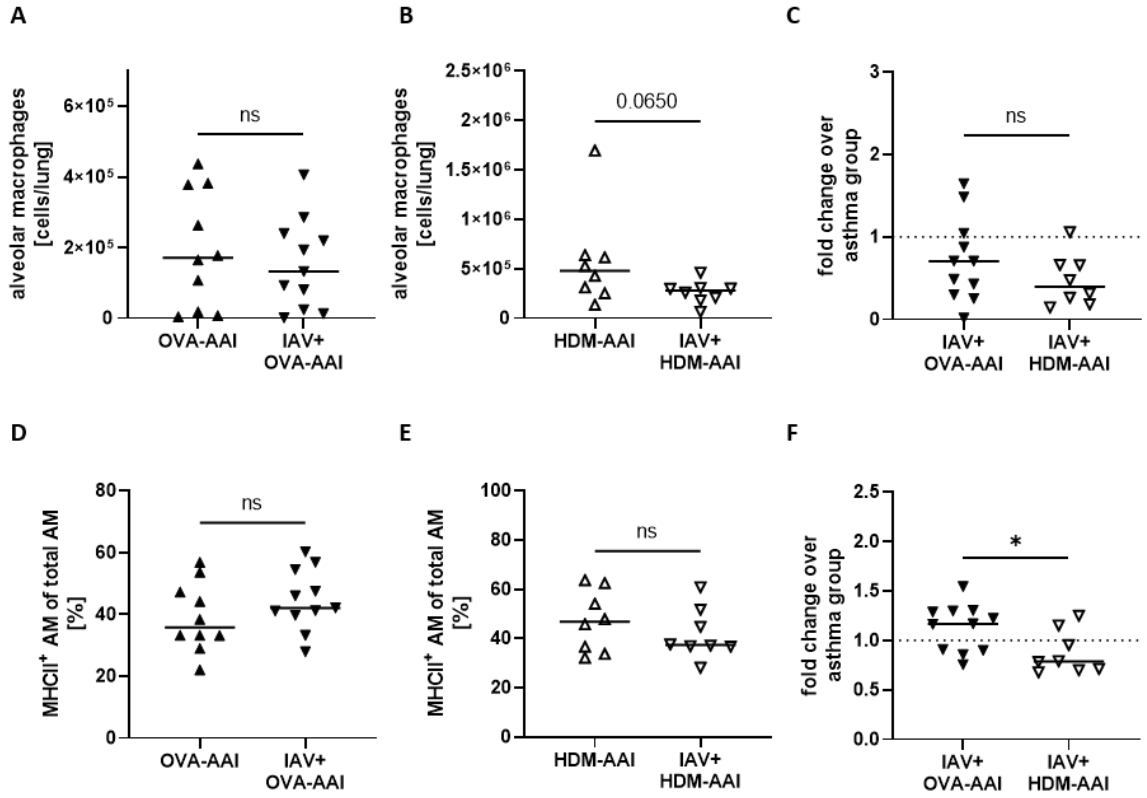


**figure 34: Impact of resolved IAV infection on absolute numbers and the frequency of MHCII expression of alveolar macrophages in the lung.**
Mice were *i.n*. infected with IAV or treated with PBS. After recovery, allergic airway inflammation (AAI) was induced. Mice were treated with ovalbumin (OVA) (and aluminum hydroxide (alum) for sensitization) or house dust mite extract (HDM) as described. On day 39 (OVA model) and day 37 (HDM model), respectively, absolute numbers of alveolar macrophages (AM) (A-C) and the frequency of their MHCII expression (D-F) were assessed. Data compiled from at least three independent experiments are shown for individual mice with the median. *$p < 0.05$, ns = not significant.

The absolute numbers of AM in the lung were unchanged in IAV + OVA-AAI and moderately decreased in IAV + HDM-AAI as compared to AAI alone (figure 34 A, B). This reduction however did not reach statistical significance (p = 0.065). Furthermore, comparing the IAV-mediated changes between the models, the median fold change over the respective AAI only group was decreased comparing IAV + HDM-AAI and IAV + OVA-AAI, pointing at stronger reduction of AM numbers in IAV + HDM although it did not reach statistical significance between the

models (figure 34 C). Effects of previous IAV infection on the frequency of MHCII-positive AM significantly differed between the two models. While the OVA-AAI model showed a marginal increase in the frequency of MHCII$^+$ AM in AAI induced after IAV infection, the IAV + HDM-AAI model rather showed a reduction as compared to HDM-AAI alone (figure 34 D, E). While both changes themselves did not reach statistical significance, this difference resulted in a significant difference in the fold change over the respective AAI group comparing IAV + OVA-AAI and IAV + HDM-AAI (figure 34 F).

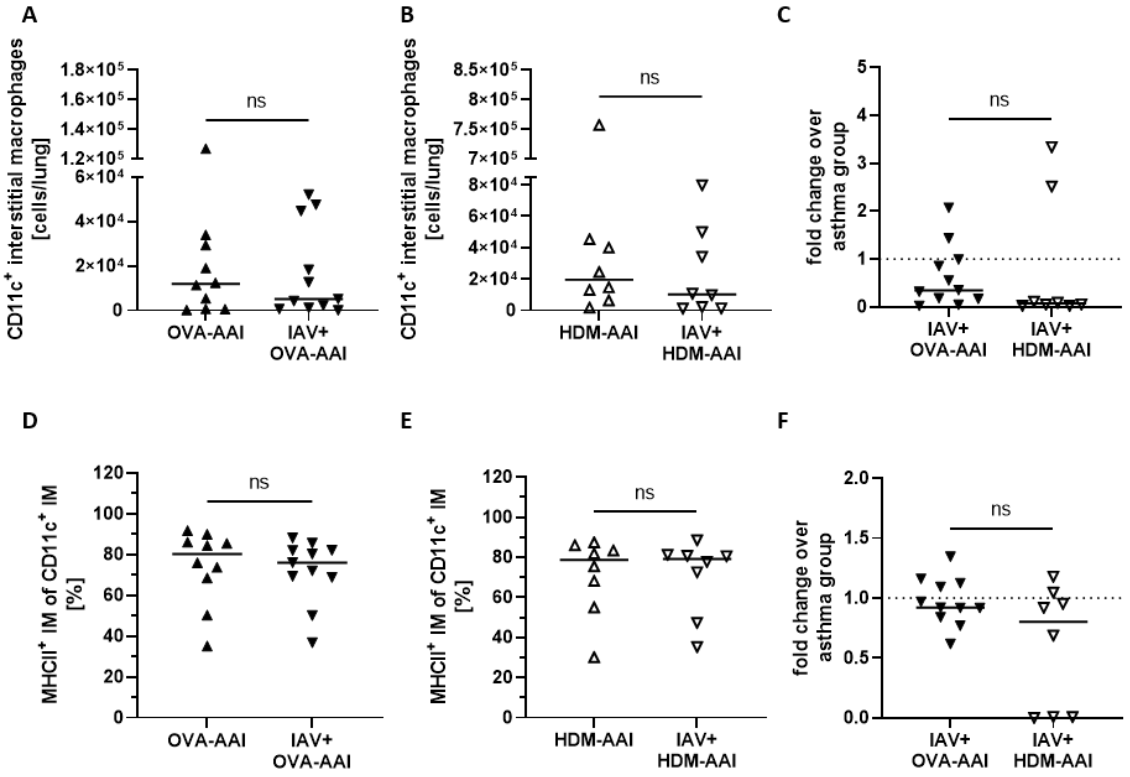


Figure continued on the next page.

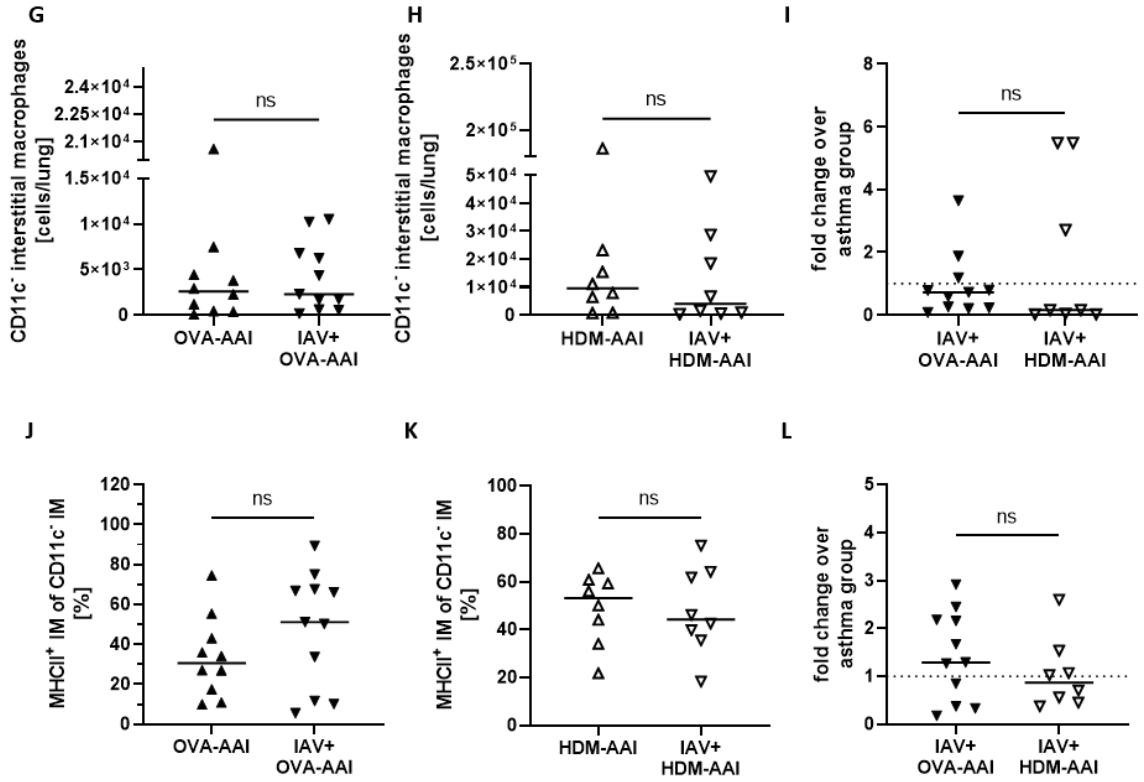


**figure 35: Resolved IAV infection did not significantly affect absolute numbers of lung IM and their frequency of MHCII expression in AAI.**
Mice were *i.n*. infected with IAV or treated with PBS. After recovery, allergic airway inflammation (AAI) was induced. Mice were treated with ovalbumin (OVA) (and aluminum hydroxide (alum) for sensitization) or house dust mite extract (HDM) as described. On day 39 (OVA model) and day 37 (HDM model), respectively, absolute numbers of $CD11c^+$ interstitial macrophages (IM) (A-C) and $CD11c^-$ IM (G-I) and their frequency of MHCII expression (D-F and J-L) were assessed. Data compiled from at least three independent experiments are shown for individual mice with the median. ns = not significant.

Both, $CD11c^+$ and $CD11c^-$ IM numbers were not significantly changed in AAI induced after IAV infection as compared to AAI alone in either model (figure 35 A-C and G-I). Also, the frequency of MHCII expression of $CD11c^+$ IM in AAI was not affected by previous IAV infection in both models (figure 35 D-F). As in AM, the MHCII expression of $CD11c^-$ IM differed between both models. While it rather decreased in IAV + HDM-AAI as compared to HDM-AAI alone, there was a slight increase in IAV + OVA-AAI as compared to OVA-AAI alone (figure 35 J, K). In

contrast to AM, the fold change over the respective AAI only group did not reach statistical significance between the two models (figure 35 L).

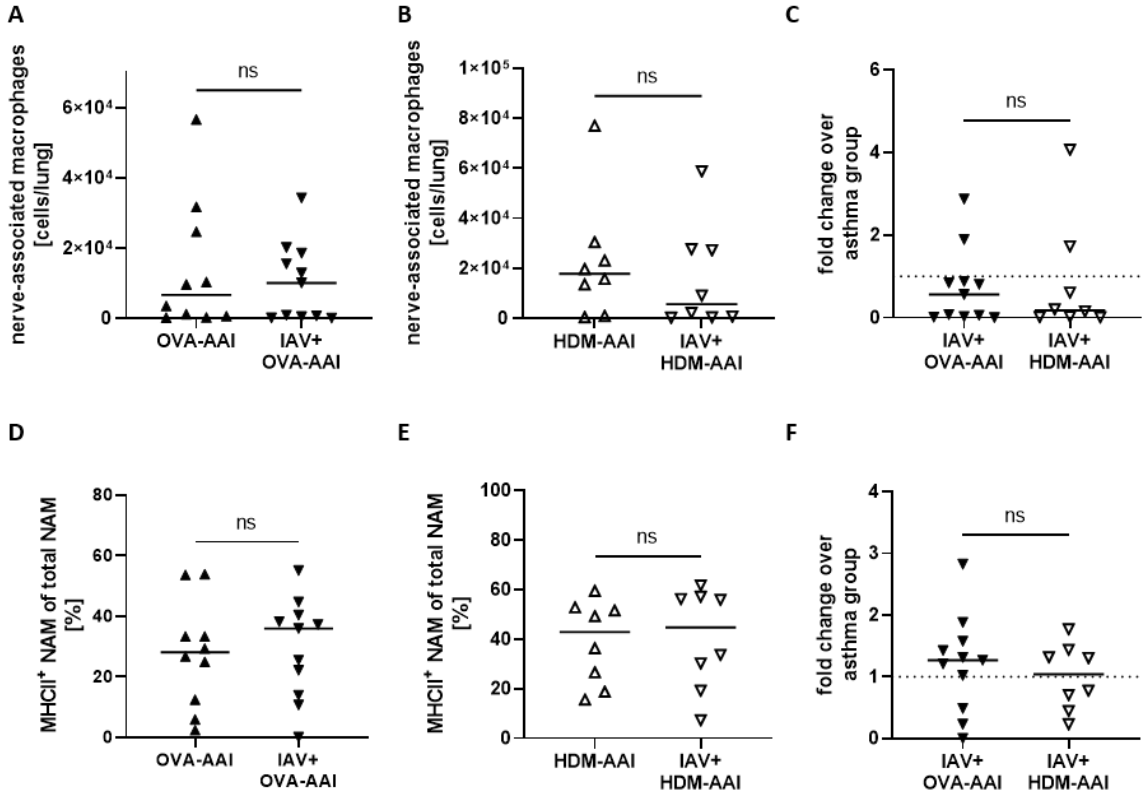


**figure 36: The effect of IAV infection on nerve-associated macrophage numbers and their frequency of MHCII expression in OVA-AAI and HDM-AAI.**
Mice were *i.n.* infected with IAV or treated with PBS. After recovery, allergic airway inflammation (AAI) was induced. Mice were treated with ovalbumin (OVA) (and aluminum hydroxide (alum) for sensitization) or house dust mite extract (HDM) as described. On day 39 (OVA model) and day 37 (HDM model), respectively, absolute numbers of nerve-associated macrophages (NAM) (A-C) and the frequency of their MHCII expression (D-F) were assessed. Data compiled from at least three independent experiments are shown for individual mice with the median. ns = not significant.

As for the other macrophage subsets, NAM were not significantly affected in IAV + AAI as compared to AAI alone in either model. However, whereas in IAV + OVA-AAI no change was observed, in IAV + HDM-AAI the number of NAM was marginally decreased in comparison to

AAI alone (figure 36 A, B). Despite this difference, the fold change over the respective AAI group was not significantly different between both models (figure 36 C). The frequency of MHCII expression of NAM was not altered in either IAV + OVA-AAI nor IAV + HDM-AAI as compared to AAI alone (figure 36 D, E, F).

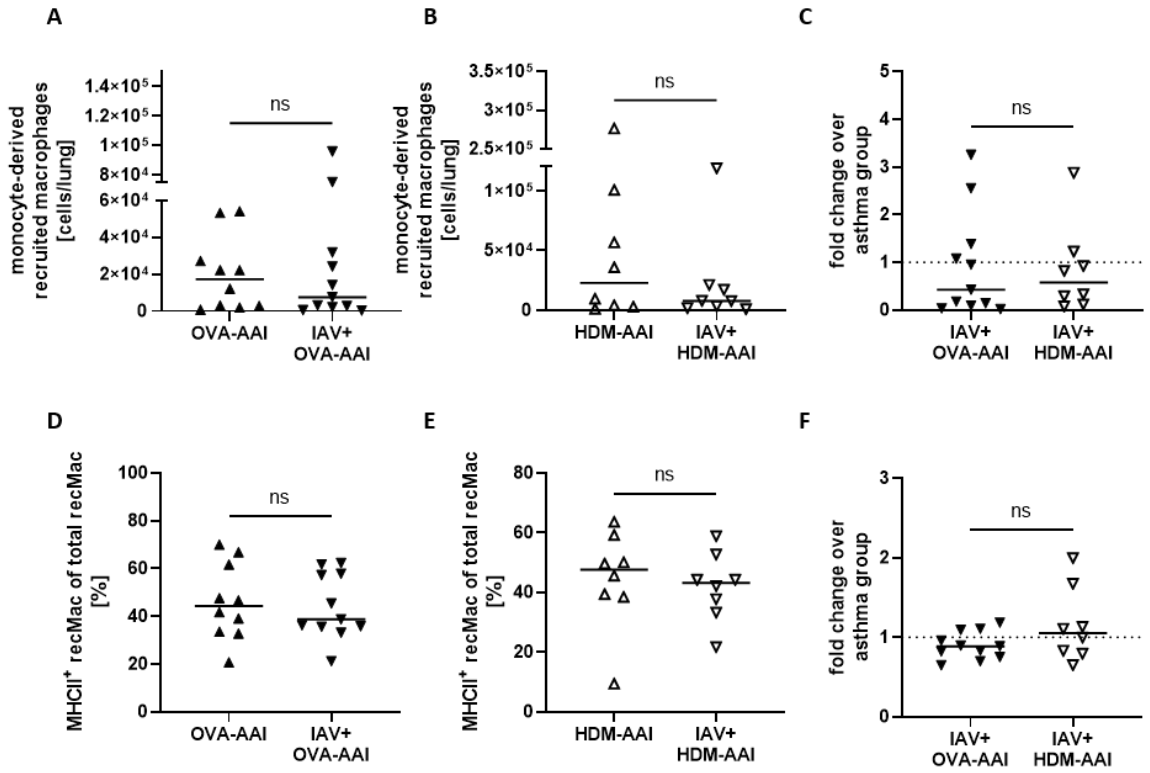


**figure 37: Monocyte-derived recruited macrophages were not affected by previous IAV infection in OVA-AAI or HDM-AAI.**

Mice were *i.n*. infected with IAV or treated with PBS. After recovery, allergic airway inflammation (AAI) was induced. Mice were treated with ovalbumin (OVA) (and aluminum hydroxide (alum) for sensitization) or house dust mite extract (HDM) as described. On day 39 (OVA model) and day 37 (HDM model), respectively, (A-C) absolute numbers of monocyte-derived recruited macrophages (recMacs) and (D-F) the frequency of their MHCII expression were assessed. Data compiled from at least three independent experiments are shown for individual mice with the median. ns = not significant.

Although the absolute numbers of lung recMac also did not change significantly in IAV + AAI in both models, they were likewise decreased by trend as compared to OVA-AAI and HDM-AAI alone, respectively (figure 37 A-C). The frequency of MHCII expression on recMac was unchanged between AAI without and previous IAV infection (figure 37 D-F).

Taken together, in both AAI models there were no significant differences in absolute numbers for all analyzed macrophage subsets if AAI was induced following IAV infection as compared to AAI alone. While the same was generally true for lung macrophage MHCII expression, the minor effects of IAV in OVA-AAI and HDM-AAI at times diverged, leading to a significant difference in the fold change over AAI alone for MHCII expression of AM between both models.

#### 4.2.2.3 Impact of resolved IAV infection on the lung dendritic cell compartment in subsequently induced OVA-AAI and HDM-AAI

As for macrophages, comparative characterization of OVA-AAI and HDM-AAI revealed strong involvement of DC that was partly subset- and model-specific. Therefore, these DC subsets were analyzed in AAI preceded by IAV infection in both models.

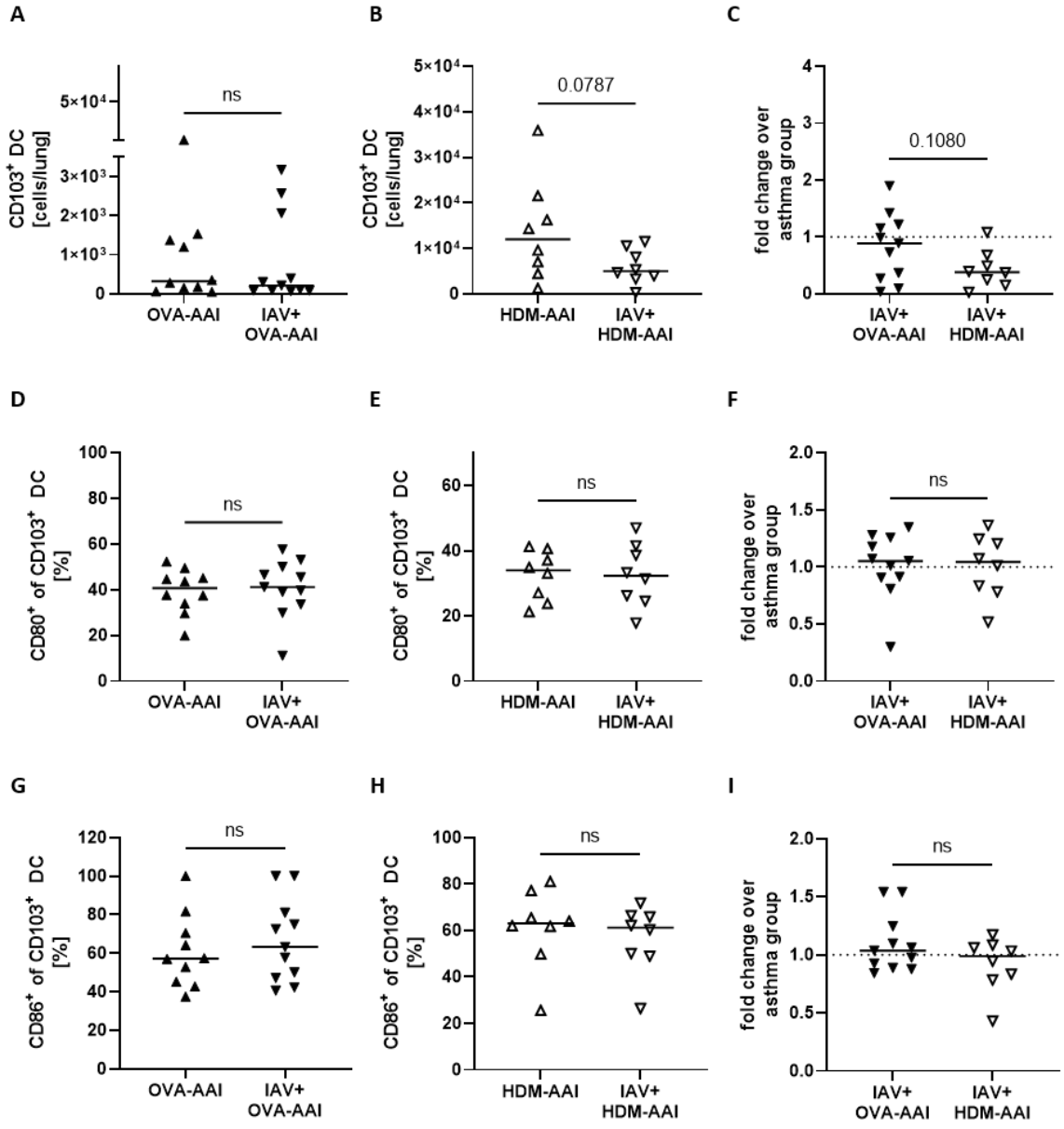


**figure 38: Absolute numbers and activation marker expression of CD103⁺ DC in OVA-AAI and HDM-AAI induced following resolution of IAV infection.**

Mice were infected with a sublethal dose of IAV or treated with PBS. After recovery, allergic airway inflammation (AAI) was induced. Mice were treated with ovalbumin (OVA) (and aluminum hydroxide (alum) for sensitization) or house dust mite extract (HDM) as described. On day 39 (OVA model) and day 37 (HDM model), respectively, lung leukocytes were analyzed for cell numbers of (A-C) CD103⁺ dendritic cells (DC). The activation status of these DC was analyzed using activation markers (D-F) CD80 and (G-I) CD86. Data compiled from at least three independent experiments are shown for individual mice with the median. ns = not significant.

Lung CD103$^+$ DC numbers were not altered in IAV + OVA-AAI in comparison to OVA-AAI alone (figure 38 A). In IAV + HDM-AAI, the numbers of CD103$^+$ DC were decreased as compared to HDM-AAI, but this decrease did not reach statistical significance ($p = 0.0787$, figure 38 B). The difference in the outcome of this comparison between the models resulted in decreased fold change over AAI alone in IAV + HDM-AAI as compared to IAV + OVA-AAI ($p = 0.1080$; figure 38 C). Of note, CD103$^+$ DC were strongly and significantly increased in HDM-AAI as compared to OVA-AAI (figure 20). Comparing the frequency of the activation markers CD80 and CD86 on CD103$^+$ DC, no differences were observed in IAV + OVA-AAI and IAV + HDM-AAI, respectively as compared to AAI alone (figure 38 D, E, G, H).

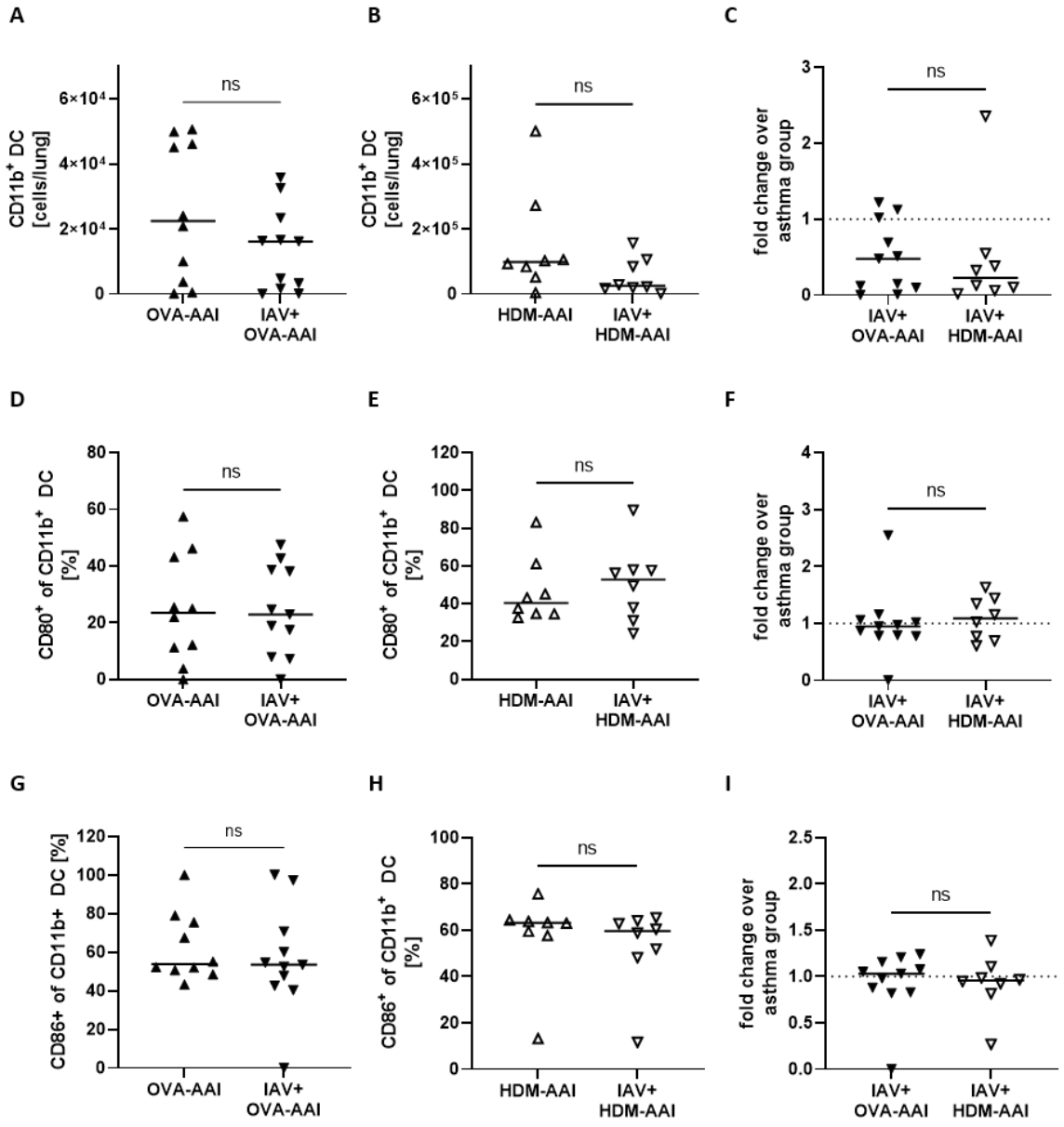


**figure 39: Absolute numbers and activation marker expression of CD11b$^+$ DC in OVA-AAI and HDM-AAI induced following resolution of IAV infection.**

Mice were infected with a sublethal dose of IAV or treated with PBS on day 0. After recovery, allergic airway inflammation (AAI) was induced. Mice were treated with ovalbumin (OVA) (and aluminum hydroxide (alum) for sensitization) or house dust mite extract (HDM) as described. On day 39 (OVA model) and day 37 (HDM model), respectively, lung leukocytes were analyzed for cell numbers of (A-C) CD11b$^+$ dendritic cells (DC). The activation status of CD11b$^+$ DC was analyzed using the activation markers (D-F) CD80 and (G-I) CD86. Data compiled from at least three independent experiments are shown for individual mice with the median. ns = not significant.

The absolute cell numbers of CD11b$^+$ DC were not significantly changed in IAV + OVA-AAI or IAV + HDM-AAI as compared to the respective AAI group (figure 39 A, B). There was a marginal reduction in lung CD11b$^+$ DC in IAV + AAI, that was similar in both models (figure 39 A-C). Moreover, the activation status (frequency of marker expression) of CD11b$^+$ DC did not differ between AAI with and without previous IAV infection with respect to both activation markers, CD80 and CD86 (figure 39 D-I). In the HDM model, a slight increase of the frequency of CD80$^+$ CD11b$^+$ DC could be observed in IAV + AAI, although it was marginal and did not reach statistical significance (figure 39 E).

In summary, a previous IAV infection did not significantly change the number and activation status of CD103$^+$ and CD11b$^+$ DC in the lung in both, OVA-AAI and HDM-AAI.

#### 4.2.2.4 Impact of resolved IAV infection on the monocyte compartment in the lung in subsequently induced OVA-AAI and HDM-AAI

Lung Ly6C$^+$ and Ly6C$^-$ monocytes were significantly increased in OVA-AAI and HDM-AAI (see 4.1.4). Therefore, the impact of a previous IAV infection on the numbers of monocytes in AAI was analyzed in the following.

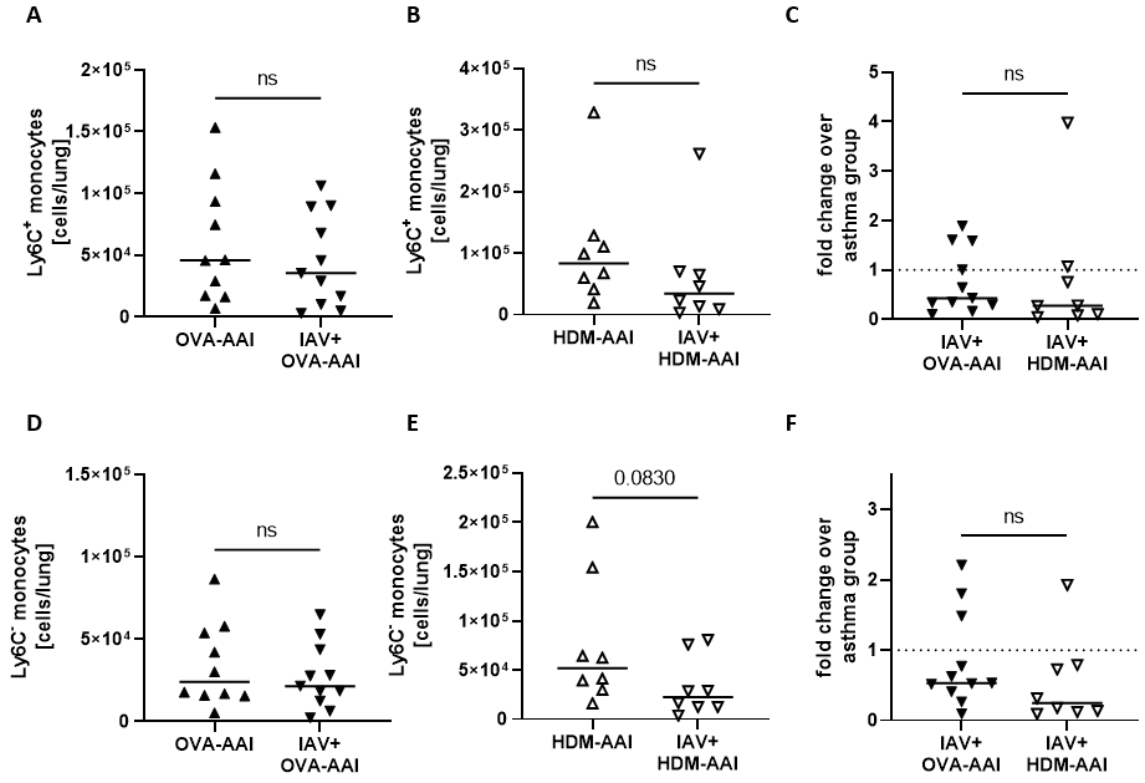


**figure 40: Analysis of Ly6C$^+$ and Ly6C$^-$ monocytes in OVA-AAI and HDM-AAI induced following IAV infection.** Mice were *i.n*. infected with IAV or treated with PBS on day 0. After recovery, allergic airway inflammation (AAI) was induced. Mice were treated with ovalbumin (OVA) (and aluminum hydroxide (alum) for sensitization) or house dust mite extract (HDM) as described. On day 39 (OVA model) and day 37 (HDM model), respectively, absolute numbers of Ly6C$^+$ monocytes (A-C) and Ly6C$^-$ monocytes (D-F) in the lung were assessed. Data compiled from at least three independent experiments are shown for individual mice with the median. ns = not significant.

The absolute numbers of Ly6C$^+$ and Ly6C$^-$ monocytes in the lung did not change significantly in OVA-AAI or HDM-AAI following IAV infection, as compared to AAI alone (figure 40 A, B, D, E). Nevertheless, a slight decrease in lung monocytes in AAI induced after IAV infection was observed in both OVA-AAI and HDM-AAI as compared to AAI groups alone (figure 40 A-F). This decrease was most apparent in IAV + HDM-AAI for Ly6C$^-$ monocytes ($p = 0.0830$, figure 40 E). There was no significant difference in the fold change of lung monocyte numbers comparing AAI without and with previous IAV infection between IAV + OVA-AAI and IAV + HDM-AAI (figure 40 C, F).

# 5 Discussion

Due to the high heterogeneity of the symptoms and chronic inflammation in allergic asthma, its treatment can be difficult and the underlying mechanisms and factors are of special interest and require further elucidation. Research in this field could lead to the development of new, specific therapeutic approaches and prophylactic measures to prevent the development of allergic asthma. Next to the analysis of clinical samples, different mouse models for allergic asthma are available for mechanistic studies. In this thesis, two common AAI mouse models, OVA- and HDM-mediated, were compared regarding the involvement of distinct myeloid cell subsets and the impact of a previous IAV infection.

One main cause of allergic asthma are viral upper respiratory tract infections, including IAV (Busse *et al.* 2010). IAV infections are associated with increased inflammatory gene expression in the respiratory tract (Forbester *et al.* 2021). Previous studies have already shown a long-lasting effect of IAV infection in the lung in both, mice and humans. In the present study, previous observations of the group were extended to long-term consequences of IAV infection for the lung immune micromilieu with a focus on lung macrophages and DC.

***Spectral flow cytometry of lung macrophages and DC:***

Knowledge of how IAV infection sustainably alters stationary lung immune cells is incomplete. In this context, our understanding of lung macrophages in lung health and disease has substantially increased and novel macrophage populations with distinct developmental origins, phenotypes and functions have been identified. To study, how IAV infection affects lung immunity and in turn changes AAI in the long term, macrophage and DC subsets not typically resolved in conventional flow cytometry were included in the analysis and displayed a central focus of this thesis. Conventional flow cytometry allowed the superficial differentiation between AM and IM, but the analysis of different cellular subtypes was limited, mainly because of restrictions in the number of detectable markers.

High-parameter spectral flow cytometry allows for staining of a high number of cellular markers and thereby for the acquisition of comprehensive phenotypic data in heterogeneous cell suspensions with a high sensitivity to detect rare populations. In conventional flow cytometry the problem arises, that the more fluorophores are used, the more overlapping of their signals takes place and it becomes increasingly difficult to distinguish the individual signals. The use of a spectral flow cytometer with spectral deconvolution algorithms has the potential for a more comprehensive and flexible approach to multi-color or multi-parameter analysis. Further, it allows handling of autofluorescence (AF) signals to increase the resolution in flow cytometric analyses. AF is a principle feature of all cell types with strong variations (Wanner *et al.* 2022). Especially macrophages and eosinophils exhibit high AF. Also in the spectral flow cytometric analysis in this thesis, it became apparent that AF plays a decisive role (Camp *et al.* 2024). In the literature, many markers for different macrophage and DC subpopulations in the murine lung were described (Helft *et al.* 2010, Chakarov *et al.* 2019, Ural *et al.* 2020). Based on the known markers, a staining panel was created, which allowed the simultaneous identification of several cellular subpopulations. Furthermore, it allowed the detection of key effector cells in allergic asthma such as eosinophils, T and B cells as well as the detection of the expression of the functional markers MHCII, CD80 and CD86. Several studies describe different macrophage and DC subsets in the mouse lung (e.g. Helft *et al.* 2010, Chakarov *et al.* 2019, Ural *et al.* 2020, Aegerter *et al.* 2022). Pulmonary macrophages are highly plastic and respond to the local microenvironment by adopting dynamic, multidimensional phenotypic profiles (Xue *et al.* 2014). During homeostasis, two main subsets of macrophages coexist in the lung and of these, AM are the major embryonically derived population found in the alveolar spaces. Further, IM, thought to originate from bone marrow-derived monocytes, reside within the lung parenchyma and comprise phenotypically distinct subpopulations (Misharin *et al.* 2013, Chakarov *et al.* 2019). However, also monocytes can differentiate into AM (Hou *et al.* 2021).

Spectral flow cytometry allowed the successful detection of the target populations AM, $CD11c^+$ and $CD11c^-$ IM, NAM, recMac, $CD103^+$ and $CD11b^+$ DC, next to monocytes and other

key effectors of AAI in the lung. It thus enabled their analyses in i) the mouse models OVA-AAI and HDM-AAI, in ii) resolved IAV infection and in iii) AAI preceded by IAV infection.

***Comprehensive analysis of lung macrophages and DC in two murine models of AAI:***

Several subsets of macrophages, i.e. AM, CD11c$^{+}$ and CD11c$^{-}$ IM, NAM and recMac, were significantly involved in experimental OVA-AAI and HDM-AAI. This likewise applied to CD103$^{+}$ DC and CD11b$^{+}$ DC as well as Ly6C$^{+}$ and Ly6C$^{-}$ monocytes. Next to the overall strong involvement of these cells and cellular subsets in AAI, distinct differences between the models were observed. The detected changes in the macrophage, DC and monocyte compartments were accompanied by classical effectors such as lung eosinophils, neutrophils, T cells and B cells as well as elevated Th1, Th2 and pro-inflammatory cytokines in the BAL and elevated systemic IgE levels in both, OVA-AAI and HDM-AAI.

Even though AM populate the airspaces, substantial AM numbers in the lung that were specifically increased in HDM-AAI as compared to OVA-AAI were detected. In these experiments, cells isolated from lavaged lungs were analyzed. Presumably, these AM also represent AM from remaining cells after lavage (Chang *et al.* 2023). The frequency of MHCII expression on the detected AM increased in AAI, which is in line with MHCII expression of inflammatory (M2) rather than homeostatic (M1) AM (Bissonnette *et al.* 2020) and further demonstrates plasticity of the AM pool in AAI, especially when mediated by HDM. The expression of MHCII and other costimulatory molecules is essential for the activation of CD4$^{+}$ T cells (Fulton *et al.* 2004). Professional antigen-presentation to T cells is mainly attributed to DC and AM have originally been ascribed rather regulatory roles (Holt 1993). So far, relatively little is known with respect to their functional roles in the induction and maintenance of AAI. They have been shown to support the induction of regulatory T cells (Soroosh *et al.* 2013) but also to promote cytokine production by allergen-specific Th2 cells, involving the expression of

CD80 and CD86 (Burastero *et al.* 1999, Balbo *et al.* 2001). In the results presented in this thesis, the MFI of the CD80 staining on $CD80^+$ AM was likewise nearly unchanged in OVA- and HDM-AAI as compared to controls. In contrast, the increase in CD86 expression (MFI) on $CD86^+$ AM between AAI and the respective control was significantly elevated in HDM-AAI as compared to OVA-AAI. Indeed, Balbo *et al*. reported CD86, but not CD80 to increase on AM following allergen challenge in patients allergic to *Dermatophagoides*. Since similar results were detected in HDM- but not OVA-AAI in mice, this possibly displays an HDM-specific mechanism in allergic asthma. However, clearly more detailed analyses will be needed to further explore on this issue und clarify its relevance in the differences observed between OVA- and HDM-AAI.

NAM are morphologically and transcriptionally distinct from AM suggesting a specialized role. They have been described to expand and to regulate inflammatory responses during acute IAV infection (Ural *et al.* 2020), making them also interesting with regard to the analysis of the long lasting effects of IAV infection in the lung. While there is increasing evidence for neuro-immune crosstalk in allergic asthma (Camp *et al.* 2021), a possible role for these cells in regulating AAI has also not been addressed. In this thesis, an increased number of NAM in the lungs in OVA-AAI and HDM-AAI was observed. While transcription of MHCII genes in NAM has been described (Ural *et al.* 2020), the frequency of $MHCII^+$ NAM was not affected in either AAI model. NAM were identified according to their described surface marker expression and their true nature will need to be confirmed by imaging *in situ* in the lung tissue upon AAI.

IM can be divided into several subpopulations such as $CD11c^+$ and $CD11c^-$ IM (Gibbings *et al.* 2017, Schyns *et al.* 2018, Ural *et al.* 2020). Further, monocytes developing into macrophages are recruited to the lung under inflammatory conditions. Analyzing the accumulation pattern of these macrophage subsets in the lung, model-specific differences were observed. $CD11c^+$ IM significantly increased in OVA-AAI and HDM-AAI, while $CD11c^-$ IM and recMac were significantly increased only in OVA-AAI. The frequency of MHCII expression on these IM was generally higher than that on AM, but it was not (recMac) or only marginally ($CD11c^+$ and

CD11c$^-$ IM) affected by AAI. In line with that, MHCII expression is reported to be expressed higher in IM as compared to AM (Schworer *et al.* 2024). A role for MHCII on lung IM in providing a niche for tissue-resident CD4$^+$ T cells has been suggested, but its precise function in this context remains unclear (Snyder *et al.* 2021).

Further, resident macrophages associated to the bronchi (BAM) have recently been described to capture and present antigens and thereby activate Th2 cells in the lung (Tang *et al.* 2022). These BAM are CD11c$^+$ IM characterized by high CX3CR1 and MHCII expression. While the established spectral flow cytometry antibody panel would in principle have allowed their identification with respect to the expression of these markers, this study at this point did not include imaging of lung tissue to validate their identity as BAM. Therefore, further studies combining spectral flow cytometry with imaging and molecular approaches such as *in situ* transcriptomics will be required to parse out the functional involvement of the different macrophage subsets in AAI.

In mice, the lung parenchyma contains two conventional DC (cDC) populations that accumulate near the small airway epithelia: CD103$^+$ and CD11b$^+$ DC (Helft *et al.* 2010). Both, CD103$^+$ and CD11b$^+$ DC, have been recognized as critical regulators of allergen-driven immune responses in the lung (Plantinga *et al.* 2013, Vroman *et al.* 2017). Plantinga *et al*. identified CD11b$^+$ cDC as the main subset inducing Th2 cell-mediated immunity in HDM-mediated experimental AAI (Plantinga *et al.* 2013). While the contribution of CD11b$^+$ cDC to AAI is widely accepted, the function of CD103$^+$ remains controversially discussed. CD103$^+$ DC may play a role in pulmonary tolerance, but have also been shown to stimulate Th2 responses to HDM and could mediate the recruitment of eosinophils in a mouse model of chronic asthma (Lajiness *et al.* 2023). Overall, significantly increased numbers of DC of both populations in the lung independent of the AAI model were detected in this thesis, which is contrast to reports of unchanged numbers of CD103$^+$ DC in mouse models of AAI (Lajiness *et al.* 2023). Significantly elevated numbers of CD103$^+$ as well as CD11b$^+$ DC in HDM-AAI as compared to OVA-AAI however pointed at a stronger involvement of DC in HDM-mediated inflammation.

This is underscored by significantly elevated (as compared to controls) frequencies of $CD80^+$ and $CD86^+$ $CD103^+$ DC as well as $CD86^+$ $CD11b^+$ DC exclusively in HDM-AAI, but not OVA-AAI. Further, this finding demonstrates not only a numeric increase in DC numbers but also significantly increased functional activation specifically in this model of AAI. Given the central role of DC in driving Th2-inflammation in AAI (Plantinga *et al.* 2013), their increased number and activation are well in line with the significantly elevated levels of IL-4 detected in the BAL in HDM-AAI as compared to OVA-AAI. Comparing the treatment regimen of the two AAI models, increased activation and accumulation of DC (and other cells) in the lung in HDM-AAI could well result from the extended period of airway challenges in this model as compared to OVA-AAI. While in HDM-AAI allergen was applied in weekly intervals over two weeks prior to analysis, respiratory allergen challenges in OVA-AAI only occurred for three consecutive days before analysis. Presumably, upstream involvement of the respiratory epithelium fundamentally differs between OVA-AAI and HDM-AAI due to the extended time-span of respiratory allergen-treatments, protease activity of the allergen and local innate immune stimulation in HDM-AAI (Wan *et al.* 1999, Hammad *et al.* 2009, Jacquet 2023), which is in turn likely to contribute to model-specific characteristics in inflammation. In this context, the likewise significantly elevated and comparable serum albumin levels detected in the BAL for both AAI models appear even more remarkable.

To gain insight into the involvement of monocytes in AAI in the context of macrophage and DC accumulation, monocyte numbers were also analyzed. Mouse monocyte subsets are characterized by differential expression of the inflammatory monocyte marker Ly6C (Geissmann *et al.* 2003). Inflammatory, $Ly6C^+$ monocytes are found in higher numbers in asthmatic patients and contribute to increased inflammation in mice with AAI (Yang *et al.* 2014, Zaslona *et al.* 2014, Niessen *et al.* 2021). In line with this, $Ly6C^+$ monocytes in the lungs were significantly elevated in both OVA- and HDM-AAI. Significant accumulation of $Ly6C^-$ monocytes was only detected in HDM-AAI. These results demonstrate that AAI in these models harbors distinct characteristics also with respect to the accumulation of monocytes in

the lungs and they further support the conclusion, that there is not generally elevated inflammation in HDM-AAI as compared to OVA-AAI. According to a recent report however, it cannot be excluded, these monocytes are of vascular rather than parenchymal origin, complicating interpretation of the data (Chang *et al.* 2023).

Next to an overall strong involvement of macrophages, DC and monocytes in the lung, several model-specific characteristics in the response were observed in this thesis. OVA-AAI, as it was induced here, involved peripheral, adjuvanted sensitizations followed by respiratory challenges with OVA-protein alone. In HDM-AAI, a natural mixture of allergens with protease-activity was administered exclusively *via* the airways without an additional adjuvant. Since these models differed in more than one variable, at this point, one can only speculate whether the detected differences resulted from the nature of the allergen, adjuvant-use, the route of sensitization or a combination of these factors. Further, the analyses performed cannot distinguish, whether the accumulation of specific subsets of macrophages and DC results from a recruitment to the inflamed tissue or their local expansion.
In conclusion, both models of AAI showed several hallmark features important for the further analysis of AAI in the context of resolved IAV infection: A significant increase in absolute numbers of macrophages, DC, eosinophils, relevant cytokines and IgE levels could be shown in the respiratory tract and serum, respectively.

Significant differences between OVA-AAI and HDM-AAI lay in the accumulation of AM and the accumulation as well as functional marker expression of DC. Therefore, when studying the role of the respiratory epithelium e.g. for macrophage or DC responses in AAI, the fundamental differences between OVA-AAI and HDM-AAI such as peripheral pre-sensitization in OVA-AAI, protease activity of HDM acting on the epithelial barrier and the time span, over which respiratory allergen treatments are performed, need to be taken into account. Generally, HDM-AAI might be more suitable as compared to OVA-AAI for AM- or DC-focused questions. The overall more intense inflammatory response in HDM-AAI as compared to OVA-AAI however, may make it less suitable for studying modulation of AAI, e.g. by interventions.

Further, it may prove beneficial to clearly separate the induction of allergen-specific sensitization from the allergen-challenge in terms of the compartment and the timing. In OVA-AAI, acute respiratory allergic responses can be studied in naïve airways of pre-sensitized hosts, while discrimination between sensitization, allergic reaction and direct airway inflammation can be difficult in HDM-AAI (De Alba *et al.* 2010). Such considerations likewise need to be applied when interpreting data generated in any model of AAI. In the context of the hypothesis of this thesis and the presumably differential involvement of the respiratory epithelium in both models, it is important to bear in mind that IAV targets the epithelium for replication and that it is substantially involved in the processes of infection, immune defense and resolution (Kalil *et al.* 2019). Therefore, the distinct differences between the two analyzed AAI models revealed in this thesis supported the analysis of the long-term effects of IAV infection on subsequently induced AAI in both of these models.

***Effects of IAV infection on lung myeloid cells and the lung immune milieu beyond acute infection:***

Previous studies have already shown a long-lasting effect of IAV infection on the lung in both, mice and humans. Epithelial changes related to repair mechanisms have been described up to 200 days after infection with the IAV PR8 strain (Kanegai *et al.* 2016), metaplasia of mucus-producing cells has been described up to 21 days after PR8 infection (Buchweitz *et al.* 2007) and goblet cell hyperplasia up to 28 days after X31 IAV infection (Wohlleben *et al.* 2003). Furthermore, persistent lymphocytic infiltration up to 21 days after IAV PR8 infection had already been observed histologically (Sharma-Chawla *et al.* 2016). Even though clinical data of long-term consequences of influenza infections on respiratory health and immunity are scarce, substantial effects on lung function and health loss in the post-acute phase of illness have been reported (Liu *et al.* 2015, Xie *et al.* 2024). Experimentally, several studies have shown sustained effects of IAV infection to the respiratory micromilieu in mouse models

(Didierlaurent *et al.* 2008, Kanegai *et al.* 2016, Sharma-Chawla *et al.* 2016, Keeler *et al.* 2018, Wu *et al.* 2020). Underlying the hypothesis and aims of this thesis, a previous study of the group has shown persisting changes in the pulmonary immune cell composition in a mouse model 39 days after sublethal IAV infection. Amongst other findings, significantly elevated numbers and MHCII expression of $CD11c^{+}SiglecF^{+}$ macrophages were detected in the lung but were not further specified (Wu *et al.* 2020). In this thesis, macrophages and DC as well as relevant soluble mediators were analyzed in more detail in a similar experimental setup.

Generally, IAV PR8 infection with a sublethal dose led to transient weight loss, from which mice recovered by day 14 post infection. This observation was in line with results from previous studies (Felgenhauer *et al.* 2020, Wu *et al.* 2020, George *et al.* 2021).
Using conventional flow cytometry for the analysis of lung immune cells 39 days post infection, the numbers of AM ($CD64^{+}MerTK^{+}F4/80^{+}CD11c^{+}CD169^{+}$) and IM ($CD64^{+}MerTK^{+}F4/80^{+}CD11c^{low}CD169^{low}CX3CR1^{+}$) were significantly increased after resolved IAV infection as compared to the control group. This finding confirmed previous results from Wu *et al.* and increased the resolution of the pulmonary macrophage pool to discriminate AM and IM (Wu *et al.* 2020). Significantly increased numbers of $SiglecF^{+}CD11c^{+}MerTK^{+}CD64^{+}$ AM in the lung 28 days post IAV infection (strain X31, H3N2) have previously been described in the context of secondary bacterial infection. These AM produced increased levels of IL-6 upon stimulation, protecting mice from secondary pneumococcal infection. In contrast to resident AM, they were found to be monocyte-derived and to harbor independent functional, transcriptional and epigenetic profiles (Aegerter *et al.* 2020). While origin and other aspects were not addressed in this thesis, the description of significantly increased AM numbers long following IAV infection with H1N1 PR8 and H3N2 IAV strains points at presumably general mechanisms in the antiviral defense that mediate this sustained increase. Further, altered responses to secondary bacterial pathogens possibly also imply altered responses also to other immunological triggers. For AM and IM different roles in the lung are postulated. AM are tightly adherent and in close contact to alveolar epithelial cells, primarily remove

surfactant and cellular debris and are also responsible for the phagocytosis of pathogens, the initiation and the resolution of immune responses in the lung (Joshi *et al.* 2018). IM, on the other hand, reside in the mesothelium and have functions in antigen-presentation and modulation of tissue-injury in lung immune defense (Somerville *et al.* 2020). Their documented functions in regulating respiratory immune reactions and their contribution to the resolution of infections together with the observation of significantly elevated cell numbers 39 days following IAV infection made AM and IM particularly interesting in the context of sustained IAV-mediated effects on the lung immune micromilieu and possible consequences for subsequently induced AAI. The established spectral flow cytometry panel allowed the analysis of multiple macrophage and DC subpopulations, respectively, in the lung in the context of resolved IAV infection. In these analyses however, none of the analyzed macrophage subpopulations (AM, $CD11c^+$ and $CD11c^-$ IM, NAM and recMac) were significantly changed in cell numbers in the lung 39 days after IAV infection. At first sight, these results were in contrast to the increased numbers of AM and IM detected by conventional flow cytometry. However, albeit the lack in statistical significance, trends for at time substantially increased numbers of AM, $CD11c^+$ and $CD11c^-$ IM, NAM and recMac as compared to uninfected controls were observed. A possible reason for this discrepancy to the findings of the conventional flow cytometry approach might be the fact, that the macrophages isolated from the lung (particularly IM) were subdivided into several subtypes, thereby spreading and reducing differences.

Previous experiments had shown significantly increased DC numbers in the BAL (Wu *et al.* 2020) and a trend for increased DC numbers in the lung (unpublished results) on day 39 post IAV infection. In that study, DC had been crudely defined as $CD11c^+SiglecF^-MHCII^+$ cells without any discrimination of subtypes or further analysis of functional markers. This thesis has substantially extended these previous analyses in a similar experimental setting. The addressed lung DC subsets ($CD103^+$ and $CD11b^+$ DC) were however not significantly altered in their numbers or functional marker expression 39 days after IAV infection. Nevertheless, a minor increase in $CD103^+$ DC and a substantial increase in $CD11b^+$ DC were detected in the

lungs, albeit a lack in statistical significance. In principle, this observation recapitulates previous results and does not exclude sustained changes to lung DC numbers following IAV infection. Indeed, published data previously described an increased number of DC ($CD11c^{+}MHCII^{low}$ and $CD11c^{+}MHCII^{high}$) in the lungs on day 30 after X31 IAV infection (Dahl *et al.* 2004). In this study, analysis of lung DC after undergoing IAV infection revealed increased expression of the functional, co-stimulatory surface molecules CD80 and CD86 (increased mean fluorescence intensity), which was associated with increased allergic disease and Th1 and Th2 responses in subsequent AAI. In contrast, in this thesis no significant effects of previous IAV infection on the frequency of CD80 and CD86 expressing DC were detected. However, even though not statistically significant, the frequency of CD80-expressing $CD11b^{+}$ DC was substantially increased 39 days following IAV infection, further pointing at possible IAV-mediated, DC-associated changes also in the H1N1 PR8 infection model. The differences between the published results and those obtained in this thesis could be a consequence of either viral strain-specific mechanisms or differences in the analysis (gating of DC, approach for the quantification of marker expression).

The analysis of a range of inflammatory, epithelial and macrophage/DC associated cytokines in lung or BAL revealed no significant differences in the concentrations of these mediators after the resolution of IAV infection, with the exception of IL-12p40, which showed a significant increase in infected mice, while IL-12p70 was not altered. IL-12 was initially described as “natural killer cell stimulatory factor” (Kobayashi *et al.* 1989), is primarily produced by antigen-presenting cells, exerts immunoregulatory effects on natural killer and T cells and promotes Th1 responses (Jalah *et al.* 2013). Studies indicate that IL-12 plays an essential role in regulating IFN gamma production (Magram *et al.* 1996), which promotes monocyte-mediated lung injury during influenza infection (Schmit *et al.* 2022). The isoform p40 acts as a chemoattractant for macrophages and is thought to be a natural antagonist of the bioactive isoform p70 (Ling *et al.* 1995, Ethuin *et al.* 2003, Cooper *et al.* 2007). The increased numbers of macrophages in the lung could explain the increased concentration of IL12p40 in the BAL, as well as the fact, that the p40 subunit is excessed in a 10- to 50-fold

manner over the p70 subunit *in vitro* and *in vivo* (Ethuin *et al.* 2003). While no associations between increased overall AM and IM numbers long after IAV infection and candidate mediators such as IL-33 and GM-CSF (Quell *et al.* 2020) could be detected, significantly increased IL-12p40 levels provide convincing further evidence for long-term effects of IAV infection on the lung micromilieu that could well affect subsequently induced AAI.
Increased serum albumin in BAL was detectable 39 days after IAV infection in both experimental settings but seemed to be more pronounced and was statistically significant in the HDM regimen, suggesting increased capillary leakage, ongoing inflammation and sustained epithelial involvement long after IAV infection. Wu *et al*. reported epithelial hyperplasia in histology and persistent pneumonia with increased activated $CD4^+$ and $CD8^+$ lymphocytes in the same experimental setting, 39 days after infection (Wu *et al.* 2020). Further, respiratory epithelial cells respond strongly to acute IAV infection (Stegemann-Koniszewski *et al.* 2016), mucosal regeneration after resolution of infection is associated with epithelial hyperplasia (Taubenberger 2008) and long-term changes in the respiratory epithelium after IAV infection have been described (Kanegai *et al.* 2016).

Taken together, the observations made in this thesis provide support for and add novel aspects to the long-lasting effects of IAV infection in the lung. Therefore, although the analysis of specialized macrophage and DC subsets in this setting did not show significant alterations, there was a strong rationale for further analyzing sustained IAV-mediated effects on AAI.

***Effect of previous IAV infection on subsequently induced AAI:***

It is generally recognized that infectious and inflammatory events can lead to persistent changes in the lung micromilieu with significant effects on subsequent immune responses (Yoo *et al.* 2013). In this context, the concepts of “innate trained immunity” or “inflammatory imprinting”, which differ from the classical immunological memory of the adaptive immune

system, have been established (Gourbal *et al.* 2018, Wanka *et al.* 2021). Due to the early recognition and description of the synergism between IAV and respiratory bacterial pathogens and its consequences for the host, secondary bacterial infections have been the focus of investigation towards the consequences of IAV infections for respiratory immunity. Several immune-related mechanisms of IAV-associated regulation of subsequent antibacterial immune responses have been described (Rynda-Apple *et al.* 2015). It is conceivable that such regulation also affects non-infectious inflammatory conditions such as allergic asthma or AAI. Previous studies in various mouse models have indeed described significant effects of IAV infection in this context (Wohlleben *et al.* 2003, Dahl *et al.* 2004, Al-Garawi *et al.* 2009, Al-Garawi *et al.* 2011, Birmingham *et al.* 2014, Kawaguchi *et al.* 2017, Skevaki *et al.* 2018, Wu *et al.* 2020). The mechanisms underlying IAV-mediated suppression or enhancement of AAI remain unclear in many aspects and the factors that are decisive for potential beneficial or detrimental effects of previous IAV infection are unknown. The hygiene hypothesis postulates that an overall reduction of virus- or bacteria-induced responses due to increased hygiene results in a decreased ability to counterbalance Th2-driven diseases and protective cross-reactive mechanisms may occur (Layland *et al.* 2013). Available clinical data are mainly limited to altered IAV-directed immune responses in asthmatics and IAV-mediated acute exacerbations in existing allergic asthma. The role of influenza viruses in asthma development is still largely unknown (Edwards *et al.* 2017, Schwarze *et al.* 2018, Veerapandian *et al.* 2018). One aim of this work was to further elucidate the effects of resolved IAV infection on a subsequently induced AAI with a focus on lung macrophage and DC associated mechanisms.

In this thesis, limited effects of resolved IAV infection on subsequently induced OVA-AAI or HDM-AAI were detected. With respect to the accumulation of immune cells in the lung in AAI preceded by IAV infection, most of the results observed a reduction of cell numbers in IAV + AAI as opposed to IAV alone, however without significant effects. Nevertheless, the overall reduction in all analyzed cell populations underline a potential general suppression of AAI after IAV infection in both models. Crane *et al*. found that pulmonary IAV infection leads to a

suppression of the innate immune response in wound healing, underlying the potential suppressive effect of IAV (Crane *et al.* 2018). In contrast to that, in a mouse model of IAV infection and subsequent induction of OVA-AAI two weeks after the second sensitization, an enhancement of the severity of AAI-illness in addition to lung pathology could be observed (Kawaguchi *et al.* 2017).

The results of this thesis showed that the total T cell number in the lung remained unchanged in IAV + AAI as compared to AAI alone. Eosinophil numbers and neutrophil numbers in the lung and TNF-α levels in BAL were marginally, although not significantly, reduced in AAI after resolved IAV infection. This was in line with findings from Wu *et al.* (Wu *et al.* 2020). There was a significant accumulation of neutrophils in the lung in HDM-AAI and the mechanisms behind their accumulation may be modulated by previous IAV infection. An individually varying contribution of neutrophils to inflammation in patients with asthma is involved in its heterogeneity (Yamasaki *et al.* 2022). As neutrophil recruitment is associated with infectious conditions, the contribution of neutrophils to inflammation in asthma could also well be affected by concurrent or previous infections (Wark *et al*., 2002).

The analyzed macrophage subtypes in the lung showed a trend for decreased cell numbers in IAV + AAI as compared to AAI alone in both models, albeit without statistical significance. Interestingly, the fold change over AAI alone in the MHCII expression of AM was significantly different between IAV + OVA-AAI and IAV + HDM-AAI. While the frequency of $MHCII^+$ AM rather increased in IAV + OVA-AAI, the number decreases in IAV + HDM-AAI, resulting in a significantly different fold change over AAI alone between both models. Respiratory viral infections as well as IAV have been shown to induce trained immunity in respiratory macrophages (Yao *et al.* 2018, Aegerter *et al.* 2020, Wang *et al.* 2023). While the "training" or "priming" of macrophages in the lungs presumably occurs in IAV infection, it is conceivable that the consequences of such priming can at least in part be AAI-model dependent and that therefore IAV-mediated training has different effects on a subsequently induced OVA-AAI and

HDM-AAI. Such findings further underline the need for considering model-specific effects in planning and interpreting data from animal studies.

Lung $CD103^+$ and $CD11b^+$ DC were significantly increased in OVA-AAI and HDM-AAI as compared to controls, with significantly higher numbers in HDM-AAI. The number of $CD103^+$ DC in the lung was now decreased in IAV + HDM-AAI as compared to HDM-AAI alone ($p = 0.0787$), while it was unchanged in the OVA-mediated model. DC work as a first line of defense against influenza virus (Waithman *et al.* 2012). Furthermore, $CD103^+$ DC in particular are thought to play a special role during influenza infection, as they can directly be infected with IAV (Moltedo *et al.* 2011). Another group has analyzed different DC subsets with respect to their ability to induce Th2 priming during AAI. From the analyzed DC subsets, only $CD103^+$ DC retrieved from mice treated with OVA, HDM or other allergen could induce Th2 responses (Nakano *et al.* 2012). Allergen-specific Th2 cells secrete pro-allergic cytokines like IL-4 and IL-9, which lead to IgE responses. Another study has shown that selective TLR7 stimulation, which occurs when the innate immune system recognizes an IAV infection, suppresses Th2 responses. Here, the concentrations of Th2 cytokines and airway hyper-responsiveness were reduced (Xirakia *et al.* 2010). In IAV + HDM-AAI the number of $CD103^+$ DC was decreased, which in turn may underlie the by trend decreased levels of BAL IL-4 and the significantly decreased levels of BAL IL-9 and serum IgE as compared to HDM-AAI alone. These findings were exclusive for HDM-AAI, suggesting a stronger susceptibility or higher sensitivity to IAV-mediated modulation of AAI in this model. Possibly this is associated to the sensitization/challenge that occurs *via* the respiratory route in HDM-AAI, while in OVA-AAI peripheral sensitization takes place and here only the allergic challenge occurs *via* the respiratory tract. Further, the use of an adjuvant intended to boost sensitization in OVA-AAI is a potential mechanism for the diverging results between the two models with respect to IAV-mediated effects of IgE production in AAI. Alum is the most commonly used adjuvant promoting the production of Th2 cytokines during the immune response (Epstein 2004). Further, OVA-AAI alone showed significantly higher levels of serum IgE as compared to HDM-

AAI alone. It is possible that the strong IgE response in OVA-AAI marks attenuating mechanisms (such as previous IAV infection) that are in principle present, but cannot "counteract".

In summary, this study shows that AAI induced in mice after apparent recovery from IAV infection was significantly modulated with regard to total serum IgE levels and Th2 cytokine production. Overall, there was a trend for amelioration of AAI by previous IAV infection. Importantly, IAV-mediated modulation depended on the mouse model of AAI was most prominent in HDM-AAI.

As a respiratory virus, IAV directly affects the respiratory tract. Sustained, significant effects of IAV infection were detected in this thesis. Moreover, a trend for increased numbers of most analyzed macrophage and DC subsets was observed. Future functional studies will have to clarify, whether and how these IAV-mediated effects on the lung immune micromilieu are mechanistically connected to alterations in the presentation of AAI. In-depth knowledge of the decisive pathways for such modulation will potentially offer specific targets for prevention and intervention in clinical asthma, especially in the context of viral upper respiratory tract infections. In this regard, it will be essential to uncover in which instances viral infection predisposes for and exacerbates allergic asthma as opposed to when microbial triggers ameliorate respiratory allergic inflammation, as suggested by the data of this thesis and other published work. Here, next to considerations about the general transferability of mouse models, it must also be taken into account, that there are many different IAV strains that can differ significantly in the immune response they trigger and are therefore very likely to have different effects on subsequently developing AAI. The same applies to clinical studies, in which various viral pathogens and strains are encountered by patient´s individual immune system.

# 6 Conclusion and outlook

This thesis demonstrates strong, subset-specific involvement of lung macrophages and DC in two models of experimental AAI. Importantly, between the analyzed AAI models, OVA-AAI and HDM-AAI, significant model-specific characteristics with respect to immune cell accumulation and functional marker expression as well as IgE production and cytokine profiles were observed. These findings underline the need for considering the choice of the animal model in studying allergic asthma and in the interpretation of respective findings. Further, the results of this thesis emphasize, that IAV infection can have significant long-term effects on the immunological micromilieu of the respiratory tract with respect to immune cell accumulation, soluble mediators and epithelial barrier integrity and can sustainably modulate/ameliorate subsequently induced allergic inflammation, also in a model-specific manner.

It must be noted that the results from animal experiments can only be transferred to humans to a limited extend. Nevertheless, they have provided and continue to provide valuable insight into clinically relevant disease mechanisms. Based on the results of this thesis, studies towards the function of macrophages and DC present in the lung after resolved IAV infection and their response in AAI will reveal mechanistic insights. To date, there is very little data on long-term changes after IAV infection in humans, so additional clinical studies in patients are clearly needed. Such knowledge will importantly enable targeted strategies of prevention and therapy, especially in the light of the continuously high numbers of seasonal IAV infections and patients suffering from allergic asthma in the human population.

# 7 Literature

Aegerter, H.*, et al.* (2020). "Influenza-induced monocyte-derived alveolar macrophages confer prolonged antibacterial protection." Nat Immunol **21**(2): 145-157.

Aegerter, H.*, et al.* (2022). "Biology of lung macrophages in health and disease." Immunity **55**(9): 1564-1580.

Akira, S.*, et al.* (2006). "Pathogen recognition and innate immunity." Cell **124**(4): 783-801.

Al-Garawi, A.*, et al.* (2011). "Influenza A facilitates sensitization to house dust mite in infant mice leading to an asthma phenotype in adulthood." Mucosal Immunol **4**(6): 682-694.

Al-Garawi, A. A.*, et al.* (2009). "Acute, but not resolved, influenza A infection enhances susceptibility to house dust mite-induced allergic disease." J Immunol **182**(5): 3095-3104.

Amin, K. (2012). "The role of mast cells in allergic inflammation." Respir Med **106**(1): 9-14.

Aoki, M.*, et al.* (2000). "Effect of a novel anti-inflammatory compound, YM976, on antigen-induced eosinophil infiltration into the lungs in rats, mice, and ferrets." J Pharmacol Exp Ther **295**(3): 1149-1155.

Arango Duque, G.*, et al.* (2014). "Macrophage cytokines: involvement in immunity and infectious diseases." Front Immunol **5**: 491.

Arruda, L. K.*, et al.* (1995). "Molecular cloning of a major cockroach (Blattella germanica) allergen, Bla g 2. Sequence homology to the aspartic proteases." J Biol Chem **270**(33): 19563-19568.

Aun, M. V.*, et al.* (2017). "Animal models of asthma: utility and limitations." J Asthma Allergy **10**: 293-301.

Ayanoglu, G.*, et al.* (2011). "Modelling asthma in macaques: longitudinal changes in cellular and molecular markers." Eur Respir J **37**(3): 541-552.

Bach, J. F. (2002). "The effect of infections on susceptibility to autoimmune and allergic diseases." N Engl J Med **347**(12): 911-920.

Balbo, P.*, et al.* (2001). "Differential role of CD80 and CD86 on alveolar macrophages in the presentation of allergen to T lymphocytes in asthma." Clin Exp Allergy **31**(4): 625-636.

Bandeira-Melo, C.*, et al.* (2002). "The cellular biology of eosinophil eicosanoid formation and function." J Allergy Clin Immunol **109**(3): 393-400.

Barrett, E. G.*, et al.* (2003). "Effect of inhaled ultrafine carbon particles on the allergic airway response in ragweed-sensitized dogs." Inhal Toxicol **15**(2): 151-165.

Bates, J. H.*, et al.* (2009). "Animal models of asthma." Am J Physiol Lung Cell Mol Physiol **297**(3): L401-410.

Berri, F.*, et al.* (2014). "Switch from protective to adverse inflammation during influenza: viral determinants and hemostasis are caught as culprits." Cell Mol Life Sci **71**(5): 885-898.

Bijanzadeh, M.*, et al.* (2011). "An understanding of the genetic basis of asthma." Indian J Med Res **134**(2): 149-161.

Bijanzadeh, M.*, et al.* (2009). "Soluble intercellular adhesion molecule-1 and E-selectin in patients with asthma exacerbation." Lung **187**(5): 315-320.

Birmingham, J. M.*, et al.* (2014). "Influenza A infection enhances antigen-induced airway inflammation and hyperresponsiveness in young but not aged mice." Clin Exp Allergy **44**(9): 1188-1199.

Bischof, R. J.*, et al.* (2003). "Induction of allergic inflammation in the lungs of sensitized sheep after local challenge with house dust mite." Clin Exp Allergy **33**(3): 367-375.

Bissonnette, E. Y.*, et al.* (2020). "Cross-Talk Between Alveolar Macrophages and Lung Epithelial Cells is Essential to Maintain Lung Homeostasis." Front Immunol **11**: 583042.

Bodewes, R.*, et al.* (2010). "Animal models for the preclinical evaluation of candidate influenza vaccines." Expert Rev Vaccines **9**(1): 59-72.

Boulet, L. P.*, et al.* (1997). "Inhibitory effects of an anti-IgE antibody E25 on allergen-induced early asthmatic response." Am J Respir Crit Care Med **155**(6): 1835-1840.

Bourdin, A.*, et al.* (2024). "Phenotyping of Severe Asthma in the Era of Broad-Acting Anti-Asthma Biologics." J Allergy Clin Immunol Pract **12**(4): 809-823.

Bousquet, J.*, et al.* (2000). "Asthma. From bronchoconstriction to airways inflammation and remodeling." Am J Respir Crit Care Med **161**(5): 1720-1745.

Bradding, P.*, et al.* (2006). "The role of the mast cell in the pathophysiology of asthma." J Allergy Clin Immunol **117**(6): 1277-1284.

Bridges, C. B.*, et al.* (2003). "Transmission of influenza: implications for control in health care settings." Clin Infect Dis **37**(8): 1094-1101.

Britt, R. D., Jr.*, et al.* (2023). "Macrophages Orchestrate Airway Inflammation, Remodeling, and Resolution in Asthma." Int J Mol Sci **24**(13).

Buchweitz, J. P*., et al.* (2007). "Time-Dependent Airway Epithelial and Inflammatory Cell Responses Induced by Influenza Virus A/PR/8/34 in C57BL/6 Mice." Toxicologic Pathology **35**(3): 424-435.

Bui, T. M*., et al.* (2020). "ICAM-1: A master regulator of cellular responses in inflammation, injury resolution, and tumorigenesis." J Leukoc Biol **108**(3): 787-799.

Burastero, S. E*., et al.* (1999). "Increased expression of the CD80 accessory molecule by alveolar macrophages in asthmatic subjects and its functional involvement in allergen presentation to autologous TH2 lymphocytes." J Allergy Clin Immunol **103**(6): 1136-1142.

Busse, W. W*., et al.* (2010). "Role of viral respiratory infections in asthma and asthma exacerbations." Lancet **376**(9743): 826-834.

Caminati, M*., et al.* (2018). "Type 2 immunity in asthma." World Allergy Organ J **11**(1): 13.

Camp, B*., et al.* (2024). "Comprehensive analysis of lung macrophages and dendritic cells in two murine models of allergic airway inflammation reveals model- and subset-specific accumulation and phenotypic alterations." Front Immunol **15**: 1374670.

Camp, B*., et al.* (2021). "Infection-Associated Mechanisms of Neuro-Inflammation and Neuro-Immune Crosstalk in Chronic Respiratory Diseases." Int J Mol Sci **22**(11).

Campbell, C. D*., et al.* (2023). "The role of the respiratory microbiome in asthma." Front Allergy **4**: 1120999.

Carr, T. F*., et al.* (2016). "Asthma heterogeneity and severity." World Allergy Organ J **9**(1): 41.

Centers for Disease Control and Prevention (CDC). “Key facts about Influenza (Flu).” https://www.cdc.gov/flu/about/keyfacts.htm. Accessed on 29.04.2024.

Chakarov, S*., et al.* (2019). "Two distinct interstitial macrophage populations coexist across tissues in specific subtissular niches." Science **363**(6432).

Chang, M. Y*., et al.* (2023). "Multicompartmental analysis of the murine pulmonary immune response by spectral flow cytometry." Am J Physiol Lung Cell Mol Physiol **325**(4): L518-l535.

Chen, J*., et al.* (2017). "Long term outcomes in survivors of epidemic Influenza A (H7N9) virus infection." Sci Rep **7**(1): 17275.

Chen, X*., et al.* (2018). "Host Immune Response to Influenza A Virus Infection." Front Immunol **9**: 320.

Cheng, D.*, et al.* (2014). "Epithelial interleukin-25 is a key mediator in Th2-high, corticosteroid-responsive asthma." Am J Respir Crit Care Med **190**(6): 639-648.

Clohisey, S.*, et al.* (2019). "Host susceptibility to severe influenza A virus infection." Crit Care **23**(1): 303.

Cooper, A. M.*, et al.* (2007). "IL-12p40: an inherently agonistic cytokine." Trends Immunol **28**(1): 33-38.

Crane, M. J.*, et al.* (2018). "Pulmonary influenza A virus infection leads to suppression of the innate immune response to dermal injury." PLoS Pathog **14**(8): e1007212.

Dahl, M. E.*, et al.* (2004). "Viral-induced T helper type 1 responses enhance allergic disease by effects on lung dendritic cells." Nat Immunol **5**(3): 337-343.

De Alba, J.*, et al.* (2010). "House dust mite induces direct airway inflammation in vivo: implications for future disease therapy?" Eur Respir J **35**(6): 1377-1387.

Denney, L.*, et al.* (2018). "The role of respiratory epithelium in host defence against influenza virus infection." Biomed J **41**(4): 218-233.

Deutsche Gesellschaft für Pneumologie und Beatmungsmedizin e.V. (DGP). "S2k-Leitlinie zur fachärtzlichen Diagnostik und Therapie von Asthma 2023." https://register.awmf.org/assets/guidelines/020-009l_S2k_Fachaerztliche-Diagnostik-Therapie-von-Asthma_2023-03.pdf. Accessed on 19.04.2024.

Didierlaurent, A.*, et al.* (2008). "Sustained desensitization to bacterial Toll-like receptor ligands after resolution of respiratory influenza infection." J Exp Med **205**(2): 323-329.

Doras, C.*, et al.* (2018). "Lung responses in murine models of experimental asthma: Value of house dust mite over ovalbumin sensitization." Respir Physiol Neurobiol **247**: 43-51.

Dou, D.*, et al.* (2018). "Influenza A Virus Cell Entry, Replication, Virion Assembly and Movement." Front Immunol **9**: 1581.

Eberl, G. (2016). "Immunity by equilibrium." Nat Rev Immunol **16**(8): 524-532.

Edwards, M. R.*, et al.* (2017). "Viral infections in allergy and immunology: How allergic inflammation influences viral infections and illness." J Allergy Clin Immunol **140**(4): 909-920.

Egan, R. W.*, et al.* (1999). "Effect of Sch 55700, a humanized monoclonal antibody to human interleukin-5, on eosinophilic responses and bronchial hyperreactivity." Arzneimittelforschung **49**(9): 779-790.

Epstein, M. M. (2004). "Do mouse models of allergic asthma mimic clinical disease?" Int Arch Allergy Immunol **133**(1): 84-100.

Ethuin, F.*, et al.* (2003). "Regulation of interleukin 12 p40 and p70 production by blood and alveolar phagocytes during severe sepsis." Lab Invest **83**(9): 1353-1360.

Fahy (2014). "Type 2 inflammation in Asthma."

Fahy, J. V.*, et al.* (1997). "The effect of an anti-IgE monoclonal antibody on the early- and late-phase responses to allergen inhalation in asthmatic subjects." Am J Respir Crit Care Med **155**(6): 1828-1834.

Feleszko, W.*, et al.* (2006). "Parental tobacco smoking is associated with augmented IL-13 secretion in children with allergic asthma." J Allergy Clin Immunol **117**(1): 97-102.

Felgenhauer, J. L.*, et al.* (2020). "Evaluation of Nutritional Gel Supplementation in C57BL/6J Mice Infected with Mouse-Adapted Influenza A/PR/8/34 Virus." Comp Med **70**(6): 471-486.

Forbester, J. L.*, et al.* (2021). "Genetic influences on viral-induced cytokine responses in the lung." Mucosal Immunol **14**(1): 14-25.

Foster, P. S.*, et al.* (2017). "Modeling TH 2 responses and airway inflammation to understand fundamental mechanisms regulating the pathogenesis of asthma." Immunol Rev **278**(1): 20-40.

Fröde, T. S.*, et al.* (2005). "The puzzle of asthma treatment: animal models to genetic studies." Curr Pharm Des **11**(19): 2515-2524.

Fulton, S. A.*, et al.* (2004). "Inhibition of major histocompatibility complex II expression and antigen processing in murine alveolar macrophages by Mycobacterium bovis BCG and the 19-kilodalton mycobacterial lipoprotein." Infect Immun **72**(4): 2101-2110.

Gamblin, S. J.*, et al.* (2010). "Influenza hemagglutinin and neuraminidase membrane glycoproteins." J Biol Chem **285**(37): 28403-28409.

Gascoigne, M. H.*, et al.* (2003). "The effect of anti-integrin monoclonal antibodies on antigen-induced pulmonary inflammation in allergic rabbits." Pulm Pharmacol Ther **16**(5): 279-285.

Geissmann, F.*, et al.* (2003). "Blood monocytes consist of two principal subsets with distinct migratory properties." Immunity **19**(1): 71-82.

Geissmann, F.*, et al.* (2010). "Development of monocytes, macrophages, and dendritic cells." Science **327**(5966): 656-661.

George, J. A.*, et al.* (2021). "Exacerbation of Influenza A Virus Disease Severity by Respiratory Syncytial Virus Co-Infection in a Mouse Model." Viruses **13**(8).

Ghebrehewet, S.*, et al.* (2016). "Influenza." Bmj **355**: i6258.

Gibbings, S. L.*, et al.* (2017). "Three Unique Interstitial Macrophages in the Murine Lung at Steady State." Am J Respir Cell Mol Biol **57**(1): 66-76.

Gordon, S.*, et al.* (2020). "Plasma membrane receptors of tissue macrophages: functions and role in pathology." J Pathol **250**(5): 656-666.

Gourbal, B.*, et al.* (2018). "Innate immune memory: An evolutionary perspective." Immunol Rev **283**(1): 21-40.

Hall, S., *et al.* (2014). Key mediators in the immunopathogenesis of allergic asthma. *International immunopharmacology*, *23*(1), 316–329.

Hammad, H.*, et al.* (2009). "House dust mite allergen induces asthma via Toll-like receptor 4 triggering of airway structural cells." Nat Med **15**(4): 410-416.

Hanania, N. A.*, et al.* (2016). "Efficacy and safety of lebrikizumab in patients with uncontrolled asthma (LAVOLTA I and LAVOLTA II): replicate, phase 3, randomised, double-blind, placebo-controlled trials." Lancet Respir Med **4**(10): 781-796.

Helft, J.*, et al.* (2010). "Origin and functional heterogeneity of non-lymphoid tissue dendritic cells in mice." Immunol Rev **234**(1): 55-75.

Herz, U.*, et al.* (2004). "Animal models of type I allergy using recombinant allergens." Methods **32**(3): 271-280.

Holgate, S. T.*, et al.* (2015). "Asthma." Nat Rev Dis Primers **1**: 15025.

Holt, P. G. (1993). "Regulation of antigen-presenting cell function(s) in lung and airway tissues." Eur Respir J **6**(1): 120-129.

Holt, P. G. (2000). "Antigen presentation in the lung." Am J Respir Crit Care Med **162**(4 Pt 2): S151-156.

Hou, F.*, et al.* (2021). "Diversity of Macrophages in Lung Homeostasis and Diseases." Front Immunol **12**: 753940.

Hussell, T.*, et al.* (2014). "Alveolar macrophages: plasticity in a tissue-specific context." Nature Reviews Immunology **14**(2): 81-93.

Hutchinson, E. C*., et al.* (2013). "Transport of the influenza virus genome from nucleus to nucleus." Viruses **5**(10): 2424-2446.

Jacquet, A. (2011). "The role of innate immunity activation in house dust mite allergy." Trends Mol Med **17**(10): 604-611.

Jacquet, A. (2023). "The HDM allergen orchestra and its cysteine protease maestro: Stimulators of kaleidoscopic innate immune responses." Mol Immunol **156**: 48-60.

Jalah, R*., et al.* (2013). "The p40 subunit of interleukin (IL)-12 promotes stabilization and export of the p35 subunit: implications for improved IL-12 cytokine production." J Biol Chem **288**(9): 6763-6776.

Jartti, T*., et al.* (2020). "Role of viruses in asthma." Semin Immunopathol **42**(1): 61-74.

Jorde, I., *et al.* (2020). "Modulation of Allergic Sensitization and Allergic Inflammation by *Staphylococcus aureus* Enterotoxin B in an Ovalbumin Mouse Model." *Frontiers in immunology*, *11*, 592186.

Joshi, N*., et al.* (2018). "Alveolar Macrophages." Cell Immunol **330**: 86-90.

Kaiko, G. E*., et al.* (2008). "Immunological decision-making: how does the immune system decide to mount a helper T-cell response?" Immunology **123**(3): 326-338.

Kalil, A. C*., et al.* (2019). "Influenza virus-related critical illness: pathophysiology and epidemiology." Crit Care **23**(1): 258.

Kanegai, C. M*., et al.* (2016). "Persistent Pathology in Influenza-Infected Mouse Lungs." Am J Respir Cell Mol Biol **55**(4): 613-615.

Kantrow, S. P*., et al.* (2009). "Neutrophil-mediated lung permeability and host defense proteins." Am J Physiol Lung Cell Mol Physiol **297**(4): L738-745.

Kawaguchi, A*., et al.* (2017). "Impacts of allergic airway inflammation on lung pathology in a mouse model of influenza A virus infection." PLoS One **12**(2): e0173008.

Kay, A. B. (2006). "The role of T lymphocytes in asthma." Chem Immunol Allergy **91**: 59-75.

Keeler, S. P*., et al.* (2018). "Influenza A Virus Infection Causes Chronic Lung Disease Linked to Sites of Active Viral RNA Remnants." J Immunol **201**(8): 2354-2368.

Khumalo, J*., et al.* (2020). "Therapeutic and prophylactic deletion of IL-4Ra-signaling ameliorates established ovalbumin induced allergic asthma." Allergy **75**(6): 1347-1360.

Kobayashi, M.*, et al.* (1989). "Identification and purification of natural killer cell stimulatory factor (NKSF), a cytokine with multiple biologic effects on human lymphocytes." J Exp Med **170**(3): 827-845.

Kumar, R. K.*, et al.* (2008). "The "classical" ovalbumin challenge model of asthma in mice." Curr Drug Targets **9**(6): 485-494.

Kuruvilla, M. E.*, et al.* (2019). "Understanding Asthma Phenotypes, Endotypes, and Mechanisms of Disease." Clin Rev Allergy Immunol **56**(2): 219-233.

Lajiness, J. D.*, et al.* (2023). "Catching Our Breath: Updates on the Role of Dendritic Cell Subsets in Asthma." Adv Biol (Weinh) **7**(6): e2200296.

Lambrecht, B. N.*, et al.* (2009). "Biology of lung dendritic cells at the origin of asthma." Immunity **31**(3): 412-424.

Lambrecht, B. N.*, et al.* (2012). "The airway epithelium in asthma." Nat Med **18**(5): 684-692.

Lambrecht, B. N.*, et al.* (2015). "The immunology of asthma." Nat Immunol **16**(1): 45-56.

Layland, L. E.*, et al.* (2013). "Schistosoma mansoni-mediated suppression of allergic airway inflammation requires patency and Foxp3+ Treg cells." PLoS Negl Trop Dis **7**(8): e2379.

Li, N.*, et al.* (2015). "Influenza infection induces host DNA damage and dynamic DNA damage responses during tissue regeneration." Cell Mol Life Sci **72**(15): 2973-2988.

Li, Y. F.*, et al.* (2005). "Maternal and grandmaternal smoking patterns are associated with early childhood asthma." Chest **127**(4): 1232-1241.

Ling, P.*, et al.* (1995). "Human IL-12 p40 homodimer binds to the IL-12 receptor but does not mediate biologic activity." J Immunol **154**(1): 116-127.

Liu, W.*, et al.* (2015). "Pulmonary Function and Clinical Manifestations of Patients Infected with Mild Influenza A Virus Subtype H1N1: A One-Year Follow-Up." PLoS One **10**(7): e0133698.

Luo, W.*, et al.* (2022). "Distinct spatial and temporal roles for Th1, Th2, and Th17 cells in asthma." Front Immunol **13**: 974066.

Magram, J.*, et al.* (1996). "IL-12-deficient mice are defective in IFN gamma production and type 1 cytokine responses." Immunity **4**(5): 471-481.

Mass, E.*, et al.* (2016). "Specification of tissue-resident macrophages during organogenesis." Science **353**(6304).

McInnes, L.*, et al.* (2018). "UMAP: Uniform Manifold Approximation and Projection." Journal of Open Source Software **3**(29).

McMillan, S. J.*, et al.* (2004). "Prolonged allergen challenge in mice leads to persistent airway remodelling." Clin Exp Allergy **34**(3): 497-507.

Mebrahtu, T. F.*, et al.* (2015). "Childhood body mass index and wheezing disorders: a systematic review and meta-analysis." Pediatr Allergy Immunol **26**(1): 62-72.

Megremis, S.*, et al.* (2018). "Rhinovirus Species-Specific Antibodies Differentially Reflect Clinical Outcomes in Health and Asthma." Am J Respir Crit Care Med **198**(12): 1490-1499.

Mellman, I. (2013). "Dendritic cells: master regulators of the immune response." Cancer Immunol Res **1**(3): 145-149.

Merad, M.*, et al.* (2013). "The dendritic cell lineage: ontogeny and function of dendritic cells and their subsets in the steady state and the inflamed setting." Annu Rev Immunol **31**: 563-604.

Mettelman, R. C.*, et al.* (2022). "Mucosal immune responses to infection and vaccination in the respiratory tract." Immunity **55**(5): 749-780.

Mikušová, M.*, et al.* (2022). "The Contribution of Viral Proteins to the Synergy of Influenza and Bacterial Co-Infection." Viruses **14**(5).

Mims, J. W. (2015). "Asthma: definitions and pathophysiology." Int Forum Allergy Rhinol **5 Suppl 1**: S2-6.

Misharin, A. V.*, et al.* (2013). "Flow cytometric analysis of macrophages and dendritic cell subsets in the mouse lung." Am J Respir Cell Mol Biol **49**(4): 503-510.

Moltedo, B.*, et al.* (2011). "Unique type I interferon responses determine the functional fate of migratory lung dendritic cells during influenza virus infection." PLoS Pathog **7**(11): e1002345.

Mostafa, D. H. D.*, et al.* (2022). "Characterization of sex-related differences in allergen house dust mite-challenged airway inflammation, in two different strains of mice." Sci Rep **12**(1): 20837.

Motta, A.*, et al.* (2004). "Phleum pratense pollen starch granules induce humoral and cell-mediated immune responses in a rat model of allergy." Clin Exp Allergy **34**(2): 310-314.

Nakagawa, H.*, et al.* (2017). "Optic neuritis and acute anterior uveitis associated with influenza A infection: a case report." Int Med Case Rep J **10**: 1-5.

Nakano, H.*, et al.* (2012). "Pulmonary CD103(+) dendritic cells prime Th2 responses to inhaled allergens." Mucosal Immunol **5**(1): 53-65.

Nials, A. T.*, et al.* (2008). "Mouse models of allergic asthma: acute and chronic allergen challenge." Dis Model Mech **1**(4-5): 213-220.

Niessen, N. M.*, et al.* (2021). "Neutrophilic asthma features increased airway classical monocytes." Clin Exp Allergy **51**(2): 305-317.

Noonan, M.*, et al.* (2013). "Dose-ranging study of lebrikizumab in asthmatic patients not receiving inhaled steroids." J Allergy Clin Immunol **132**(3): 567-574.e512.

Ntontsi, P.*, et al.* (2021). "Genetics and Epigenetics in Asthma." Int J Mol Sci **22**(5).

O'Byrne, P. M. (2000). "Leukotriene bronchoconstriction induced by allergen and exercise." Am J Respir Crit Care Med **161**(2 Pt 2): S68-72.

Ohshima, Y.*, et al.* (1997). "Expression and function of OX40 ligand on human dendritic cells." J Immunol **159**(8): 3838-3848.

Ong, J. W. J.*, et al.* (2019). "Insights into Early Recovery from Influenza Pneumonia by Spatial and Temporal Quantification of Putative Lung Regenerating Cells and by Lung Proteomics." Cells **8**(9).

Palese, P.*, et al.* (2011). "Why do influenza virus subtypes die out? A hypothesis." mBio **2**(5).

Papi, A.*, et al.* (2018). "Asthma." The Lancet **391**(10122): 783-800.

Peteranderl, C.*, et al.* (2016). "Human Influenza Virus Infections." Semin Respir Crit Care Med **37**(4): 487-500.

Peters, S. P. (2014). "Asthma phenotypes: nonallergic (intrinsic) asthma." J Allergy Clin Immunol Pract **2**(6): 650-652.

Plantinga, M.*, et al.* (2013). "Conventional and monocyte-derived CD11b(+) dendritic cells initiate and maintain T helper 2 cell-mediated immunity to house dust mite allergen." Immunity **38**(2): 322-335.

Platts-Mills, T.*, et al.* (2001). "Sensitisation, asthma, and a modified Th2 response in children exposed to cat allergen: a population-based cross-sectional study." Lancet **357**(9258): 752-756.

Price, J. D.*, et al.* (2015). "The Role of Dendritic Cell Subsets and Innate Immunity in the Pathogenesis of Type 1 Diabetes and Other Autoimmune Diseases." Front Immunol **6**: 288.

Quell, K. M.*, et al.* (2020). "GM-CSF and IL-33 Orchestrate Polynucleation and Polyploidy of Resident Murine Alveolar Macrophages in a Murine Model of Allergic Asthma." Int J Mol Sci **21**(20).

Rashid, F.*, et al.* (2023). "Roles and functions of IAV proteins in host immune evasion." Front Immunol **14**: 1323560.

Robert-Koch-Institut (RKI). "Influenza: Erkrankung durch saisonale Influenzaviren." https://www.rki.de/DE/Content/Infekt/EpidBull/Merkblaetter/Ratgeber_Influenza_saisonal.html#doc2382022bodyText3. Accessed on 22.04.2024.

Romanet-Manent, S.*, et al.* (2002). "Allergic vs nonallergic asthma: what makes the difference?" Allergy **57**(7): 607-613.

Roquet, A.*, et al.* (1997). "Combined antagonism of leukotrienes and histamine produces predominant inhibition of allergen-induced early and late phase airway obstruction in asthmatics." Am J Respir Crit Care Med **155**(6): 1856-1863.

Roubidoux, E. K.*, et al.* (2021). "Animal Models Utilized for the Development of Influenza Virus Vaccines." Vaccines (Basel) **9**(7).

Rouse, B. T.*, et al.* (2010). "Immunity and immunopathology to viruses: what decides the outcome?" Nat Rev Immunol **10**(7): 514-526.

Rynda-Apple, A.*, et al.* (2015). "Influenza and Bacterial Superinfection: Illuminating the Immunologic Mechanisms of Disease." Infect Immun **83**(10): 3764-3770.

Schmit, T.*, et al.* (2022). "Interferon-γ promotes monocyte-mediated lung injury during influenza infection." Cell Rep **38**(9): 110456.

Schwarze, J.*, et al.* (2018). "Influenza burden, prevention, and treatment in asthma-A scoping review by the EAACI Influenza in asthma task force." Allergy **73**(6): 1151-1181.

Schworer, S. A.*, et al.* (2024). "Pulmonary Interstitial Macrophages stIMulate Regulatory T Cell Responses." Am J Respir Cell Mol Biol.

Schyns, J.*, et al.* (2018). "Lung Interstitial Macrophages: Past, Present, and Future." J Immunol Res **2018**: 5160794.

Sharma-Chawla, N.*, et al.* (2016). "Influenza A Virus Infection Predisposes Hosts to Secondary Infection with Different Streptococcus pneumoniae Serotypes with Similar Outcome but Serotype-Specific Manifestation." Infect Immun **84**(12): 3445-3457.

Shay, L. A.*, et al.* (2015). "Where is the evidence? A systematic review of shared decision making and patient outcomes." Med Decis Making **35**(1): 114-131.

Shimizu, H.*, et al.* (2013). "Critical role of interleukin-5 in the development of a mite antigen-induced chronic bronchial asthma model." Inflamm Res **62**(10): 911-917.

Sjöberg, L. C.*, et al.* (2017). "Interleukin 33 exacerbates antigen driven airway hyperresponsiveness, inflammation and remodeling in a mouse model of asthma." Sci Rep **7**(1): 4219.

Skarbinski, J.*, et al.* (2011). "Hospitalized patients with 2009 pandemic influenza A (H1N1) virus infection in the United States--September-October 2009." Clin Infect Dis **52 Suppl 1**: S50-59.

Skevaki, C.*, et al.* (2018). "Influenza-derived peptides cross-react with allergens and provide asthma protection." J Allergy Clin Immunol **142**(3): 804-814.

Snyder, M. E.*, et al.* (2021). "Human Lung-Resident Macrophages Colocalize with and Provide Costimulation to PD1(hi) Tissue-Resident Memory T Cells." Am J Respir Crit Care Med **203**(10): 1230-1244.

Somerville, L.*, et al.* (2020). "Alveolar Macrophages in Influenza A Infection Guarding the Castle with Sleeping Dragons." Infect Dis Ther (San Antonio) **1**(1).

Song, P.*, et al.* (2022). "Global, regional, and national prevalence of asthma in 2019: a systematic analysis and modelling study." J Glob Health **12**: 04052.

Soroosh, P.*, et al.* (2013). "Lung-resident tissue macrophages generate Foxp3+ regulatory T cells and promote airway tolerance." J Exp Med **210**(4): 775-788.

Stegemann-Koniszewski, S.*, et al.* (2016). "Alveolar Type II Epithelial Cells Contribute to the Anti-Influenza A Virus Response in the Lung by Integrating Pathogen- and Microenvironment-Derived Signals." mBio **7**(3).

Stegemann, S.*, et al.* (2009). "Increased susceptibility for superinfection with Streptococcus pneumoniae during influenza virus infection is not caused by TLR7-mediated lymphopenia." PLoS One **4**(3): e4840.

Steinke, J. W.*, et al.* (2001). "Th2 cytokines and asthma. Interleukin-4: its role in the pathogenesis of asthma, and targeting it for asthma treatment with interleukin-4 receptor antagonists." Respir Res **2**(2): 66-70.

Takazono, T.*, et al.* (2017). "Aspergillus in chronic lung disease: Modeling what goes on in the airways." Med Mycol **55**(1): 39-47.

Tang, X. Z*., et al.* (2022). "Bronchus-associated macrophages efficiently capture and present soluble inhaled antigens and are capable of local Th2 cell activation." Elife **11**.

Taramarcaz, P*., et al.* (2005). "Ragweed (Ambrosia) progression and its health risks: will Switzerland resist this invasion?" Swiss Med Wkly **135**(37-38): 538-548.

Taubenberger (2008). "The pathology of influenza virus infections."

Thangavel, R. R*., et al.* (2014). "Animal models for influenza virus pathogenesis, transmission, and immunology." J Immunol Methods **410**: 60-79.

Torrent, M*., et al.* (2007). "Early-life allergen exposure and atopy, asthma, and wheeze up to 6 years of age." Am J Respir Crit Care Med **176**(5): 446-453.

Toufen, C., Jr*., et al.* (2011). "Follow-up after acute respiratory distress syndrome caused by influenza a (H1N1) virus infection." Clinics (Sao Paulo) **66**(6): 933-937.

Toward, T. J*., et al.* (2004). "Early and late bronchoconstrictions, airway hyper-reactivity, leucocyte influx and lung histamine and nitric oxide after inhaled antigen: effects of dexamethasone and rolipram." Clin Exp Allergy **34**(1): 91-102.

Tscherne, D. M*., et al.* (2011). "Virulence determinants of pandemic influenza viruses." J Clin Invest **121**(1): 6-13.

Ural, B. B*., et al.* (2020). "Identification of a nerve-associated, lung-resident interstitial macrophage subset with distinct localization and immunoregulatory properties." Sci Immunol **5**(45).

van Helden, M. J*., et al.* (2013). "Dendritic cells in asthma." Curr Opin Immunol **25**(6): 745-754.

van Tilburg Bernardes, E*., et al.* (2017). "Hygiene Hypothesis in Asthma Development: Is Hygiene to Blame?" Arch Med Res **48**(8): 717-726.

Veerapandian, R*., et al.* (2018). "Influenza in Asthmatics: For Better or for Worse?" Front Immunol **9**: 1843.

Vogelmeier, C. F*., et al.* (2017). "Global Strategy for the Diagnosis, Management, and Prevention of Chronic Obstructive Lung Disease 2017 Report: GOLD Executive Summary." Eur Respir J **49**(3).

von Mutius, E*., et al.* (2020). "Primary prevention of asthma: from risk and protective factors to targeted strategies for prevention." Lancet **396**(10254): 854-866.

Vroman, H*., et al.* (2017). "Dendritic Cell Subsets in Asthma: Impaired Tolerance or Exaggerated Inflammation?" Front Immunol **8**: 941.

Waithman, J*., et al.* (2012). "Dendritic cells and influenza A virus infection." Virulence **3**(7): 603-608.

Walsh, K. B*., et al.* (2011). "Suppression of cytokine storm with a sphingosine analog provides protection against pathogenic influenza virus." Proc Natl Acad Sci U S A **108**(29): 12018-12023.

Wan, H*., et al.* (1999). "Der p 1 facilitates transepithelial allergen delivery by disruption of tight junctions." J Clin Invest **104**(1): 123-133.

Wang, T*., et al.* (2023). "Influenza-trained mucosal-resident alveolar macrophages confer long-term antitumor immunity in the lungs." Nat Immunol **24**(3): 423-438.

Wang, X*., et al.* (1999). "Characterization of mouse interleukin-12 p40 homodimer binding to the interleukin-12 receptor subunits." European Journal of Immunology **29**(6): 2007-2013.

Wanka, L*., et al.* (2021). "Trained immunity and allergy: State of the art and future perspectives." Allergy **76**(4): 1265-1267.

Wanner, N*., et al.* (2022). "Using the Autofluorescence Finder on the Sony ID7000(TM) Spectral Cell Analyzer to Identify and Unmix Multiple Highly Autofluorescent Murine Lung Populations." Front Bioeng Biotechnol **10**: 827987.

Wark, P. A*., et al.* (2002). "Neutrophil degranulation and cell lysis is associated with clinical severity in virus-induced asthma." Eur Respir J **19**(1): 68-75.

Whetstone, C. E*., et al.* (2022). "The Role of Airway Epithelial Cell Alarmins in Asthma." Cells **11**(7).

Wills-Karp, M. (2004). "Interleukin-13 in asthma pathogenesis." Immunol Rev **202**: 175-190.

Wohlleben, G*., et al.* (2003). "Influenza A virus infection inhibits the efficient recruitment of Th2 cells into the airways and the development of airway eosinophilia." J Immunol **170**(9): 4601-4611.

Woodruff, P. G*., et al.* (2009). "T-helper type 2-driven inflammation defines major subphenotypes of asthma." Am J Respir Crit Care Med **180**(5): 388-395.

World Health Organization (WHO). “Influenza (seasonal).” https://www.who.int/news-room/fact-sheets/detail/influenza-(seasonal). Accessed on 19.04.2024.

Wu, Q*., et al.* (2020). "Resolved Influenza A Virus Infection Has Extended Effects on Lung Homeostasis and Attenuates Allergic Airway Inflammation in a Mouse Model." Microorganisms **8**(12).

Xie, Y*., et al.* (2024). "Long-term outcomes following hospital admission for COVID-19 versus seasonal influenza: a cohort study." Lancet Infect Dis **24**(3): 239-255.

Xirakia, C*., et al.* (2010). "Toll-like receptor 7-triggered immune response in the lung mediates acute and long-lasting suppression of experimental asthma." Am J Respir Crit Care Med **181**(11): 1207-1216.

Xu, Y*., et al.* (2016). "Macrophages transfer antigens to dendritic cells by releasing exosomes containing dead-cell-associated antigens partially through a ceramide-dependent pathway to enhance CD4(+) T-cell responses." Immunology **149**(2): 157-171.

Xue, J*., et al.* (2014). "Transcriptome-based network analysis reveals a spectrum model of human macrophage activation." Immunity **40**(2): 274-288.

Yamasaki, A*., et al.* (2022). "Neutrophils and Asthma." Diagnostics (Basel) **12**(5).

Yang, J*., et al.* (2014). "Monocyte and macrophage differentiation: circulation inflammatory monocyte as biomarker for inflammatory diseases." Biomark Res **2**(1): 1.

Yao, Y*., et al.* (2018). "Induction of Autonomous Memory Alveolar Macrophages Requires T Cell Help and Is Critical to Trained Immunity." Cell **175**(6): 1634-1650.e1617.

Ye, Q*., et al.* (2003). "MHC class II-associated invariant chain isoforms regulate pulmonary immune responses." J Immunol **170**(3): 1473-1480.

Yeo, I.-K*., et al.* (2000). "A New Family of Power Transformations to Improve Normality or Symmetry." Biometrika **87**(4): 954-959.

Yoo, J. K*., et al.* (2013). "Viral infection of the lung: host response and sequelae." J Allergy Clin Immunol **132**(6): 1263-1276; quiz 1277.

Yoon, S. W*., et al.* (2014). "Evolution and ecology of influenza A viruses." Curr Top Microbiol Immunol **385**: 359-375.

Yoshikawa, S*., et al.* (2004). "Time and pressure dependence of transvascular Clara cell protein, albumin, and IgG transport during ventilator-induced lung injury in mice." Am J Physiol Lung Cell Mol Physiol **286**(3): L604-612.

Yu, W. C*., et al.* (2011). "Viral replication and innate host responses in primary human alveolar epithelial cells and alveolar macrophages infected with influenza H5N1 and H1N1 viruses." J Virol **85**(14): 6844-6855.

Zarnegar, B*., et al.* (2017). "Influenza Infection in Mice Induces Accumulation of Lung Mast Cells through the Recruitment and Maturation of Mast Cell Progenitors." Front Immunol **8**: 310.

Zaslona, Z*., et al.* (2014). "Resident alveolar macrophages suppress, whereas recruited monocytes promote, allergic lung inflammation in murine models of asthma." J Immunol **193**(8): 4245-4253.

Żeromski, J*., et al.* (2020). "Pattern Recognition Receptors: Significance of Expression in the Liver." Arch Immunol Ther Exp (Warsz) **68**(5): 29.

Zosky, G. R*., et al.* (2007). "Animal models of asthma." Clin Exp Allergy **37**(7): 973-988.

Zuo, W*., et al.* (2015). "p63(+)Krt5(+) distal airway stem cells are essential for lung regeneration." Nature **517**(7536): 616-620.

# 8 Ehrenerklärung

Ich versichere hiermit, dass ich die vorliegende Arbeit ohne unzulässige Hilfe Dritter und ohne Benutzung anderer als der angegebenen Hilfsmittel angefertigt habe; verwendete fremde und eigene Quellen sind als solche kenntlich gemacht. Ich habe insbesondere nicht wissentlich:

- Ergebnisse erfunden oder widersprüchlich Ergebnisse verschwiegen,
- statistische Verfahren absichtlich missbraucht, um Daten in ungerechtfertigter Weise zu interpretieren,
- fremde Ergebnisse oder Veröffentlichungen plagiiert,
- fremde Forschungsergebnisse verzerrt wiedergegeben.

Mir ist bekannt, dass Verstöße gegen das Urheberrecht Unterlassungs- und Schadensersatzansprüche des Urhebers sowie eine strafrechtliche Ahndung durch die Strafverfolgungsbehörden begründen kann.
Ich erkläre mich damit einverstanden, dass die Arbeit ggf. mit Mitteln der elektronischen Datenverarbeitung auf Plagiate überprüft werden kann. Die Arbeit wurde bisher weder im Inland noch im Ausland in gleicher oder ähnlicher Form als Dissertation eingereicht und ist als Ganzes auch noch nicht veröffentlicht.

Magdeburg, den 24. Mai 2024

_____

Belinda Camp